FT-ICR Studies of Transition Metal Cluster Ions

Iulia Balteanu

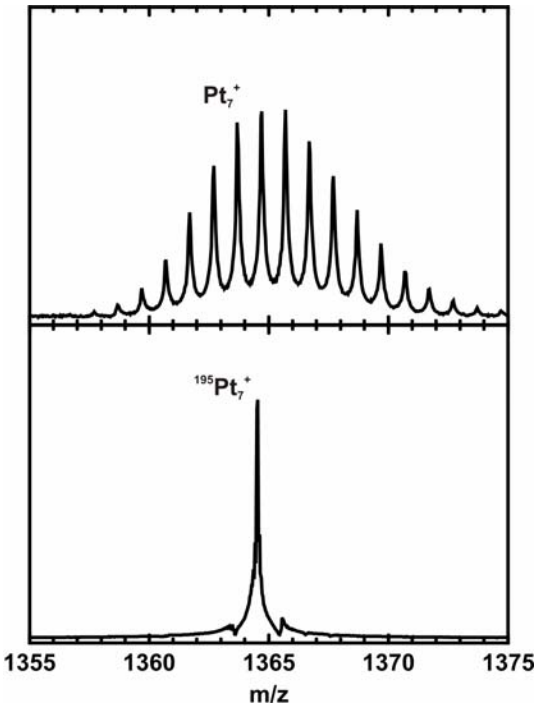

Dissertation

Technische Universität München

Technische Universität München
Fakultät für Chemie
- Lehrstuhl II für Physikalische Chemie -

FT-ICR Studies of Transition Metal Cluster Ions

Iulia Balteanu

Vollständiger Abdruck der von der Fakultät für Chemie der Technischen Universität München zur Erlangung des akademischen Grades eines

Doktors der Naturwissenschaften

genehmigten Dissertation.

Vorsitzender: Univ.-Prof. Dr. U. K. Heiz

Prüfer der Dissertation:

1. Univ.-Prof. V. E. Bondybey, Ph.D. (Univ. of California, Berkeley, USA)
2. Univ.-Prof. Dr. K. Köhler

Die Dissertation wurde am 11.01.2005 bei der Technischen Universität München eingereicht und durch die Fakultät für Chemie am 11.02.2005 angenommen.

For Buni

In memory of my grandmother, Mémé

Contents

1. Introduction

Investigations of the interactions between transition metals, both clusters and surfaces, and different adsorbed substances has been the focus of intensive studies for many years. The chemistry and the structure of transition metal clusters and their compounds, with their multitude of oxidation states is of long standing interest because of their potential use as catalysts[1] which have numerous applications in technology and industry. Over the last 20 years such investigations provided considerable insights into the details of metal-adsorbate interactions, including reaction on metal surfaces. There have been many studies[2-12] involving transition metal clusters and their reactivity with a large variety of small molecules, for example nitrogen oxide, carbon monoxide, molecular hydrogen, oxygen and benzene. In spite of this lively interest, the detailed mechanism of their chemisorption on transition metal clusters is still poorly understood.

The Fourier transform ion cyclotron resonance (FT-ICR) mass spectrometry is very well suited for studies of ionic cluster reactions. Its ability to trap and store the ions for 10^{-1}s - 1000s makes it possible to investigate the reactions at very low pressure, under strictly binary collision conditions. Its inherent extremely high resolution permits an unambiguous identification of the elemental composition of the reactant ions and of their reaction products. The laser vaporization source used for the experiments described in this work can produce both cationic and anionic metal clusters of almost any material. Large ionic metal clusters up to 25 atoms were generated from the laser vaporisation source and their reactions with different molecules were investigated using the FT-ICR technique.

Coinage metals being relatively unreactive occur in nature in native, elemental

form, and have therefore been known to man since antiquity. Gold specifically is one of the heaviest stable elements and its compounds are often viewed as prototypes for investigating relativistic effects.[13-17] Its reactivity studies initially concentrated on the adsorption efficiency of various molecules.[18,19] Since oxidation of CO catalyzed by transition metal ions is probably the first metal-catalysed cycle studied by mass spectrometric methods in the gas phase,[20,21] the interest in supported gold cluster catalysts has initiated a series of theoretical and experimental studies of CO and O_2 adsorption[22-26] and coadsorption[27-30] on anionic, neutral and cationic gold clusters. Chapter 3 deals with first results on the reactivity of gold anionic clusters Au_n^- with up to 16 atoms towards CO. A novel approach was developed in order to extract absolute bimolecular rate constants from a pulsed-valve experiment in an FT-ICR, due to the fact that the rate constants observed were in most cases too low to be measured by the standard method with a constant backing pressure.

The azides due to their strong exotermicity in reactions and to their explosive properties, have a significant importance in industry and technology both as chemical intermediates as well as end products, and are used in numerous applications. Lead azide is the most common primary explosive used in detonators,[31-32] while sodium azide is the most frequently used propellant in automobile air bags.[33-34] Also organic, covalent azides have found applications in photoresists,[35] vulcanization[36] and polymer coupling.[37] Increasingly, they are also used in chemical vapor deposition for generating nitride films.[38-40] In chapter 4 reactions and surface-activated decomposition of one simple representative of covalent azides, azidoacetonitrile, are investigated. Gas-phase reactions of anionic and cationic rhodium clusters with azidoacetonitrile N_3CH_2CN are studied by FT-ICR mass spectroscopy under near-thermal conditions as a function of their size and charge state.

Every catalytic process requires adsorption of the reactants on the metal surface, occurrence of its reaction, and then desorption of the products. Rhodium metal has a number of advantages for investigating hydrocarbon reactions. It does not have a very high affinity to carbon[41] and lies in the area of the periodic table where the elements are rather reactive towards hydrogen. A great advantage of rhodium is that, unlike other typical catalysts like palladium or platinum, it is monoisotopic. Investigation of the reactions of small cationic rhodium clusters Rh_n^+, n = 1 – 23 with C_2H_6 in order to observe the size dependence of the ethane dehydrogenation on the cluster surfaces makes the subject of chapter 5.

Platinum, palladium and rhodium are useful dehydrogenation catalysts,[42,43] but are also used extensively in removing toxic oxides such as carbon monoxide or nitrogen oxides from automotive exhaust.[44,45] Platinum and palladium have been studied in less detail because unlike rhodium which is a monoisotopic element, both metals have six stable isotopes each. For larger clusters, this very quickly leads to dilution of the signal among many isotopomers, and overlapping of the products with the reactants. Both effects together so far have limited the cluster sizes accessible in reactivity studies. The laser vaporization source requires only minor amounts of materials, permitting work with isotopically enriched samples. In chapter 6 highly isotopically enriched platinum was used to investigate the reactions of $^{195}Pt_n^{+/-}$ clusters, n = 1-24, with small molecules like N_2O and CO as well the saturation reactions with CO and catalytic oxidation of CO on gas phase platinum clusters.

It is well known that transition metals can activate unreactive C-H bonds of different molecules. Several groups have investigated in detail the interaction between methane and catalysts in order to understand the methane activation mechanism.[6,43,46-49] The Garching group has previously studied methane activation by gas phase $Pt_n^{+/-}$ cluster

ions with a normal isotopic distribution, thus the study was limited to small species up to nine atoms.[43] In chapter 7 highly isotopically enriched platinum ^{195}Pt was used to investigate the reactions of $^{195}Pt_n^{+/-}$ clusters, n = 1-24, with methane CH_4 and deuterated methane CD_4

References

(1) T. A O'Brien, K. Albert, M. C. Zerner, *J. Chem. Phys.*, **2000**, *112*, 3192**.**

(2) W. T. Wallace, R. L. Whetten, *J. Phys. Chem. B*, **2000**, *104*, 10964.

(3) C. Berg, M. Beyer, T. Schlinder, G Niedner-Schatteburg, V. Bondybey, *J. Chem. Phys.*, **1996**, *104*, 20.

(4) C. Berg, M. Beyer, U. Achatz, S. Joos, G. Niedner-Schatteburg, V. E. Bondybey, *J. Chem. Phys.*, **1998**, *108*, 5398.

(5) V. Bondybey, M. Beyer, *J. Phys Chem. A*, **2001**, *105*, 951.

(6) U. Achatz, M Beyer, S. Joos, B. S. Fox, G. Niedner-Schatteburg, V. E. Bondybey, *J. Phys. Chem. A*, **1999**, *103*, 8200.

(7) T. Mineva, N. Russo, H-J. Freund, *J. Phys. Chem. A*, **2001**, *105*, 10723.

(8) M. B. Knickelbein, G. M. Koretsky, *J. Phys. Chem.*, **1998**, *102*, 580.

(9) M. B. Knickelbein, *J. Chem. Phys.*, **2001**, *115*, 1983.

(10) H. Grönbeck, A. Rosén, W. Andreoni, *Z. Phys. D.*, **1997**, *40*, 206.

(11) A. Lupinetti, S. Fau, G. Frenking, S. H. Strauss, *J. Phys. Chem. A*, **1997**, *101*, 9551.

(12) M. B. Knickelbein, *Annu. Rev. Phys. Chem.*, **1999**, *50*, 79.

(13) K. S. Pitzer, *Acc. Chem. Res.*, **1979**, *12*, 271.

(14) P. Pyykkö, J.-P. Desclaux, *Acc. Chem. Res.*, **1979**, *12*, 276.

(15) P. Pyykkö, *Chem. Rev.*, **1988**, *88*, 563.

(16) K. Balasubramanian, *J. Phys. Chem.*, **1989**, *93*, 6585.

(17) D. Schröder, H. Schwarz, J. Hrušak, P. Pyykkö, *Inorg. Chem.*, **1998**, *37*, 624.

(18) D. M. Cox, R. Brickman, K. Creegan, A. Kaldor, *Z. Phys. D*, **1991**, *19*, 353.

(19) M. A. Nygren, P. E. M. Siegbahn, C.-M. Jin, T. Guo, R. E. Smalley, *J. Chem. Phys.*, **1991**, *95*, 6181.

(20) M. M. Kappes, R. H. Staley, *J. Am. Chem. Soc.*, **1981**, *103*, 1286.

(21) Y. Shi, K. M. Ervin, *J. Chem. Phys.*, **1998**, *108*, 1757.

(22) T. H. Lee, K. M. Ervin, *J. Phys. Chem.*, **1994**, *98*, 10023.

(23) W. T. Wallace, R. L. Whetten, *J. Phys. Chem. B*, **2000**, *104*, 10964.

(24) B. E. Salisbury, W. T. Wallace, R. L. Whetten, *Chem. Phys.*, **2000**, *262*, 131.

(25) G. Mills, M. S.Gordon, H. Metiu, *Chem. Phys. Lett.*, **2002**, *359*, 493.

(26) X. Wu, L. Senapati, S. K. Nayak, *J. Chem. Phys.*, **2002**, *117*, 4010.

(27) H. Häkkinen, U. Landman, *J. Am. Chem. Soc.*, **2001**, *123*, 9704.

(28) W. T. Wallace, R. L. Whetten, J. *Am. Chem. Soc.*, **2002**, *124*, 7499.

(29) J. Hagen, L. D. Socaciu, M. Elijazyfer, U. Heiz, T. M. Bernhardt, L. Wöste, *Phys. Chem. Chem. Phys.*, **2002**, *4*, 1707.

(30) N. Lopez, J. K. Nørskov, *J. Am. Chem. Soc.*, **2002**, *124*, 11262.

(31) V. R. P. Verneker, A. C. Forsyth, *J. Phys. Chem.*, **1968**, *72*, 111-115.

(32) V. R. P. Verneker, *J. Phys. Chem.*, **1968**, *72*, 1733-1736.

(33) T. L. Chant, K. B. Gross, R. G. Wooley, *Aerosol Sci. Tech.*, **1990**, *13*, 349-355.

(34) J. M. Berger, P. B. Butler, *Combust. Sci. Technol.*, **1995**, *104*, 93-114.

(35) T. Urano, K. Takahama, T. Yamaoka, *Imaging Sci. J.*, **1999**, *47*, 133-140.

(36) A. Marcos, J. L. de Benito, L. Ibarra, A. Rodriguez, L. Gonzalez, *Polym. Int.*, **1991**, *25*, 7-12.

(37) M. A. L. Manchado, J. M. Kenny, *Rubber Chem. Technol.*, **2001**, *74*, 198-210.

(38) R. A. Fischer, H. Sussek, A. Miehr, H. Pritzkow, E. Herdtweck, *J. Organomet. Chem.*, **1997**, *548*, 73-82.

(39) F. Falk, J. Meinschien, K. Schuster, H. Stafast, *Carbon*, **1998**, *35*, 765-769.

(40) J. J. Wang, E. G. Gillan, *Thin Solid Films*, **2002**, *422*, 62-68.

(41) W. Andreoni, C. M. Varma, *Phys. Rew. B*, **1981**, *23 (2)*, 437-444.

(42) C. Berg, M. Beyer, T. Schindler, G. Niedner-Schatteburg, V. E. Bondybey, *J. Chem. Phys.*, **1996**, *104*, 7940-7946.

(43) U. Achatz, C. Berg, S. Joos, B. S. Fox, M. K. Beyer, G. Niedner-Schatteburg, V. E. Bondybey, *Chem. Phys. Lett.*, **2000**, *320*, 53-58.

(44) S. H. Yang, D. A. Drabold, J. B. Adams, P. Ordejon, K. Glassford, *Journal of Physics-Condensed Matter*, **1997**, *9*, L39-L45.

(45) K. Koszinowski, D. Schroder, H. Schwarz, *J. Phys. Chem. A*, **2003**, *107*, 4999-5006.

(46) D. J. Trevor, R. L. Whetten, D. M. Cox, A. Kaldor, *J. Am. Chem. Soc.*, **1985**, *107*, 518-519.

(48) M. Pavlov, M. R. A. Blomberg, P. E. M. Siegbahn, R. Wesendrup, C. Heinemann, H. Schwarz, *J. Phys. Chem. A*, **1997**, *101*, 1567-1579.

(47) C. Heinemann, R. Wesendrup, H. Schwarz, *Chem. Phys. Lett.*, **1995**, *239*, 75

(49) G. Albert, C. Berg, M. K. Beyer, U. Achatz, S. Joos, G. Niedner-Schatteburg, V. E. Bondybey, *Chem. Phys. Lett.*, **1997**, *268*, 235-241.

2. Experimental and Theoretical Methods

2.1. Fourier Transform Ion Cyclotron Resonance Mass Spectrometry

2.1.1. General

A charged particle moving in the presence of a spatially uniform magnetic field $\vec{B}_0$ is forced to move on a circular trajectory by the Lorentz force:

$$\vec{F} = m\frac{d\vec{v}}{dt} = q\vec{v} \times \vec{B}_0 \qquad (1)$$

in which *m*, *q*, and *v* are the ionic mass, charge, and velocity in a plane perpendicular to $\vec{B}_0$, and $\times$ the vector cross product, showing that the direction of the Lorentz force is perpendicular on the plane determined by $\vec{v}$ and $\vec{B}_0$. If the ion motion is collision free, the magnetic field bends the ion trajectory into a circle of radius *r*, as displayed in Figure 1. Using the angular velocity ω, $v = \omega \times r$ and the angular acceleration $\left|d\vec{v}/dt\right| = v^2/r$ the cyclotron frequency of a charged particle can be determined as:

$$\nu_c = \frac{qB_0}{2\pi m} \qquad (2)$$

Ion Cyclotron Resonance Mass Spectrometry (ICR-MS) uses the possibility to determine the mass of an ion with charge q by measuring its cyclotron frequency v_c in a high magnetic field B_0.

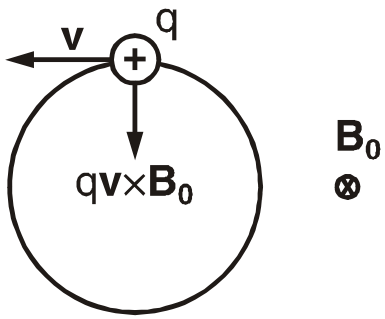

Figure 1: Origin of the cyclotron motion: A particle with charge q and velocity v perpendicular to the magnetic field $\vec{B}_0$ is forced to move on a circular path by the Lorentz force.

One can see in equation (2) that the cyclotron frequency does not depend on the velocity of the charged particle, therefore all the ions with the same mass-to-charge ratio, m/q have the same cyclotron frequency, v_c, independent of their velocity.

The frequency can be measured with very high accuracy.[1] Thus, ICR-MS allows to determine masses with an accuracy of $\Delta m/m=10^{-6}$ or better.[2] In this way, the composition of ions with the same nominal mass can be determined by their mass defect. For example, N_2^+ with a mass of 28.0056 amu and CO^+ with a mass of 27.9944 amu are represented by two separated peaks.[2] A.G. Marshall and M.B. Comisarow[3] extended the ICR technology by using the Fourier transformation, allowing the acquisition of mass spectra over a continuous mass range. Therefore, Fourier Transform Ion Cyclotron Resonance Mass Spectrometry (FT-ICR MS) became a universal tool for chemical analysis and basic research.

The most important part of every FT-ICR setup is the ICR-cell, placed in ultra-high vacuum, in a static, homogenous and very high magnetic field, ranging from 1 to 15 T. To transform the cyclotron motion shown in Figure 1 into a detectable electronic signal the ions are trapped in the ICR-cell by applying an electrostatic potential of the order of less 5V, applying the storage scheme of a Penning trap. Some widely used cell geometries are shown in Figure 2. For detection, the ions are excited on larger radii by a broadband high frequency signal which contains all the frequencies in the desired mass range. The excitation results in formation of coherent ion packages, as shown schematically in Figure 3. The ion packages induce a small electric potential between the detection plates which oscillates with the cyclotron frequency ν_c. This signal is amplified, recorded with an analog-digital converter and then stored as the digitized transient. Fourier transformation of the transient yields a frequency spectrum, which is converted to a mass spectrum by applying equation (2), as is displayed schematically in Figure 4.

Coulomb repulsion among the ions and collisions with the background gas present in the ICR-cell destroy the coherence of the ion packages and result in an exponential decay of the signal. This leads to peak broadening which limits the mass resolution. Ultra high vacuum, with pressures lower than 10^{-8} mbar, can minimize the collisional broadening.

The quadrupol potential used to trap the ions leads to additional oscillations of the ions, these are the magnetron motion and trapping oscillations.[2]

Ions of a defined mass can be accelerated by application of a resonant radio frequency signal which is utilized to perform energy resolved studies,[4] or to eject unwanted ions from the cell. This is done under software control. Highly sophisticated multiple mass spectrometry schemes MS^n can be devised, limited only by the capabilities of the electronics and by the trapping characteristics of the ICR-cell.

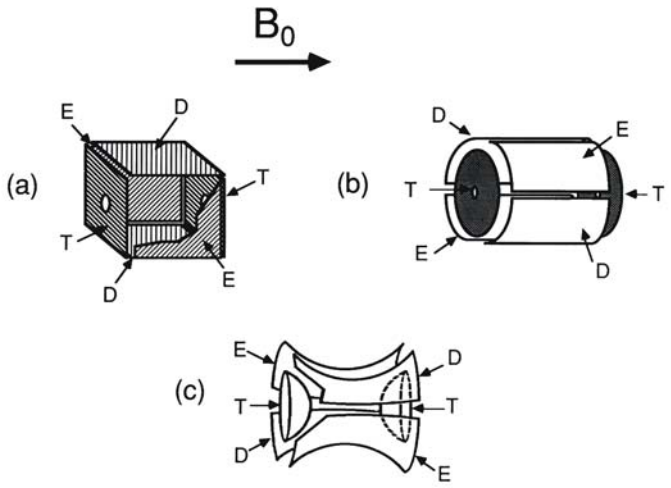

Figure 2: Different ICR cell geometries: (a) cubic cell, (b) cylindric cell, (c) hyperbolic cell. T indicates the trapping electrodes, D the detection electrodes and E the excitation electrodes.[5]

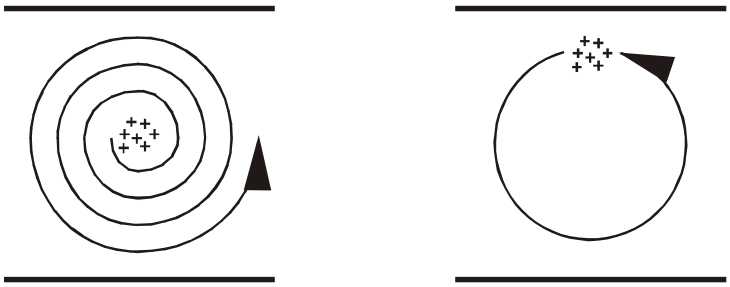

Figure 3: The initially incoherent cyclotron motion of the ions is transformed into a coherent and detectable motion upon irradiation of radio frequency.[5]

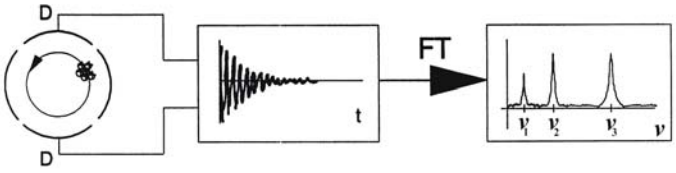

Figure 4: The coherent ion package induces a potential difference between the detection plates which oscillates with the cyclotron frequency ν_c. Coulomb repulsion among the ions and collisions with the background gas lead to an exponential decay of the transient. Fourier transformation of the transient yields a frequency spectrum.

2.1.2. The Garching FT-ICR Mass Spectrometer

All the experiments described in the next chapters were performed with an FT-ICR[6-8] displayed schematically in Figure 5 which is a modified Bruker/Spectrospin CMS47X. It is equipped with a 4.7 T superconducting magnet with cylindrical room temperature bore, a cylindrical 60 mm x 60 mm infinity cell[9] and a differentially pumped ultra high vacuum system with external ion transfer optics. The experiment is controlled by an APEX III data station. The instrument has been fitted with a supplementary source chamber with an additional differential pumping stage which allows the application of pulsed, supersonic expansion molecular beam ion sources with a high gas load.[8,10] A gate valve separates UHV and source region and allows changing the expansion gas and the metal target and cleaning the source chamber without disturbing the ultra high vacuum (UHV) in the ICR cell.

The ions are generated in the source chamber using a molecular beam ion source, then they are confined by a cylindrical mesh and accelerated downstream from a 1.0 mm skimmer which acts as a first flow constraint separating the source chamber from the next differential pumping stages. The ion beam is transferred by the subsequent ion optics into the high field region of the superconducting magnet. To direct the ion beam against the magnetic mirror effect[11], into the homogenous high field region of the magnet it needs to be accelerated to 3 keV kinetic energy. Then the beam is stepwisely decelerated below the trapping potentials and the ions are trapped using the Caravatti method.[12] A small potential gradient is applied perpendicular to the velocity of the ions, thus a part of the kinetic energy of the ions is converted from translational energy along the magnetic field axis into cyclotron motion.

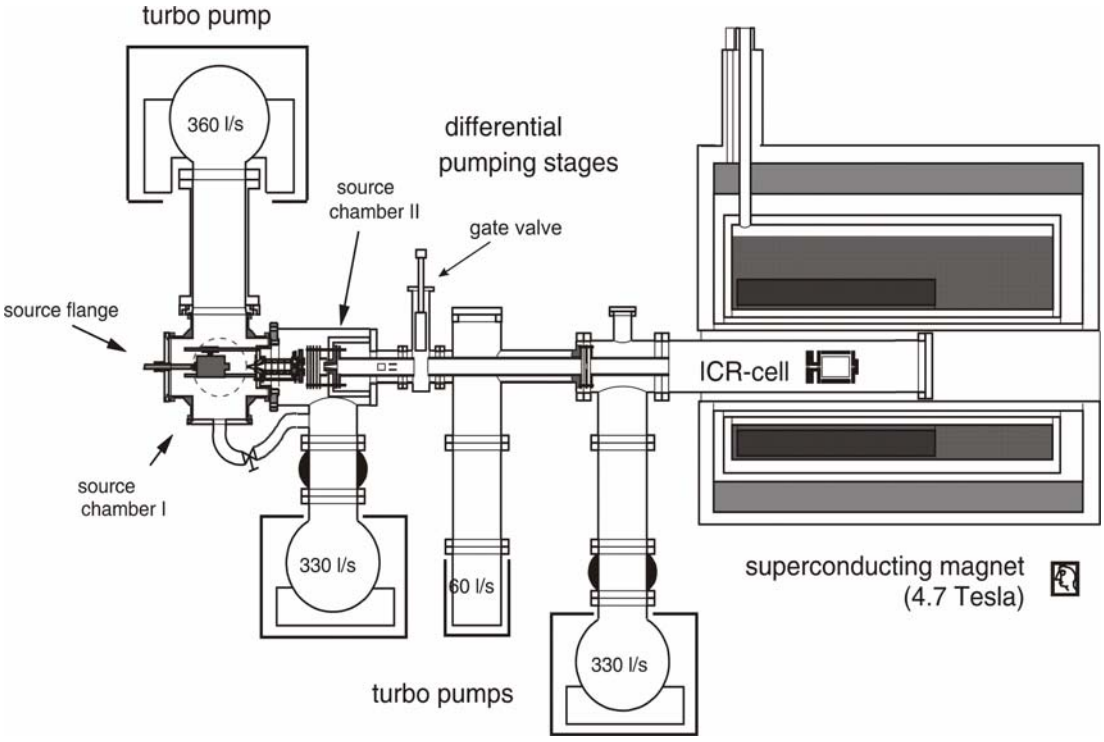

Figure 5: Side-view of the Garching FT-ICR mass spectrometer. Ions are produced in the source chamber and transferred to the ICR-cell inside the magnet by a system of electrostatic lenses. Four differential pumping stages allow the application of molecular beam ion sources with a high gas load.

In the ICR-cell the ions can be stored for times ranging from milliseconds to minutes. If desired, the ions can be individually selected and their chemistry and reaction rates quantitatively studied under well-defined temperature and pressure conditions. Switching between cations and anions is accomplished by inverting the polarity of the transfer ion optic and of the trapping voltages.

The turbomolecular pumps which provide the ultra high vacuum in the ICR-cell are shielded against the strong magnetic field with soft iron, while the rotary roughing pumps which support the previous ones are not shielded. For turbomolecular pumps and rotary pumps the pumping speeds are 360 l/s and respectively 8 m^3/h in the source chamber, 330 l/s and 16 m^3/s in the second stage of differential pumping, and 60 l/s, 330 l/s and 8 m^3/h in the

UHV region. This differential pumping stage setup provides typical pressures without gas load of 5×10^{-6} mbar in the source chamber, 3×10^{-7} mbar in the second pumping stage and less than 1×10^{-10} mbar in the UHV region. Reactant gases can be introduced in the UHV region via two needle valves, type Balzers UHD40, one of them is corrosion gas proof. Another rotary pump is attached to the needle valves inlet for cleaning purposes.

The pressure is measured by Penning ionization gauges, type Balzers IKR 020, in all the differential pumping stages. The Penning gauge in the UHV region is placed 80 cm away from the ICR cell directly on top of the turbomolecular pump. Upon introduction of a collision gas into the cell, a constant backing pressure is obtained as a stationary state between gas flowing into the cell, atoms or molecules sticking on the apparatus walls and desorbing again, and pumping. These processes are highly dependent on the specific gas, and the actual pressure in the cell is different from the pressure above the pump where the Penning ionization gauge is placed. The pressure reading is therefore corrected according to the following equation:[13]

$$p_x^{cell} = \frac{G p_x^{IG}}{R_x} \tag{3}$$

in which G is an empirical geometry factor and R_x the sensitivity of the ion gauge. The geometry factor G was experimentaly determined to have almost the same value for different reactant gases.[13] Thus in a good aproximation, the experimental value for G is 3.7±1.0.[13] The sensitivity of the ion gauge depends on the reactant gas and it is tabulated.[14,15]

An APEX III data station from Bruker was used to control all the experiments and data processing. Mass spectra are transformed to ASCII format and displayed with the public

domain graphics package XMGR.[16] For kinetic analysis the mass-intensities of the spectra are first correlated using ANALYZZE[17] and then transferred to a UNIX computer, where with help of a set of programs including LLCORR,[18] C2N,[19] NNORM,[18] LARGENORM,[17,18] FIT[19] and SPECIALFIT[17,19] are further processed.

2.1.3. The Laser Vaporization Molecular Beam Ion Source

For all experiments a laser vaporization molecular beam ion source[20-22] displayed schematically in Figure 6 was used. The ions are produced by pulsed laser vaporization of a rotating metal disk using the focused 532 nm radiation of a Continuum Surelite II Nd:YAG laser, operating at 10 Hz with up to 20 mJ per 5 ns pulse length. The spot size on the metal target is about 500 μm. The plasma produced by the laser contains enough ions with no need of post-ionization. The vaporization is synchronized with a helium pulse of 50 μs and about 20 bar from a homebuilt piezoelectric valve.[8] This is a modified version of the initial design by Proch and Trickl,[23] designed at TU Munich. The laser generated plasma entrained in the carrier gas, helium, flowing through the confining channel is thermalized by collisions with the cold carrier gas. Further cooling and clustering occur upon supersonic expansion into high vacuum.

The pressure in the inlet system is controlled by an oil-free Leybold pump, EcoDry-M 15, with a maximum pumping speed of 16m^3/h at 1200 rotates/min, to avoid the possible contamination with hydro carbides from the oil of the usual pumps.

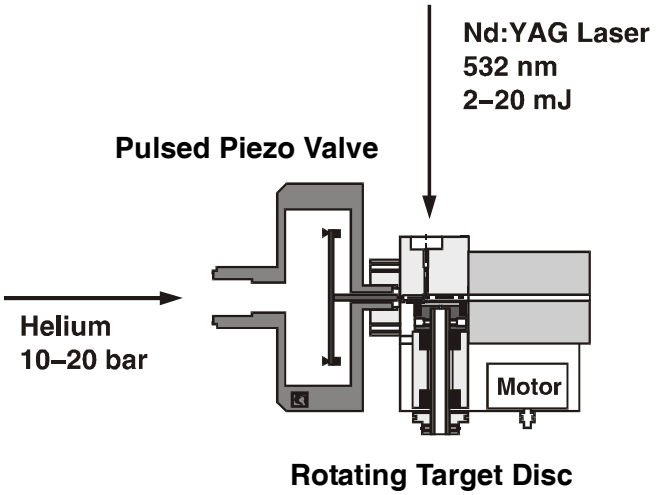

Figure 6: Laser vaporization ion source. The metal is vaporized with a 5 ns laser pulse from a rotating target disk. The hot plasma is expanded via a confining channel into high vacuum where is collisionally cooled, and metal clusters are formed in the supersonic expansion.

The pulse scheme of a typical experiment is shown in Figure 7. The cycle starts with a quench pulse P1, which cleans the ICR cell from ions that might be trapped at the beginning of the experiment. The cell is subsequently filled with typically 20 cycles of ion generation and trapping, which consist of the firing of the flash lamps, opening of the piezoelectric valve, and laser Q-switch trigger. The so-called gate-pulse P2 lowers the trapping voltage of the first trapping plate to 0 V, which allows the ions to enter the cell. Shifting D5 and P2, one can utilize time of flight-effects to select a certain ion distribution. The amount of ions produced as well as their composition, are critically dependent on the relative timing between the gas pulse and the laser pulse. Ion generation is typically followed by optional mass selection, by a variable reaction delay, and by detection of the mass spectrum.

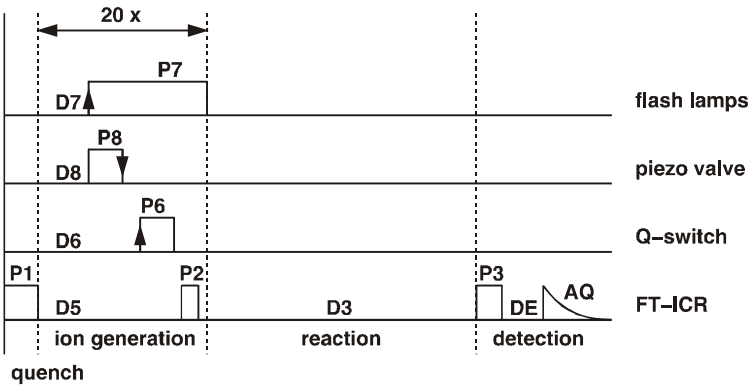

Figure 7: Pulse sequence of a typical ICR-experiment with the laser vaporization source. The quench pulse P1 ejects all charged particles from the cell, which is subsequently filled in typically 20 ion generation cycles. The piezoelectric valve is triggered with the falling edge of the pulse, which allows 1 μs accuracy. After a reaction delay, the ions in the cell are accelerated by the broad-band pulse P3, and the transient is recorded during AQ. The short delay DE ensures that the transient is not affected by the pulse P3.

2.2. Ion-molecule Reactions

To study bimolecular cluster ion-molecule reactions, for every experiment mass spectra are taken after varying reaction delays. Relative rate constants are obtained by fitting the observed time dependence of the parent and the reaction product ion intensities assuming pseudo-first order kinetics, and converted into absolute rate constants, using equation (3) for pressure calibration, through:[13]

$$k_{abs} = \frac{k_{rel} k_B T}{p_x^{cell}} = \frac{k_{rel} k_B T R_x}{G p_x^{IG}} \qquad (4)$$

in which k_B is the Boltzmann constant and T the temperature. If R_x the sensitivity of the ion

gauge can not be found in tabels, it can be calculated with the empirical formula:[15]

$$R_x = 0.36\alpha + 0.3 \tag{5}$$

where α represents the polarizability of the reactant gas molecule.

The Average Dipole Orientation theory (ADO) introduced in 1973 by Su and Bowers[24] allows the calculation of a theoretical collision rate, k_{ADO}:[13]

$$k_{ADO} = \frac{q}{2\varepsilon_0\sqrt{\mu}}\left(\sqrt{\alpha} + \mu_D\sqrt{\frac{2}{\pi k_B T}}\right) \tag{6}$$

in which q is ionic charge, ε_0 electric permittivity, $\mu = m_1 m_2/(m_1 + m_2)$ the reduced mass, α polarizability of the gas molecule, and μ_D permanent dipole moment. The factor c is the dipole locking constant and is tabulated.[25]

The reaction efficiency can be defined as:

$$\Phi = \frac{k_{abs}}{k_{ADO}} \tag{7}$$

2.3. References:

(1) D. J. Wineland, *Science*, **1984**, *226*, 395.

(2) A. G. Marshall, P. B. Grosshans, *Anal. Chem.*, **1991**, *63*, 215A-229A.

(3) M. B. Comisarow, A. G. Marshall, *Chem. Phys. Lett.* **1974**, *25*, 282.

(4) M. Beyer, V. E. Bondybey, *Rapid Commun. Mass Spectrom.* **1997**, *11*, 1588.

(5) A.G. Marshall, F.R. Verdun, *Fourier Transforms in NMR, Optical, and Mass Spectrometry*; Elsevier: Amsterdam, 1990.

(6) C. Berg, T. Schindler, G. Niedner-Schatteburg, V. E. Bondybey, *J. Chem. Phys.* **1995**, *102*, 4870.

(7) T. Schindler, *Dissertation.* Fakultät für Chemie, Biologie und Geowissenschaften, Technische Universität München, Garching, 1996.

(8) C. Berg, *Dissertation.* Fakultät für Chemie, Biologie und Geowissenschaften, Technische Universität München, Garching, 1995.

(9) P. Caravatti, M. Allemann, *Org. Mass Spectrom.* **1991***, 26*, 514.

(10) C. Berg, *Diplomarbeit.* Physik Department, Technische Universität München, Garching, 1992.

(11) J. D. Jackson, *Klassische Elektrodynamik;* de Gruyter: Berlin, New York, 1983.

(12) P. Caravatti, USA Patent Nr. 4 924 089, May 8, 1990.

(13) T. Schindler, *Diplomarbeit*. Physik Department, Technische Universität München, Garching, 1992.

(14) R. L. Summers, NASA Technical Note TN D-5285, 1969.

(15) J. E. Bartmess, R. M. Georgiadis, *Vacuum*, **1983**, *33*, 149.

(16) P. J. Turner, Beaverton, 1994; A. Thoma, G. Schallmoser, A. Lammers, Garching, 1995; A. Lammers, Garching, 1996.

(17) M. Beyer, Garching, 2004.

(18) T. Schindler, Garching, 1994; Beyer, M. Garching, 1996.

(19) T. Schindler, Garching, 1994.

(20) V. E. Bondybey, J. H. English, *J. Chem. Phys.* **1981**, *74*, 6978.

(21) V.E. Bondybey, *Science* **1985**, *227*, 4683.

(22) T. G. Dietz, M. A. Duncan, D. E. Powers, R. E. Smalley, *J. Chem. Phys.* **1981**, *74*, 6511.

(23) D. Proch, T. Trickl, *Rev. Sci. Instrum.* **1989**, *60*, 713.

(24) T. Su, M. T. Bowers, *J. Chem. Phys.* **1973**, *58*, 3027.

(25) T. Su, M. T. Bowers, *Int. J. Mass. Spectrom. Ion Phys.*, **1975**, *17*, 211.

3. CO Adsorption on Anionic Gold Clusters: Implications for Catalytic Activity

3.1. Introduction

The chemistry of coinage metals and of gold and its clusters in particular has been a topic of considerable interest for a variety of reasons. On one hand, the elements are transition metals, but on the other, with their closed d-electron shell and a simple $d^{10}s^1$ configuration, they share some similarities with the alkali metals. Their half occupied ns shell with a single valence electron results in a relatively simple electronic structure of their clusters, to which the simplified "particle in a box" jellium model has been applied by several authors with considerable success.[1,2] Gold specifically is one of the heaviest stable elements, and its compounds are often viewed as prototypes for investigating relativistic effects.[3-7]

Coinage metals being relatively unreactive occur in nature in native, elemental form, and have therefore been known to man since antiquity. In spite of the inertness of the metals, there has recently been a considerable increase in investigations of the chemistry of their clusters and supramolecular assemblies.[8,9] This enhanced activity has been at least partially due to the discovery, that finely dispersed, supported clusters of gold exhibit interesting catalytic properties.[10-14] These can activate a variety of important C1 reactions, including industrially important processes such as methanol synthesis or water-gas shift reaction, as well as a variety of oxygen transfer processes such as CO oxidation or NO reduction.[11] They appear to show efficiencies comparable to those of more

conventional catalysts, while operating at lower temperatures and exhibiting a better tolerance to moisture and catalyst "poisoning". The catalytic activity depends critically on the degree of dispersion, and in a variety of studies it was argued that the optimum occurs for particles with less than 100 atoms,[12] with the range of 8-20 atoms being given in some works.[13,14]

Finite gas phase clusters of metal atoms provide suitable, relatively tractable models for investigating dispersed metal catalysts.[15-19] Properties of anionic gold clusters have been studied by ultraviolet photoelectron spectroscopy[20] and by theory,[21,22] while the structures of cationic clusters were recently probed by ion mobility measurements and by density functional calculations.[23] Even doubly charged gold anions starting from sizes of 29 gold atoms have been generated by laser vaporization,[24] and triply charged clusters starting at size 54 by electron attachment.[25]

Reactivity studies of gold clusters initially concentrated on the adsorption efficiency of various molecules.[26,27] Since oxidation of CO catalyzed by transition metal ions is probably the first metal-catalysed cycle studied by mass spectrometric methods in the gas phase,[28,29] the above mentioned interest in supported gold cluster catalysts has initiated a series of theoretical and experimental studies of CO and O_2 adsorption[30-34] and coadsorption[35-38] on anionic, neutral and cationic gold clusters. For Au_n^-, with the exception of Au_{16}^-, a strict odd-even oscillation in reactivity with O_2 was reported, with only even *n* species adsorbing O_2.[30,32] This was rationalized by oxygen acting as an electron acceptor, forming essentially an O_2^- superoxide adsorbed on a neutral, even-electron gold cluster.[32] Speaking in a more physical picture, one of the singly occupied π^* orbitals of O_2 is able to interact with the half-filled HOMO of the Au_n^- cluster, if *n* is even, resulting in a stronger interaction than with the odd *n* clusters.[30] A completely different situation was encountered with CO. Reactivity sharply increases from n = 4 to n = 7,[30,31]

reaching essentially a plateau with a sharp peak at n = 11 and a broader feature of somewhat increased reactivity around n = 15. In the CO, O_2 coadsorption studies, a promotional effect of preadsorbed CO on the reactivity with O_2 is observed for certain cluster sizes.[37,36] These coadsorbed species $Au_n(CO)(O_2)^-$ are useful model systems for theoretical studies of the catalytic activity of supported gold clusters.[35]

All studies of gold cluster anion reactions so far were undertaken in the presence of a buffer gas in a flow reactor[30-32,36] or ion trap,[37] while the early study of Au_n^+ with CO[27] indicates that observable reactivity may also occur under the strictly single collision conditions of a Fourier-transform ion cyclotron resonance (FT-ICR) mass spectrometer. In this chapter first results on the reactivity of Au_n^-, n = 1 - 16, with CO under these conditions are presented. A novel approach was developed to extract absolute bimolecular rate constants from a pulsed-valve experiment in an FT-ICR. This was necessary, since the rate constants observed were in most cases too low to be measured by the standard method with a constant backing pressure. These results show some marked and interesting deviations from previous flow reactor studies.

3.2. Experimental Details

The experimental apparatus and techniques used were described in details elsewhere,[39,40] and will be here presented only briefly. The studies are carried out on a commercial FT-ICR mass spectrometer. The gold clusters were produced by laser vaporization of the metal in the presence of high pressure (20 bar) helium carrier gas. In the process of sample cooling and adiabatic expansion not only neutral, but also ionic clusters are formed, both negatively and positively charged. Even though, for reasons which we do not quite understand at this time, in contrast with most other metals the

formation of cationic clusters of coinage metals in our source is rather inefficient, cold anionic clusters Au_n^-, with $n \leq 17$ could be produced and investigated.

The ionic clusters are accelerated along the field axis of the superconducting magnet through several stages of differential pumping, steered towards the mass spectrometer, and eventually decelerated and trapped in the ICR cell. The reactant, molecular carbon monoxide, can be admitted to the instrument via adjustable leak valves. In the present case, the reactions of the gold clusters with CO were found to be relatively slow, so that in the mode we usually carry out this type of experiment, that is with the reactant pressure adjusted in the 10^{-9} - 10^{-8} mbar range, very little product was formed. To circumvent this problem, a pulsed valve (General Valve Series 99) was used, which raised momentarily the reactant pressure in the ICR cell into the 10^{-5} mbar range. The reactivity of clusters to between 1-20 such pulses of the reactant gas, which contained as a trace component approximately 1% of O_2 was investigated. The delay between each two pulses was 0.2 s, and a pump down delay of 5 s was applied prior to recording the mass spectra. Under these conditions the anionic gold clusters clearly reacted with the CO, and relative rate constants as a function of the number of gas pulses can be extracted.

The disadvantage of this procedure is that the pressure in the cell is poorly defined, and varies with time during the experiment, which makes estimates of absolute reaction rates generally impossible. Fortuitously, the most reactive cluster, Au_{11}^-, exhibits a high enough rate constant which could just be measured with a fairly high steady CO reactant pressure of 8×10^{-7} mbar in the instrument, and at the same time low enough to be just measurable by the pulsed-valve approach. This experiment then provided a scaling ratio, with which the rates of all the other observed reactions could be adjusted. The systematic error associated with the absolute rate constants is estimated to be about 50%, while the relative rates have errors of less than 10%.

3.3. Results and Discussion

As explained in the experimental section, in order to explore the reactions of the anionic clusters in the nearly collision-free environment of our ICR instrument, the distribution of the clusters was first accumulated in the trap over usually 20 laser pulses. After the completed accumulation, the clusters were exposed to CO by activating a pulsed valve controlling the flow of the CO reactant. Each gas pulse raised transiently the pressure in the ICR cell to a value which is difficult to measure experimentally, but which we estimate to be about 5×10^{-5} mbar. Instead of varying the reaction time, reaction kinetics can be studied by taking mass spectra as a function of the number of gas pulses. The fact that the measured intensities follow pseudo-first order kinetics remarkably well provides strong evidence that the amounts of gas introduced are relatively stable, and that pulse to pulse fluctuations average out in the signal accumulation process.

Figure 1 displays a typical mass spectrum observed after 5 gas pulses. Clearly visible in the data is the profound effect of the number of atoms upon the reaction rates. Mainly the clusters in the range of $5 \leq n \leq 11$ exhibit an appreciable reactivity. The relative lack of reactivity for anionic clusters with $n \leq 4$ we observe is in agreement with the very low rate constants measured in previous flow reactor studies.[30,31] For Au_2^-, we detect a weak product band corresponding to addition of the molecular O_2 present as a trace component in about 1 % concentration, but no evidence of a similar complex with CO. This suggests that the formation of the former complex is at least two orders of magnitude more efficient than that of a complex with CO. For the n = 3 cluster anion, a growth of a very weak peak corresponding to Au_3CO^- complex could be detected. It appeared after exposing the clusters to two CO gas pulses, but did not seem to grow significantly upon further exposures. On the other hand, in this case there was no evidence

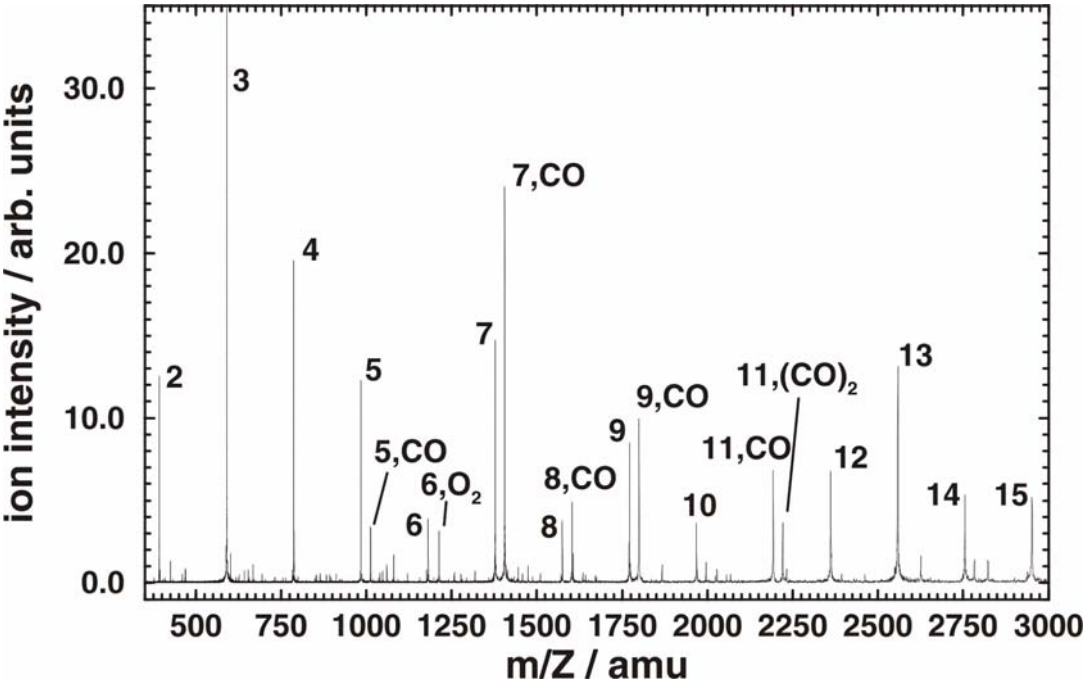

Figure 1: Mass spectrum after 5 pulses of CO. The dominant reaction products are clearly identified. The most reactive species, Au_{11}^-, is completely converted to products containing one or two CO.

for a reaction with molecular oxygen, and no O_2 complex was observed for the Au_3^- cluster.

A relatively clear peak at the mass corresponding to the Au_4CO^- complex was observable after exposing the clusters to a single CO pulse. This peak, however, completely disappeared after a few additional gas pulses, in part probably by adding an O_2 ligand. One way to interpret this result is by assuming that the initially cold clusters are capable of adding CO to some extent. The temperature of the clusters emerging from the source is estimated to be about 40-60 K. The reaction then stops, and is in fact reversed, with the complexes dissociating again, after the clusters are collisionally warmed up to the ambient temperature.

Turning now to the "reactive" region, the smallest cluster which clearly exhibits an appreciable reactivity towards CO is n = 5.

$$Au_5^- + CO \quad \rightarrow \quad Au_5CO^- \qquad (1)$$

Figure 2 depicts the relative intensities of the Au_5^- cluster reactant and of the Au_5CO^- product as a function of the number of the reactant gas pulses. The data follow fairly smoothly pseudo-first order reaction kinetics. If stabilizing collisions would be needed for the reaction to occur, this should have a visible effect on the data: with increasing the number of gas pulses, the average pressure in the cell is increased, and this would accelerate the reaction for higher number of pulses. This is an indication for the single-collision conditions. The rate constant is derived in units of (no. of pulses)$^{-1}$, which is then, as described above, converted to absolute rate. In agreement with the flow reactor studies, no O_2 product is observed. After longer exposures, a very weak peak, attributable to the $Au_5(CO)_2^-$ secondary product can also be detected.

Quite different again is the behavior of the next larger cluster, Au_6^-. This exhibits a small concentration of the carbon monoxide complex after the reaction with a single CO gas pulse. This, however, disappears after longer exposures, and is replaced by a much stronger peak corresponding to the complex with molecular oxygen, $Au_6O_2^-$. The relative intensity profiles of the reaction sequence in Figure 3 suggests that both direct addition of O_2 to the gold cluster anion, as well as ligand exchange with the Au_6CO^- complex contribute to the $Au_6O_2^-$ formation. After still longer exposures, a secondary/tertiary product $Au_6O_2CO^-$ grows in, apparently due to the adsorption of an additional CO

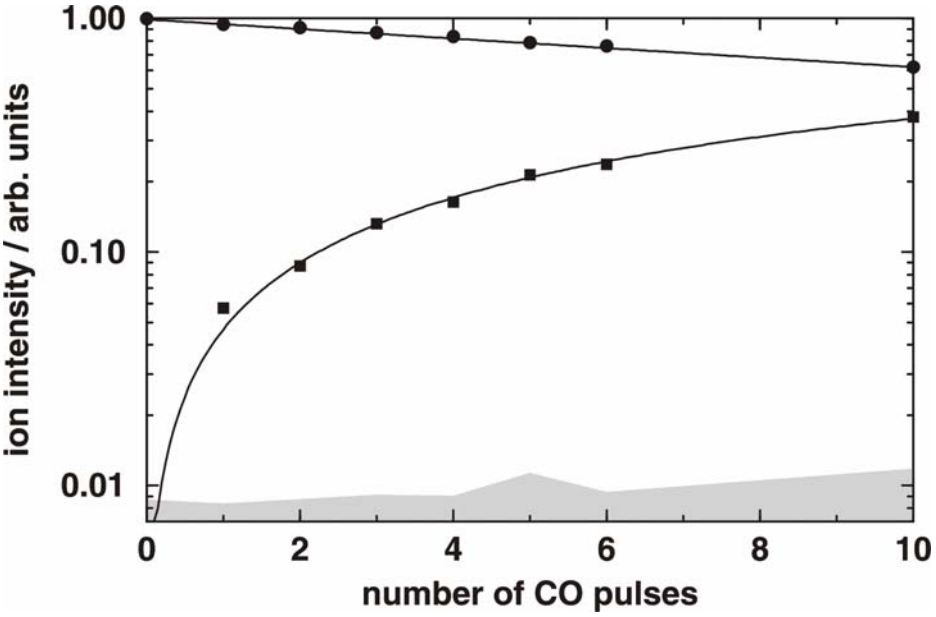

Figure 2: Kinetic fit of Au_5^- + CO → Au_5CO^-, ion intensities as a function of the number of reaction gas pulses, ● Au_5^-, ■ Au_5CO^-. The almost perfect fit to a pseudo-first order model indicates that the pulse-to-pulse stability is excellent and that there are no stabilizing three-body collisions involved. Grey shaded area denotes noise level.

molecule onto the $Au_6O_2^-$ complex. Similarly to the n = 4 case, the initially cold clusters are capable of adsorbing CO. After the first gas pulse, the clusters are essentially equilibrated to room temperature and become unreactive. The Au_6CO^- behaves as a primary ion, exhibiting a clean first-order decay of its intensity:

$$Au_6^- + CO \rightarrow Au_6CO^- \quad \text{only 10\% of clusters} \qquad (2)$$

$$Au_6^- + O_2 \rightarrow Au_6O_2^- \qquad (3)$$

$$Au_6CO^- + O_2 \rightarrow Au_6O_2^- + CO \qquad (4)$$

$$Au_6O_2^- + CO \rightarrow Au_6O_2CO^- \qquad (5)$$

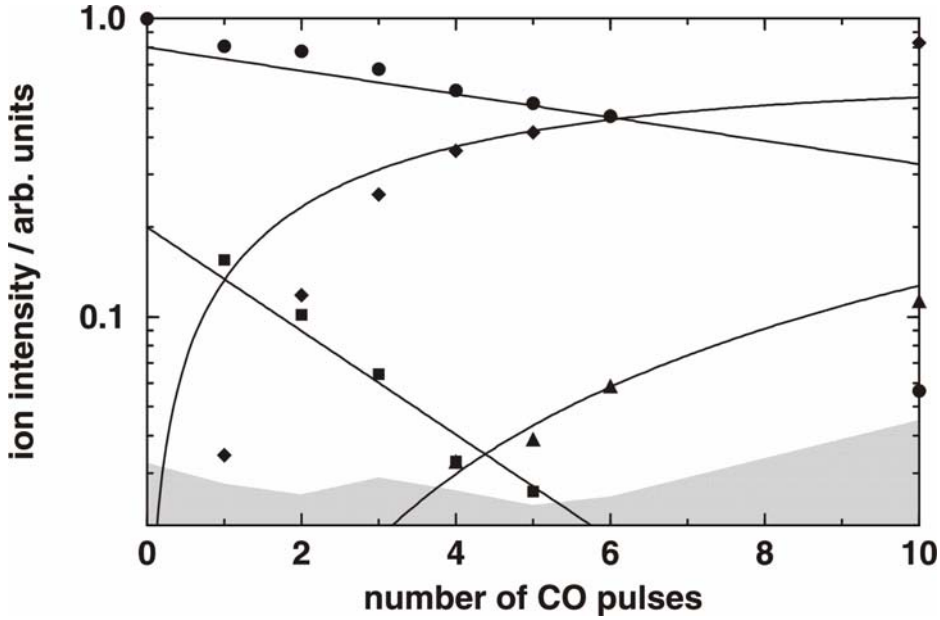

Figure 3: Kinetic fit of Au_6^- + CO, ● Au_6^-, ■ Au_6CO^-, ◆ $Au_6O_2^-$, Δ $Au_6O_2CO^-$. The initial product forms very efficiently in the first gas pulse, and is subsequently converted by ligand exchange with the O_2 impurity. Apparently thermalization and / or annealing of Au_6^- takes place during the first gas pulse, making the clusters unreactive towards CO adsorption in the later pulses. The spectrum is scaled to a Au_3^- intensity of 100. Grey shaded area denotes noise level. Fit parameters are $k_{rel}(3)$ = 0.09 (number of pulses)$^{-1}$, $k_{rel}(4)$ = 0.4 (number of pulses)$^{-1}$, $k_{rel}(5)$ = 0.034 (number of pulses)$^{-1}$.

The n = 7 cluster reacts very efficiently, with CO addition being the only observed reaction. After longer reaction times the bare gold cluster is almost completely replaced by the complex with a single CO molecule, Au_7CO^-, but no competing reactions or secondary products could be detected:

$$Au_7^- + CO \quad \rightarrow \quad Au_7CO^- \qquad (6)$$

More complex is again the chemistry of the n = 8 cluster Au_8^-. Initially, after the first gas pulse, the CO adduct Au_8CO^- is the dominant product, but this then reacts

efficiently further. As a secondary product $Au_8O_2^-$ complex ion grows in, clearly due to a ligand exchange with the primary Au_8CO^- ion. This then attaches an additional CO molecule, with the tertiary $Au_8O_2CO^-$ ion becoming the dominant final product after still longer exposures:

$$Au_8^- + CO \rightarrow Au_8CO^- \quad (7)$$

$$Au_8CO^- + O_2 \rightarrow Au_8O_2^- + CO \quad (8)$$

$$Au_8O_2^- + CO \rightarrow Au_8O_2CO^- \quad (9)$$

The n = 9 ion resembles the Au_7^- cluster in that it also forms a unique Au_9CO^- primary product complex with a CO molecule, and also with a fairly similar reaction rate:

$$Au_9^- + CO \rightarrow Au_9CO^- \quad (10)$$

Things again become more complex for the even n = 10 cluster, whose reactions exhibit some similarities to that of the n = 8. The primary product, dominant after a single reactive pulse is again the $Au_{10}CO^-$ complex, however, unlike for n = 8, no ligand exchange takes place, and no $Au_{10}O_2^-$ complex is detectable. The subsequent reactions are rather complex, and exact determination of their sequence and relative rates is somewhat difficult. Clearly, as a secondary reaction step, both the addition of a molecular oxygen and of CO can occur, resulting in the $Au_{10}O_2CO^-$ and $Au_{10}(CO)_2^-$ secondary products. The $Au_{10}(CO)_2O_2^-$ complex with three ligands which appears to be the final product is formed by a very efficient O_2 addition to the latter cluster, although it could also be reached by the addition of CO to the former. The $Au_{10}(CO)_2^-$, however, also seems to ligand exchange efficiently with O_2 and convert to $Au_{10}O_2CO^-$ so that the rates of the secondary and tertiary

reactions are correlated and their values somewhat tentative. Quite unambiguous is that CO addition is the first reaction step. It is also evident that no more than two CO molecules can be adsorbed on the cluster, and that the O_2 addition is strongly promoted by the presence of at least one CO ligand:

$$Au_{10}^- + CO \rightarrow Au_{10}CO^- \quad (11)$$

$$Au_{10}CO^- + CO \rightarrow Au_{10}(CO)_2^- \quad (12)$$

$$Au_{10}CO^- + O_2 \rightarrow Au_{10}O_2CO^- \quad (13)$$

$$Au_{10}(CO)_2^- + O_2 \rightarrow Au_{10}O_2CO^- + CO \quad (14)$$

$$\rightarrow Au_{10}O_2(CO)_2^- \quad (15)$$

$$Au_{10}O_2CO^- + CO \rightarrow Au_{10}O_2(CO)_2^- \quad (16)$$

The most reactive of the clusters within the range studied is n = 11, with CO addition being the unique primary reaction, resulting in an $Au_{11}CO^-$ anion complex. In a secondary step, this then adds a further molecule of CO, yielding a unique final product $Au_{11}(CO)_2^-$. The intensity profiles of the reactants and products observed in the pulsed valve experiments shown in Figure 4a are compared with those obtained from an experiment with a constant backing pressure presented in the panel 4b. Comparison of the rate constant derived from the two experiments yields then a scaling factor with which the rate constants in (no. gas pulses)$^{-1}$ can be converted to absolute bimolecular rate constants.

$$Au_{11}^- + CO \rightarrow Au_{11}CO^- \quad (17)$$

$$Au_{11}CO^- + CO \rightarrow Au_{11}(CO)_2^- \quad (18)$$

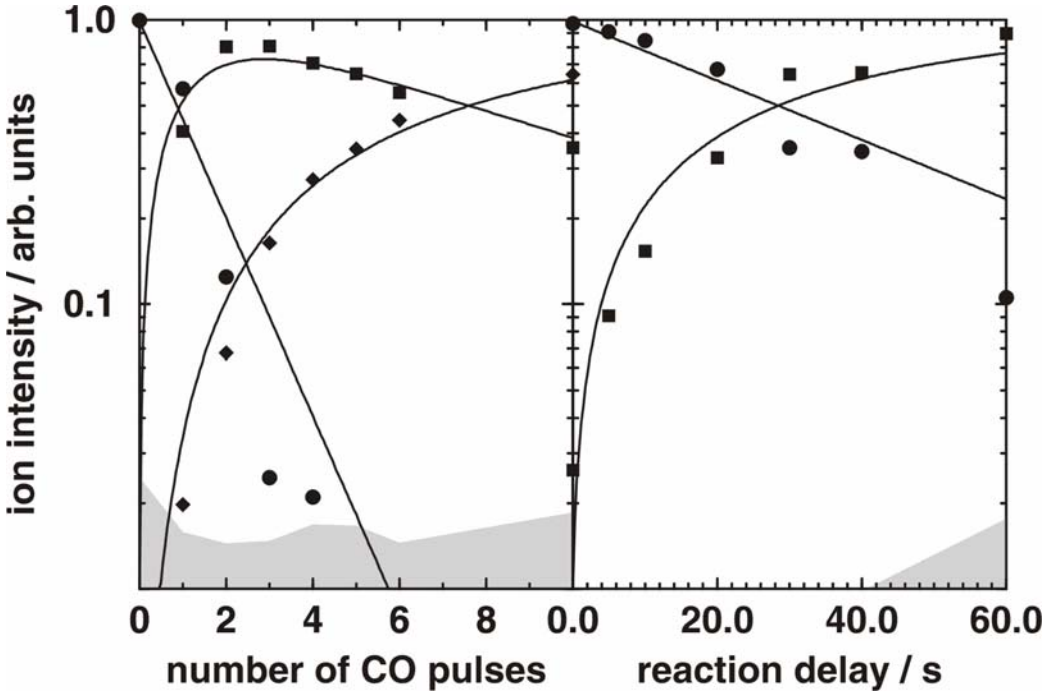

Figure 4: Kinetic fit of Au_{11}^- + CO $\rightarrow$ $Au_{11}CO^-$ measured as a function of the number of reaction gas pulses (a) and as a function of time with a constant CO backing pressure of 8.1×10^{-7} mbar (b), ● Au_{11}^-, ■ $Au_{11}CO^-$, ◆ $Au_{11}(CO)_2^-$. These two experiments provide the scaling factor for conversion of rate constants in units of (no. of pulses)$^{-1}$ to absolute rate constants. Grey shaded area denotes noise level. Fit parameters are $k_{rel}(17) = 0.8$ (number of pulses)$^{-1}$ $k_{rel}(18) = 0.11$ (number of pulses)$^{-1}$ (a) and $k_{rel}(17) = 0.024$ (number of pulses)$^{-1}$ (b).

While n = 11 is clearly the most reactive of the gold cluster anions, for still larger species the reactivities decrease sharply. The n = 12 exhibits no reaction with CO, but similar to for instance n = 6, it appears to react directly, albeit rather slowly, with molecular oxygen, with $Au_{12}O_2^-$ being the only observed product. No reactions at all were detected for n = 13. A weak adduct with CO was seen when Au_{14}^- was exposed to several carbon monoxide pulses, but the product in fact decreases upon still longer exposure times due to secondary reactions. Very weak intensities attributable to the CO adduct were also detected for n = 15 and n = 16. Unfortunately, the larger clusters of gold are formed rather

inefficiently in the source, and so the signal to noise ratio for these clusters was quite poor. This is rather surprising, since all other metals examined thus far could easily and without special effort form clusters well above the n = 30-50 range, and the reason why the coinage metals should be an exception is not yet clear.

$$Au_{14\text{-}16}^- + CO \quad \rightarrow \quad Au_{14\text{-}16}CO^- \qquad (19)$$

The bimolecular rate constants and efficiencies for the reaction of the gold anion clusters with CO calculated from the average dipole orientation theory[41-44] are summarized in Table 1, and presented graphically in Figure 5. The overall pattern seems to be in good agreement with the earlier flow reactor studies,[30,31] however the absolute values of the rate constants are almost three orders of magnitude lower.[30]

Clearly, the absence of the stabilizing collisions makes the reactions significantly less efficient, and it is in fact relatively surprising that a CO molecule may be, presumably radiatively stabilized on a small metal cluster. Given enough time without collisions, a cluster with adsorbed CO will either be radiatively stabilized, or lose the ligands. An elaborate theory allowing quantiative predictions of radiative association rate constants for organic molecules was established by Dunbar and coworkers.[46] Under ICR conditions, radiative stabilization is not only a well-established fact, it is also a method to experimentally determine binding energies from the association kinetics. In this case is surprising how efficiently, in spite of the low pressure, the complexes of even small clusters with a simple ligand like CO are formed. The experimental lifetime estimate of 10^{-9} s for the collision complex[30] lies well below typical infrared lifetimes. Radiative stabilization is surprising in the sense that at least a small fraction of the collision complexes must be much longer lived. This can be rationalized either because the collision

Table 1: Absolute bimolecular rate constants k_{abs}, collision frequency calculated by average dipole orientation theory k_{ADO},[41-44] and efficiencies k_{abs} / k_{ADO}. Even for the most efficient reaction, less than one in a thousand collisions is reactive.

Reactant	k_{abs} (10^{-13} cm^3 s^{-1})	k_{ADO} (10^{-10} cm^3 s^{-1})	Efficiency (%)
Au^-	< 0.003	6.65	< 0.00005
Au_2^-	< 0.009	6.44	< 0.00014
Au_3^-	< 0.004	6.37	< 0.00007
Au_4^-	< 0.007	6.34	< 0.00011
Au_5^-	0.208 ± 0.018	6.31	0.00330
Au_6^-	< 0.044	6.30	< 0.00070
Au_7^-	0.754 ± 0.133	6.29	0.01199
Au_8^-	0.887 ± 0.177	6.28	0.01412
Au_9^-	0.643 ± 0.111	6.28	0.01025
Au_{10}^-	0.523 ± 0.133	6.27	0.00849
Au_{11}^-	3.55 ± 0.887	6.27	0.05663
Au_{12}^-	< 0.018	6.26	< 0.00028
Au_{13}^-	< 0.009	6.26	< 0.00014
Au_{14}^-	0.266 ± 0.067	6.26	0.00425
Au_{15}^-	0.089 ± 0.089	6.26	0.00142
Au_{16}^-	0.177 ± 0.177	6.25	0.00284
$Au_6O_2^-$	0.151	6.30	0.00239
$Au_8O_2^-$	0.754	6.28	0.01201
$Au_{10}CO^-$	≈1.02	6.27	≈0.01627
$Au_{10}COO$	≈0.665	6.27	≈0.01061
$Au_{11}CO^-$	0.488	6.27	0.00779

energy was due to the individual collision parameters very small, like CO and Au_n^- moving in the same direction during the collision, or the cluster is exceptionally cold, or a very slow CO collides. All these effects would lead to a collision complex with an internal energy just above the dissociation limit. This small fraction of collision complexes would be several orders of magnitude longer lived than the above quoted estimate,[30] and probably these eventually stabilize presumably by infrared emission.

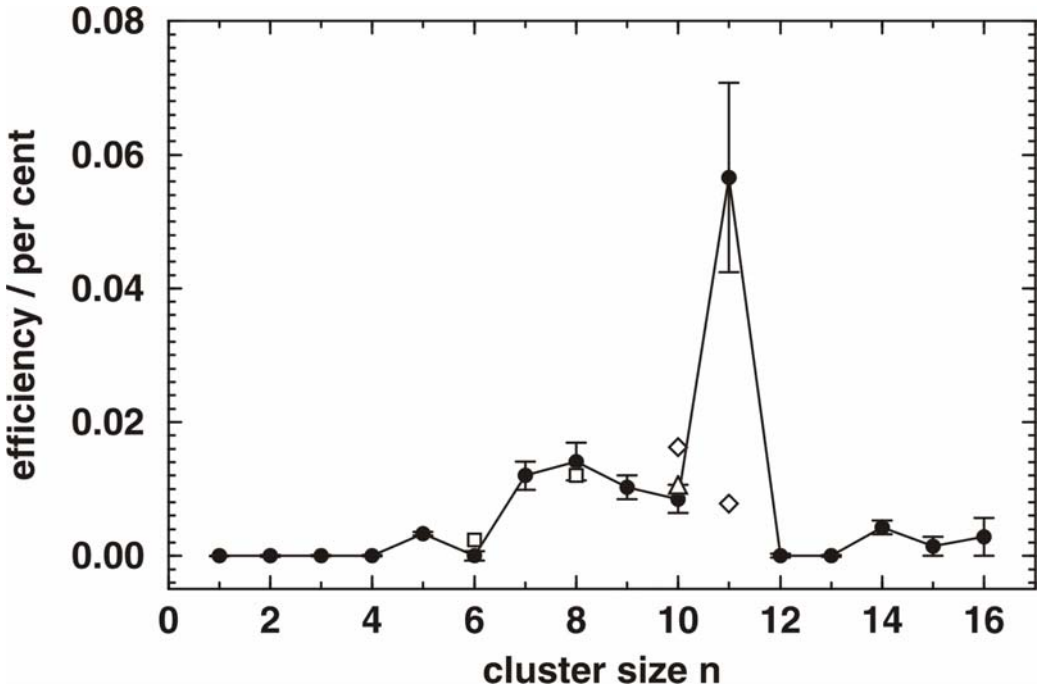

Figure 5: CO adsorption bimolecular reaction efficiencies (%) as a function of cluster size. Reactant ions: ● Au_n^-, □ (open squares) $Au_nO_2^-$, ◇ Au_nCO^-, △ $Au_nO_2CO^-$.

Collisional stabilization, however, cannot be excluded. An order of magnitude estimate of the probability for a third body colliding during the lifetime of the collision complex yields a non-zero probability. A pressure of 10^{-8} mbar corresponds to a collision rate of 1 s^{-1}. A pressure rise up to 5×10^{-5} mbar gives a conservative estimate that the collision rate never lies above 10^4 s^{-1}. The lifetimes of the collision complexes are

estimated from flow reactor studies to be in the 10^{-9} s to 10^{-8} s regime. This is a factor of 10^4 smaller than the average time between two collisions under the most unfavorable conditions in the experiment. At best one in 10^4 collisions is a three-body collision. In the case of Au_{11}^-, one out of 2000 collisions is reactive, one order of magnitude above the three-body collision probability. It should be noted that also in the flow reactor studies, at collision rates of the order of the reciprocal lifetime of the collision complex, at best one out of 30 collisions was found to be reactive.

Another, even more striking feature is that the further reactivity of the Au_nCO^- complexes is even more size selective than the first reaction step, which is in contrast with the flow reactor studies.[30,31] Only n = 10 and n = 11 are capable of sequentially adding a second CO molecule, while the n = 8 species undergo a selective and efficient ligand exchange with O_2, which is otherwise not attached to the cluster at all. Given the larger number of degrees of freedom in the Au_nCO^- complexes compared to the bare clusters, one might expect that the sequential CO addition steps would proceed more efficiently than the first step, since the radiative stabilization should be significantly more favorable. On the other hand, for Au_6^- and Au_8^-, the presence of O_2 seems to allow the addition of a second, CO ligand, whereas for n = 10 the situation is reversed, and an O_2 adsorption requires the presence of least one preadsorbed CO, a cooperativity similar to that reported previously for the Au_3^- in an ion trap study.[37]

There may be a variety of reasons for the relative lack of reactivity of the larger clusters with $n \geq 12$. In the first place, in the smaller clusters the individual gold atoms are necessarily coordinatively more unsaturated than in the larger clusters, and thus may tend more strongly towards binding additional ligands. This interpretation is supported by a recent ion mobility study,[45] which shows that the transtition from planar to three-dimensional structures occurs at n = 12, a species which exhibits both planar and three-

dimensional isomers. In the second place, if the presence of the negative charge on the cluster, and the polarization effect it exerts upon the neutral ligand is of any consequence, obviously as the size of the cluster is increased, this charge will be more and more delocalized, resulting in a weaker polarization and a less efficient reaction. Clearly, it would be quite helpful to examine in more detail also larger clusters above n = 16. Equally interesting would be similar studies of neutral clusters, as well as systematic FT-ICR studies of cluster cations. In an earlier study,[27] Au_7CO^+, $Au_{18}CO^+$ and $Au_{19}CO^+$ were identified as particularly favorable and stable species in an FT-ICR study, in accordance with shell closing in the jellium model, with CO acting as a two-electron donor. Unfortunately, no data for an extended cluster size region was given.

The lack of reactivity of the very small clusters is relatively easy to understand. Under our experimental conditions there are no three body collisions, and obviously any complex formed by two body recombination of a CO ligand with the metal cluster contains more than enough energy to again immediately dissociate. If the binding energy of the ligand, plus the kinetic energy of the reactants lost during the collision is randomly redistributed in the cluster, a longer lived complex and a "sticky collision" may result. The lifetime, and the rate of dissociation, will depend on the density of states at the total energy of the complex, and its excess over that needed for dissociation. Apparently, for the clusters with $n \leq 4$ the lifetimes are much too short to allow their stabilization by radiation. Apparently clusters with $n \geq 5$ are sufficiently long lived, so that they can be stabilized under the conditions of our experiment. Lifetime estimates based on flow reactor experiments[30] place it in the 10^{-9} s range, with a strongly nonlinear size dependence. In addition, radiative cooling is also enhanced with the increasing cluster size.

Several previous studies have employed the jellium model to interpret their results. While some of the present observations, e.g. the lack of reactivity of n = 6, 12 and 13 could be consistent with the model and shell "closures" for 8 and 14 electrons, others are not. For instance, it cannot explain the efficient addition of a second CO by the "jellium closed-shell" $Au_{11}CO^-$ complex. While the jellium model appears reasonable for large alkali clusters with 20 or more atoms, its application to small, and surely quite nonspherical transition metal clusters - note that small Au_n^- species are predicted to be planar,[21] as recently verified in ion mobility studies[45] - seems somewhat questionable. These data document clearly the previously reported preferential reactivity of even Au_n^- clusters towards oxygen. It is interesting to note that if anything, the overall reactivities towards CO somewhat seem to favor odd n clusters. Thus n = 5, 7, 9, and 11 all are highly reactive. The complete lack of reactivity of Au_{13}^- might be explained by its presumably icosahedral close-packed geometry. Note that while the reactivity of perfect bulk crystals is low, it is greatly increased by the presence of add-atoms and steps, which could explain the increased reactivity of n = 14.

The diversity of the reaction patterns which we observe for the various size clusters described above is quite amazing. The clusters in the size range we investigated can be viewed rather like discrete molecules with well defined, different geometric and also electronic structures than like small pieces of metal with freely moving valence electrons. In view of this it would seem, that geometric effects will be at least equally important for their reactivity, as the electronic shell structure. Also earlier observation that, for instance, for small rhodium clusters "magic" reactivity behavior occurs for the same size cluster anions and cations can be viewed as evidence in favor of this view.

At this time, one cannot make any statement regarding a possible activation of CO or O_2 in the species already studied, which could help in clarifying the catalytic activity of

supported gold clusters. There is no indication in any of the spectra for the formation and loss of CO_2, which could be seen as an evidence for catalytic CO oxidation. The initial cluster distribution contains a minor contamination of Au_nH^- species, and in the course of the experiment an Au_6OH^- product growing in was observed. This could be explained by adsorption of CO and O_2, followed by CO_2 formation and loss. While the resolution of the FT-ICR experiment is sufficient to unambiguously identify and assign these impurities, the intensities of these peaks were quite weak, and intermediate complexes through which the reaction would have to proceed were not detected. In view of this observation, and of the fact that the CO and O_2 adsorption efficiencies seem to be highly cooperative,[36,37] it might be worthwhile to test the influence of an additional H atom on the catalytic activity of Au_n^-.

3.4. Conclusions

In the absence of stabilizing collisions, a more distinct reactivity pattern of Au_n^- clusters with CO under FT-ICR conditions than earlier flow reactor studies is found. While some of the observations are consistent with the jellium model, others seem to contradict it. The clusters in the size range of n = 2-17 exhibit an amazing diversity in their reactivity patterns, suggesting that perhaps their distinct molecular geometries and structures are of comparable importance as electronic shell closing predicted by the jellium model. Adsorption of CO and O_2 is found to be highly cooperative and strikingly size-dependent. No convincing evidence for catalytic oxidation of CO by O_2 is found.

3.5. References

(1) W. A. de Heer, *Rev. Mod. Phys.*, **1993**, *65*, 611.

(2) M. Brack, *Rev. Mod. Phys.*, **1993**, *65*, 677.

(3) K. S. Pitzer, *Acc. Chem. Res.*, **1979**, *12*, 271.

(4) P. Pyykkö, J.-P. Desclaux, *Acc. Chem. Res.*, **1979**, *12*, 276.

(5) P. Pyykkö, *Chem. Rev.*, **1988**, *88*, 563.

(6) K. Balasubramanian, *J. Phys. Chem.*, **1989**, *93*, 6585.

(7) D. Schröder, H. Schwarz, J. Hrušak, P. Pyykkö, *Inorg. Chem.*, **1998**, *37*, 624.

(8) H. Schmidbaur, *Nature*, **2001**, *413*, 31.

(9) H. Schmidbaur, A. Hamel, N. W. Mitzel, A. Schier, S. Nogai, *P. Natl. Acad. Sci. USA*, **2002**, *99*, 4916.

(10) M. Haruta, N. Yamada, T. Kobayashi, S. Iijima, *J. Catal.*, **1989**, *115*, 301.

(11) M. Haruta, *Catal. Today*, **1997**, *36*, 153.

(12) M. Valden, X. Lai, D. W. Goodman, *Science*, **1998**, *281*, 1647.

(13) A. Sanchez, S. Abbet, U. Heiz, W.-D. Schneider, H. Häkkinen, R. N. Barnett, U. Landman, *J. Phys. Chem. A*, **1999**, *103*, 9573.

(14) U. Heiz, A. Sanchez, S. Abbet, W.-D. Schneider, *Eur. Phys. J. D*, **1999**, *9*, 35.

(15) D. M. P. Mingos, T. Slee, L. Zhenyang, *Chem. Rev.*, **1990**, *90*, 383.

(16) M. B. Knickelbein, *Ann. Rev. Phys. Chem.*, **1999**, *50*, 79.

(17) P. B. Armentrout, *Ann. Rev. Phys. Chem.*, **2001**, *52*, 423.

(18) K. M. Ervin, *Int. Rev. Phys. Chem.*, **2001**, *20*, 127.

(19) V. E. Bondybey, M. K. Beyer, *J. Phys. Chem. A*, **2001**, *105*, 951.

(20) K. J. Taylor, C. L. Pettiette-Hall, O. Cheshnovsky, R. E. Smalley, *J. Chem. Phys.*, **1992**, *96*, 3319.

(21) H. Häkkinen, U. Landman, *Phys. Rev. B*, **2000**, *62*, R2287.

(22) H. Häkkinen, M. Moseler, U. Landman, *Phys. Rev. Lett.*, **2002**, *89*, 033401.

(23) S. Gilb, P. Weis, F. Furche, R. Ahlrichs, M. M. Kappes, *J. Chem. Phys.*, **2002**, *116*, 4094.

(24) C. Stoermer, J. Friedrich, M. M. Kappes, *Int. J. Mass Spectrom.*, **2001**, *206*, 63.

(25) C. Yannouleas, U. Landman, A. Herlert, L. Schweikhard, *Eur. Phys. J. D*, **2001**, *16*, 81.

(26) D. M. Cox, R. Brickman, K. Creegan, A. Kaldor, *Z. Phys. D*, **1991**, *19*, 353.

(27) M. A. Nygren, P. E. M. Siegbahn, C.-M. Jin, T. Guo, R. E. Smalley, *J. Chem. Phys.*, **1991**, *95*, 6181.

(28) M. M. Kappes, R. H. Staley, *J. Am. Chem. Soc.*, **1981**, *103*, 1286.

(29) Y. Shi, K. M. Ervin, *J. Chem. Phys.*, **1998**, *108*, 1757.

(30) T. H. Lee, K. M. Ervin, *J. Phys. Chem.*, **1994**, *98*, 10023.

(31) W. T. Wallace, R. L. Whetten, *J. Phys. Chem. B*, **2000**, *104*, 10964.

(32) B. E. Salisbury, W. T. Wallace, R. L. Whetten, *Chem. Phys.*, **2000**, *262*, 131.

(33) G. Mills, M. S.Gordon, H. Metiu, *Chem. Phys. Lett.*, **2002**, *359*, 493.

(34) X. Wu, L. Senapati, S. K. Nayak, *J. Chem. Phys.*, **2002**, *117*, 4010.

(35) H. Häkkinen, U. Landman, *J. Am. Chem. Soc.*, **2001**, *123*, 9704.

(36) W. T. Wallace, R. L. Whetten, J. *Am. Chem. Soc.*, **2002**, *124*, 7499.

(37) J. Hagen, L. D. Socaciu, M. Elijazyfer, U. Heiz, T. M. Bernhardt, L. Wöste, *Phys. Chem. Chem. Phys.*, **2002**, *4*, 1707.

(38) N. Lopez, J. K. Nørskov, *J. Am. Chem. Soc.*, **2002**, *124*, 11262.

(39) C. Berg, T. Schindler, G. Niedner-Schatteburg, V. E. Bondybey, *J. Chem. Phys.*, **1995**, *102*, 4870.

(40) C. Berg, M. Beyer, U. Achatz, S. Joos, G. Niedner-Schatteburg, V. E. Bondybey,

J. Chem. Phys., **1998**, *108*, 5398.

(41) T. Su, M. T. Bowers, *Int. J. Mass Spectrom. Ion Phys.*, **1973**, *12*, 347.

(42) L. Bass, T. Su, W. J. Chesnavich, M. T. Bowers, *Chem. Phys. Lett.*, **1975**, *34*, 119.

(43) T. Su, M. T. Bowers, *Int. J. Mass Spectrom. Ion Phys.*, **1975**, *17*, 211.

(44) T. Su, E. C. F. Su, C. F. Elkie, M. T. Bowers, *J. Chem. Phys.*, **1978**, *69*, 2243.

(45) F. Furche, R. Ahlrichs, P. Weis, C. Jacob, S. Gilb, T. Bierweiler, M. M. Kappes, *J. Chem. Phys.*, **2002**, *117*, 6982.

(46) S. J. Klippenstein, Y.-C. Yang, V. Ryzhov, R. C. Dunbar, *J. Chem. Phys.*, **1996**, *104*, 4502.

(47) K. Hansen, E. E. B. Campbell, *Phys. Rev. E.*, **1998**, *58*, 5477.

(48) C. Walther, G. Dietrich, W. Dostal, K. Hansen, S. Krückeberg, K. Lützenkirchen, L. Schweikhard, *Phys. Rev. Lett.*, **1999**, *83*, 3816.

(49) V. A. Spasov, Y. Shi, M. K. Ervin, *Chem. Phys.*, **2000**, *262*, 75.

4. Size and Charge-state Dependent Reactivity of Azidoacetonitrile with Anionic and Cationic Rhodium Clusters $Rh_n^{+/-}$

4.1. Introduction

Hydrazoic acid, or hydrogen azide, HN_3 was first prepared in 1890 by the oxidation of aqueous hydrazine by nitrous acid,[1] while phenyl azide was discovered as early as 1864.[2] Since then, azide chemistry was extensively studied, and countless derivatives were synthesized.[3] The N_3 group as well as several other groups with large electron affinities like for instance CN or OCN, behave in many of their compounds similar to halogens, and are often referred to as pseudohalogens.[4] Their compounds are often ionic, and the N_3 anion is, similar to the isoelectronic CO_2 molecule and other 16 valence electron species, linear and centrosymmetric. In biochemistry, N_3^- acts as an enzyme inhibitor by coordinating to a metal center.[5-6] In covalent compounds the N_3 unit may deviate somewhat from linearity, and in general the lengths of the two N=N bonds are different. Most of the azide compounds react strongly exothermically, and are often quite explosive.[3]

Due to their interesting properties, organic azides played a not insignificant role in the development of modern physical chemistry. Ramsperger tested the newly developed unimolecular reaction rate theory on the thermal decomposition of hydrazoic acid and methyl azide,[7] and Pauling developed the adjacent charge rule for resonant Lewis valence structures, among other molecules, on methyl azide.[8-9]

The azides have nowadays a considerable importance in industry and technology both as chemical intermediates as well as end products, and are used in numerous applications. Lead azide is the most common primary explosive used in detonators,[10-11] while sodium azide is the most frequently used propellant in automobile air bags.[12-13] Also organic, covalent azides have found applications in photoresists,[14] vulcanization[15] and polymer coupling.[16] Increasingly, they are also used in chemical vapor deposition for generating nitride films.[17-19]

Obviously, the use of azides as propellants, fuses and detonators, as well as like sources of atoms in semiconductor processing, makes the question of the mechanisms and pathways of their decomposition particularly important. Starting from Ramsperger's work, thermal decomposition of azides has been studied for more than 70 years.[7,20-24] The availability of modern experimental techniques for the spectroscopy of transient species, like photoelectron spectroscopy[25] and matrix isolation[26] has recently renewed the interest in these species.[27-32] Also the wide distribution of computational chemistry packages in the last decade has left its mark in the azide literature.[33-39] The Curtius rearrangement (1) is the well-established decomposition pathway of alkyl azides by nitrogen elimination to form an alkyleneimine:[33]

$$R_2CH\text{-}N_3 \rightarrow R_2C{=}NH + N_2 \qquad (1)$$

Recent studies also report formation of the methylnitrene diradical upon photodissociation of methylazide.[40-41] Together with the multiconfigurational self-consistent field calculations by Arenas et al.[36-38], there is experimental as well as theoretical evidence that the alkyleneimine is a stable intermediate in the decomposition of alkyl azides.

In striking contrast to the large body of work in the gas and condensed phase, studies of the decomposition of organic azides on surfaces, as well as their gas phase ion chemistry, are rare to not available. While the adsorption of hydrazoic acid on semiconductors was studied as a possible precursor for nitride formation,[42-44] to the best of our knowledge azidoacetic acid is the only organic azide so far studied in a surface apparatus.[45] Oliveira et al.[46] have investigated the N_3CH_2COOH, $N_3CH_2COCH_3$ and $N_3CH_2CH_2OH$ compounds by mass spectrometry. For each of them they detected only a weak parent cation peak, but their spectra indicated that for each of the compounds the dominant fragment corresponds to the loss of a mass of 56 AMU, presumably the N_3CH_2 entity. Another common feature is a strong signal at a nominal mass of 28 AMU. Unfortunately the resolution of the instrument used in their study was not sufficient to differentiate between the N_2^+ and CH_2N^+ fragments with the same nominal mass. Recent high-resolution measurements by Duarte et al.[47] indicate that the m/z = 28 peak is due to CH_2N^+ ions in the EI impact spectra of aliphatic α-carbonyl azides.

Most azides readily decompose, especially if the activation barrier is lowered by the presence of a suitable catalyst. Transition metals are known to be useful catalysts for many reactions involving unsaturated compounds. One of the difficulties of studies on bulk solids is that the adsorbed species can move around on the surface, and their decomposition may be the result of a complex sequence of a number of reactions. Furthermore, detailed diagnostics of such processes is usually quite difficult. On the other hand, studies of reactions on surfaces of small ionic metal clusters in the gas phase offer a convenient, much more tractable alternative.[49-52] Since in this case the products are the result of a single bimolecular collision, where the exact masses and elemental compositions of both of the reactants and of their products are known, very unambiguous statements can often be made about the occurring reactions. Additional insight into their course and mechanisms can be gained by observing the

reactivity trends as a function of cluster size and charge state.[53-55] In this chapter the reactions and surface activated decomposition of one simple representative of aliphatic covalent azides are investigated with the help of Fourier transform ion cyclotron resonance mass spectrometry. There are presented the reactions of the azide of acetonitrile, N_3CH_2CN, on the surface of rhodium clusters as a function of their size and charge state.

4.2. Experimental Details

Most of the relevant experimental details were described elsewhere,[56] and so only a brief outline of the experiment will be given here. The ionic Rh_n clusters with about n = 1-20 are produced in an external source chamber by laser vaporization of rhodium metal. A sufficient number of both positively and negatively charged ions are formed without need for post-ionization.[53] The clusters, either anions or cations, are then transferred through several stages of differential pumping into the high vacuum of the FT- mass spectrometer, and trapped in the ICR cell, where they are exposed to a steady pressure of typically 8.0×10^{-9} mbar of the azidoacetonitrile reactant. Rhodium has only one isotope, which is favorable for mass spectrometric studies.

Preliminary experiments with size selected clusters have shown that under the conditions of our experiment, similar to previous studies,[53] no breakage of rhodium-rhodium bonds takes place, and in the course of the chemical reactions no rhodium atoms are lost from the clusters. This made it possible in the subsequent experiment to dispense entirely with mass selection, and investigate the reaction of the entire broad cluster distribution at the same time. By varying the delay between trapping of the ions and acquisition of the mass spectrum, the reaction kinetics is followed over a total period of 20 s. Relatives rate constants are obtained

by fitting the normalized data with pseudo-first order kinetics, with an accuracy of typically 10%. The absolute pressure of azidoacetonitrile inside the ICR cell cannot be determined due to the lack of published rate constants for ion-molecule reactions with azidoacetonitrile which would be necessary for calibration. Therefore, no absolute rate constants are given. The relative rate constants in this study refer to an uncalibrated azidoacetonitrile pressure of 8.0×10^{-9} mbar. The absence of rhodium-rhodium bond cleavage is again substantiated by the exponential decay of the parent ion. Loss of intensity to smaller clusters would inevitably lead to a significant curvature of the parent ion intensity in a semilogarithmic plot, which is not observed.

The compound studied here, azidoacetonitrile N_3CH_2CN, was prepared by methods described in the literature.[57] To avoid its decomposition it was kept at dry ice temperature, and prior to experiment it was degassed by three freeze-pump-thaw cycles. During the experiment the sample was maintained at room temperature and shielded from light to prevent photolysis.

Safe handling instructions: Azidoacetonitrile may decompose rapidly and spontaneously. Decomposition products include hydrogen cyanide HCN and are toxic. If possible, prepare and handle only small quantities, and ensure adequate protection. Dispose properly.

4.3. Results and Discussion

After establishing firmly that the $Rh_n^{\pm}$ clusters always react as an unbreakable unit the reactions for the entire cluster distribution, without mass selection have been carried out. This has, besides the fact that in a single experiment the reactivity data are obtained for a number of cluster sizes simultaneously, also the obvious advantage that all of them are investigated under

exactly identical conditions. Overall the reactions of azidoacetonitrile with both negatively and positively charged clusters of rhodium, Rh_n^+, n = 1 - 16, and Rh_n^-, n = 3 – 16 have been investigated. Monomer and dimer anions are not produced in sufficient quantities in our ion source.

4.3.1. Reactions of Anionic Clusters

Typical data from an experiment involving the larger clusters are exemplified by Figure 1, showing part of the mass spectra in the neighborhood of the Rh_8^- cluster and of its reaction products. Figure 1a shows the mass spectrum right after cluster accumulation at a nominal time t = 0, while the spectra after reaction delays of 2 s and 5 s, respectively, are presented in the Figure 1b and Figure 1c. It should be noted that since the rhodium clusters are accumulated over typically 20 laser pulses, and since the azidoacetonitrile reactant is present in the mass spectrometer continuously, the reactions actually take place already during the accumulation time of 2 s. Due to this, the zero nominal time corresponds actually to a nonzero reaction delay, and this is reflected in the fact that even the spectrum in Figure 1a, corresponding to time t = 0, already clearly shows the presence of reaction products.

The reactions occurring in the trap are relatively simple, and the only products correspond to the addition of a mass of 52 amu to the Rh_8^- cluster, or in other words to a loss of a mass of 30 amu from the gaseous N_3CH_2CN reactant which has a nominal mass of 82 amu:

$$Rh_8C_{2(m-1)}N_{2(m-1)}^- + N_3CH_2CN \rightarrow Rh_8C_{2m}N_{2m}^- + N_2 + H_2 \qquad m = 1 - 4 \qquad (2)$$

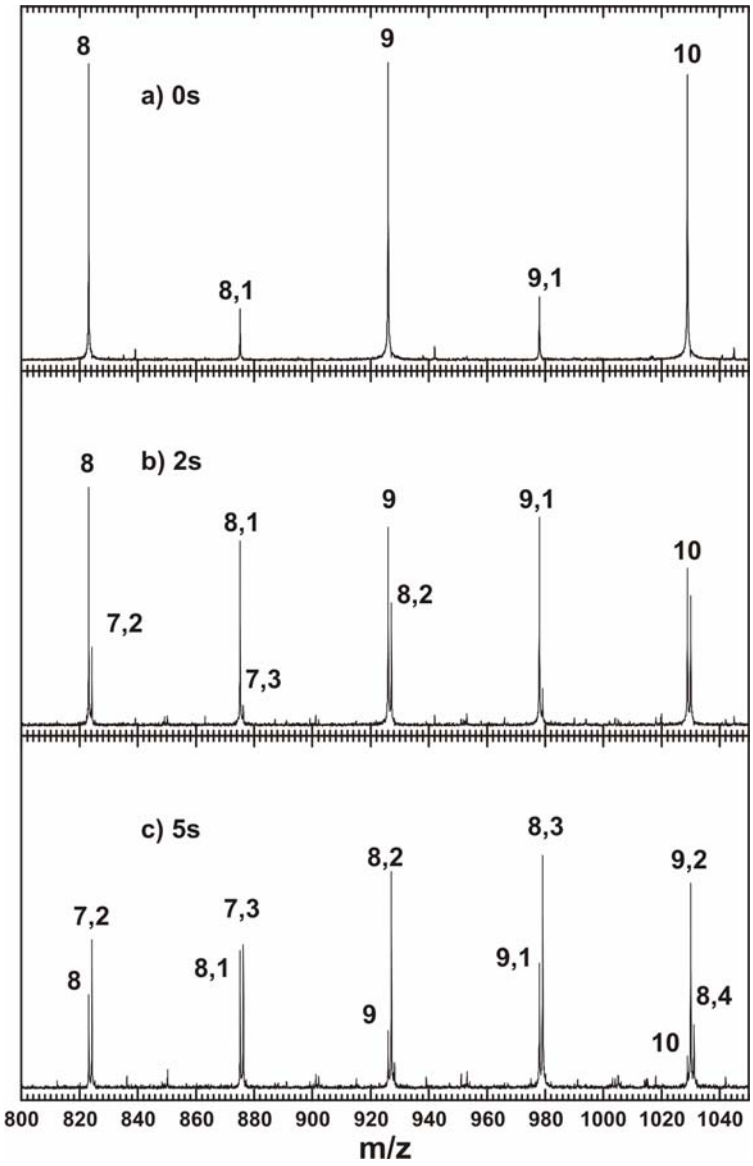

Figure 1: Mass spectra showing the neighborhood of the Rh_8^- cluster and of its reaction products at the nominal time t = 0 (a) and after reaction delays of 2 s (b) and 5 s (c). The numbers denote the cluster size n, numbers after the comma refer to the number of consecutive reaction steps. The only reaction products correspond to the sequential addition of a mass of 52 amu to the Rh_n^- cluster, $Rh_nC_{2m}N_{2m}^-$.

The products of the reaction with azidoacetonitrile thus correspond to $Rh_8C_{2m}N_{2m}^-$, with N_2 and H_2 "evaporating" from the cluster in each step. Naturally, mass spectra do not give any direct information about the departing neutral reactants, and cannot directly

distinguish between the loss of discrete N_2 and H_2 molecules, or that of an N atom together with an NH_2 radical, or perhaps even of the neutral diazene N_2H_2. Formation of the latter, however, would require quite complicated rearrangements, and its heat of formation lies with 220 kJ/mol[58] significantly above the elemental dimers. For mechanistic and thermochemical reasons, one can assume that N_2 and H_2 molecules are evaporated.

At first sight the evaporation of both the H atoms from the CH_2 entity, and on the other hand the retention of one of the nitrogen atoms from the azide N_3 group might seem surprising. It becomes, however, quite reasonable if one considers that rhodium and its neighbors in the periodic table are characterized by large affinities to nitrogen as well as carbon, with which they form very stable and refractory, so-called interstitial carbides and nitrides,[59] but on the other hand are relatively unreactive towards hydrogen. Furthermore one has to consider that the azides involved are actually metastable with respect to the loss of molecular N_2. Calculations for methyl azide suggest that roughly 200 kJ/mol are released upon N_2 elimination.[33] Overall, the reaction with the cluster surface, which may result in the formation of very strong metal-carbon or metal-nitrogen bonds, is undoubtedly highly exothermic, and the reactive cluster intermediate formed in its course must therefore be extremely hot. This high temperature must then result in the evaporation of the comparatively weakly bound hydrogen atoms, probably in the form of a molecular H_2. As an alternative to the formation of interstitial carbides and nitrides, CN groups with their thermochemically favorable triple bond may be attached to the surface.

In a typical experiment, spectra similar to those exemplified in Figure 1 were actually measured at 14 different delays ranging from nominally t = 0 up to t = 5 s. Relative intensities of reactant and product ions are extracted from these data and normalized, as displayed in Figure 2. Numerical fits assuming pseudo-first order reaction kinetics yield the appropriate

reaction rate constants. The problem noted above, that is the fact that the nominal t = 0 corresponds actually to non-zero reaction time can easily be compensated by assuming a non-zero starting intensity of the products.

Figure 2 illustrates that the first three reaction steps proceed efficiently, while the fourth N_3CH_2CN molecule reacts significantly more slowly, as can also be seen in the relative rate constants displayed in Figure 3. The numeric fit is made somewhat more difficult by the fact that the products of neighboring cluster sizes overlap, because two reaction steps add a nominal mass of 104, while the mass of a rhodium atom is 103. The upcoming secondary product of Rh_n^- overlaps with the base of the still intense unreacted clusters Rh_{n+1}^-, and its

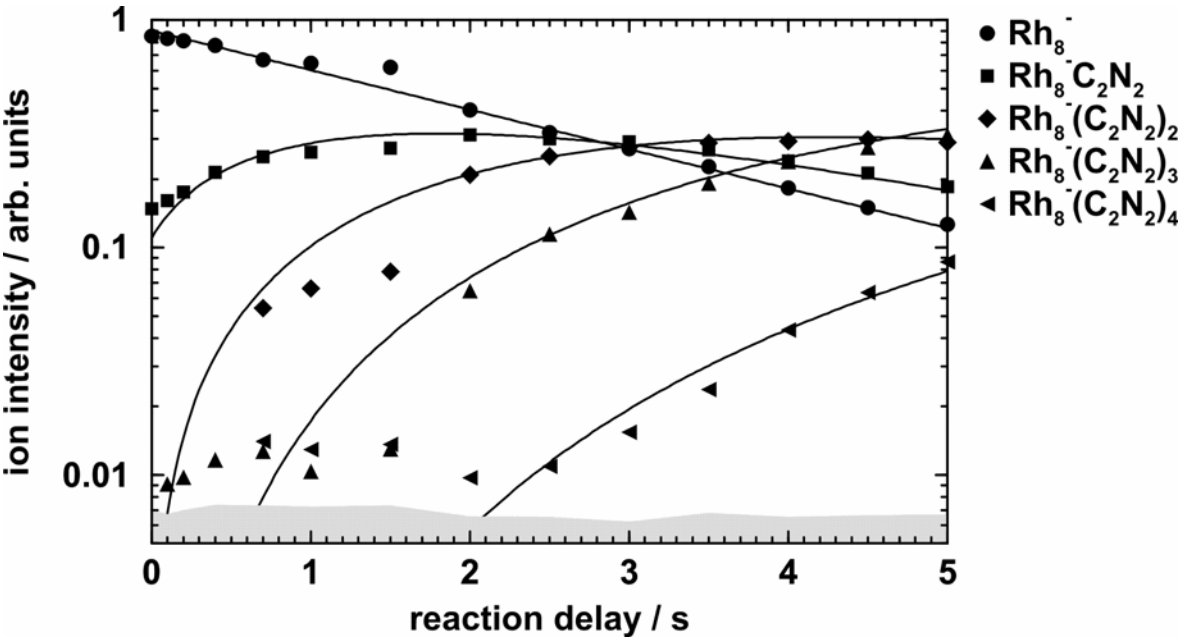

Figure 2: Time profile for the reaction of Rh_8^- with N_3CH_2CN. The first three reaction steps proceed efficiently, while the fourth N_3CH_2CN molecule reacts significantly more slowly, suggesting that a certain kind of saturation is achieved. The grey shaded area denotes the noise level. The parent ion decay is linear in the semi-logarithmic scale of the figure, indicating the absence of rhodium-rhodium bond cleavage.

intensity is not determined correctly by the data acquisition software. This problem is resolved by ignoring the unreliable intensities in the fit.

The fourth N_3CH_2CN molecule obviously faces some difficulty to find a reactive site on the cluster, indicating that a certain kind of saturation is reached. This is in line with our interpretation of the formation of interstitial carbides and nitrides. As soon as most of the interstitial sites are taken, the cluster ceases to react. The same argument, however, applies to the surface covered with CN groups.

A similar kinetic evaluation of the data was undertaken for all clusters Rh_n^-, n = 3 - 16, and the rate constants of up to five consecutive steps are summarized in Figure 3. All anionic clusters react sequentially by evaporation of N_2 and H_2 and addition of $[C_2,N_2]$ to the cluster surface:

$$Rh_nC_{2(m-1)}N_{2(m-1)}^- + N_3CH_2CN \rightarrow Rh_nC_{2m}N_{2m}^- + N_2 + H_2 \qquad (3)$$

In other words, in each consecutive step an additional N_3CH_2CN reactant molecule is decomposed on the cluster, with two additional carbon and two additional nitrogen atoms being incorporated into the product, and presumably one N_2 and one H_2 molecule escaping from the cluster. In general, the number of such steps (3), that is the maximum value of m depends on the cluster size, and increases with the number of rhodium atoms, from m=2 for the smallest clusters studied n = 3, 4 to m = 7 observed for n = 13. The larger the cluster, the more efficient the later reaction steps, and the larger the maximum number of steps. This behavior clearly indicates that the reaction proceeds at an intact part of the rhodium cluster surface. We tentatively conclude this to be the genuine behavior of a rhodium surface in the reaction with azidoacetonitrile.

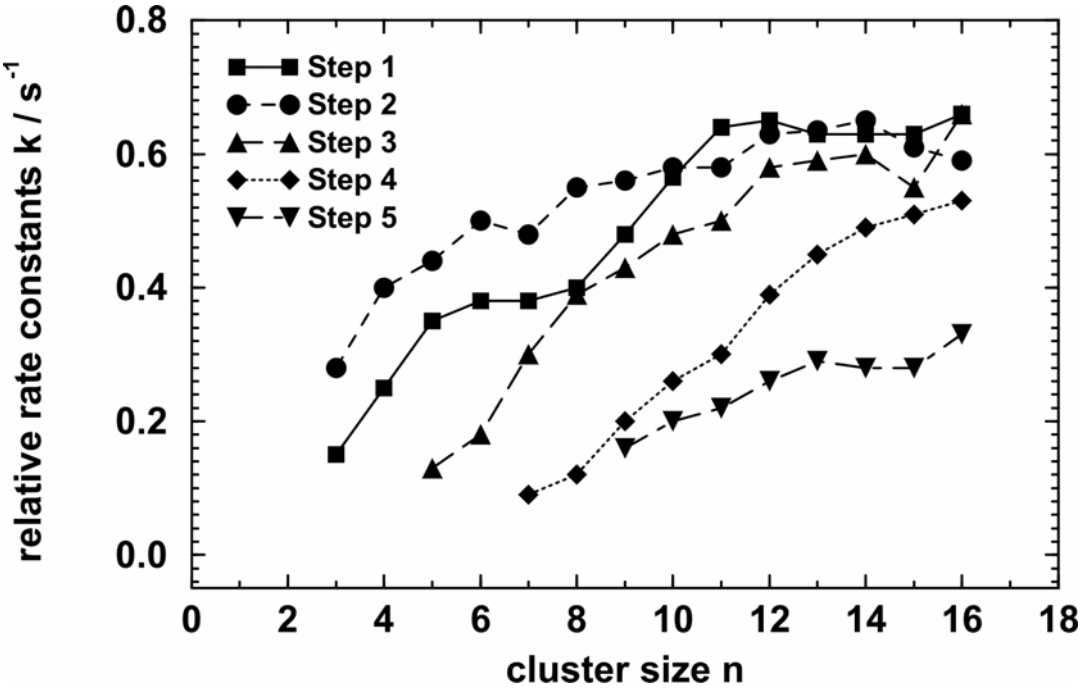

Figure 3: Relative rate constants assuming pseudo-first-order kinetics of reaction of rhodium anions Rh_n^-, n = 3-16, with azidoacetonitrile N_3CH_2CN. All anionic clusters react subsequently by evaporation of N_2 and H_2 and addition of [2C,2N] to the cluster surface. The number of efficient reaction steps increases with cluster size, which indicates that the cluster is gradually saturated with either interstitial carbides and nitrides or CN groups on its surface.

4.3.2. Reactions of Cationic Clusters

For cationic clusters, the picture is considerably more complex, since a number of competing reactions occur, which are characteristic for certain cluster sizes or size regimes. Reaction kinetics were again analyzed for reaction times of up to 5 s. Since competing reaction pathways are present, the precursors of secondary products were not always identified unambiguously. Thus the attention is concentrated here on a clear assignment of the primary products, and the results are summarized in the rate constant plot of Figure 4.

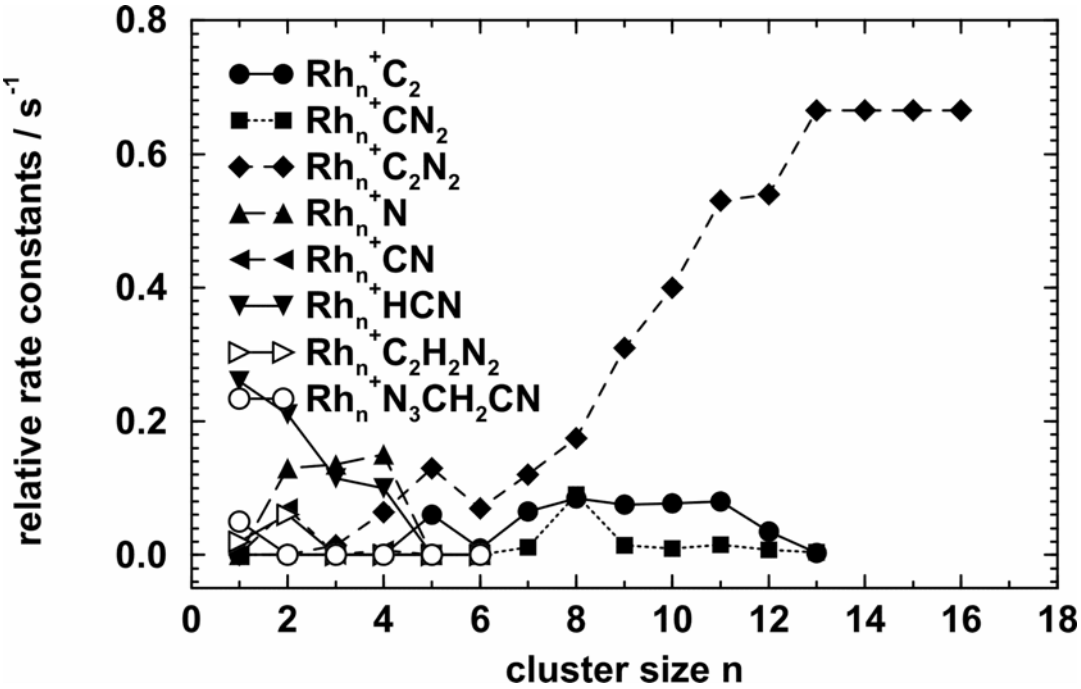

Figure 4: Relative rate constants assuming pseudo-first-order kinetics of reaction of rhodium cations Rh_n^+ , n = 1-16, with azidoacetonitrile N_3CH_2CN. For smaller clusters, the gas phase reactivity of N_3CH_2CN is responsible for the observed reaction pattern, while larger clusters show similar reactivity as the anions, which is probably characteristic of a rhodium surface.

Reaction (4) is the equivalent of reaction (3). It is the dominant reaction pathway for most clusters, and its branching ratio increases with increasing cluster size. Starting at n = 3, where it is barely observed, it becomes the dominant pathway at n = 5, with the rate constant quickly increasing until it reaches a constant value at n = 13, where it also becomes the only remaining reaction:

$$Rh_n^+ + N_3CH_2CN \rightarrow Rh_nC_2N_2^+ + N_2 + H_2 \qquad (4)$$

In an intermediate size region, n = 5-12, another process typical of surfaces is observed, formation of the pure carbide cations $Rh_nC_2^+$, which corresponds to the evaporation

of H_2 as well as of two N_2 molecules from the reactive complex according to equation (5):

$$Rh_n^+ + N_3CH_2CN \rightarrow Rh_nC_2^+ + 2N_2 + H_2 \qquad n = 5 - 12 \qquad (5)$$

In this intermediate size regime, the reaction enthalpy heats the cluster sufficiently to prevent the formation of the nitride and to enable the presumably energetically less favorable evaporation of a second N_2 molecule.

Even slower and less abundant were reactions corresponding to the loss of a nominal mass 42, resulting in the $Rh_nCN_2^+$ or $Rh_nC_2H_2N^+$ species. These were observed for n = 7 - 13 with a pronounced maximum at n = 8. Unfortunately, the mass resolution of our 4.7 T instrument is not sufficient in this mass region at this pressure to reliably distinguish between the two possible elemental compositions of the product cluster. However, looking at the possible neutral products and the overall reaction pattern, one can identify three chemically reasonable possibilities, loss of a diazomethane (6a), cyanamide (6b), or loss of the azide radical N_3 (6c):

$$Rh_n^+ + N_3CH_2CN \rightarrow Rh_nCN_2^+ + CH_2NN \qquad n = 7 - 13 \qquad (6a)$$

$$\rightarrow Rh_nCN_2^+ + NH_2CN \qquad n = 7 - 13 \qquad (6b)$$

$$\rightarrow Rh_nC_2H_2N^+ + N_3 \qquad n = 7 - 13 \qquad (6c)$$

Among these three possibilities, formation of the azide radical (6c) is unlikely, first of all because radical formation is in general less favorable than formation of closed shell neutrals as in (6a,b), and the heat of formation of N_3 is with 414 kJ/mol substantially higher than the corresponding values of 215 kJ/mol for diazomethane, CH_2NN, or 134 kJ/mol for

cyanamide, NH_2CN.[58] In addition, the hydrogen atoms do not remain on the cluster in the parallel reaction pathways (4) and (5), and a common pattern with respect to hydrogen incorporation seems reasonable. Arguing for or against (6a) vs. (6b) is much less straightforward. Mechanistically, formation of diazomethane seems much more likely, since it does not require rearrangement of C-N bonds, in contrast to cyanamide, as illustrated in Figure 5. Thermochemically, however, (6b) is favored by 81 kJ/mol over (6a), the difference between the heat of formation of diazomethane and of cyanamide.[58] The preferred occurrence of the reaction for n = 8, however, indicates a mechanistic origin, and it is quite intriguing to imagine that the initial adsorbent structure in Figure 5a is most likely realized in a relatively compact cluster structure with "sharp" edges. The complex rearrangement and survival of the CN-group required in Figure 5b must be considered unlikely, since the triple bond will interact predominantly with the cluster surface. Under these circumstances, an intact abstraction after recombination with a newly formed NH_2-group is hard to imagine.

Overall, the subsidiary reactions (5) and (6) are of decreasing importance with increasing the cluster size, so that essentially only the dominant primary reaction (4) is detected for $n \geq 13$. Two possible interpretations can be offered for this trend. One contributing factor may be that the probability of the two remaining N atoms approaching each other on the cluster surface close enough in order to recombine and form molecular N_2 is reduced with the increase of its size.

More important, however, is probably the effect of the available energy.[50] The reaction of the metal cluster according to equation (4) can be viewed as a metal catalyzed, exothermic decomposition of the metastable azide compound with the loss of molecular N_2, followed by reaction of the remaining NCH_2CN entity with the metal cluster, which results in the elimination of both hydrogen atoms in the form of molecular H_2. A large amount of energy

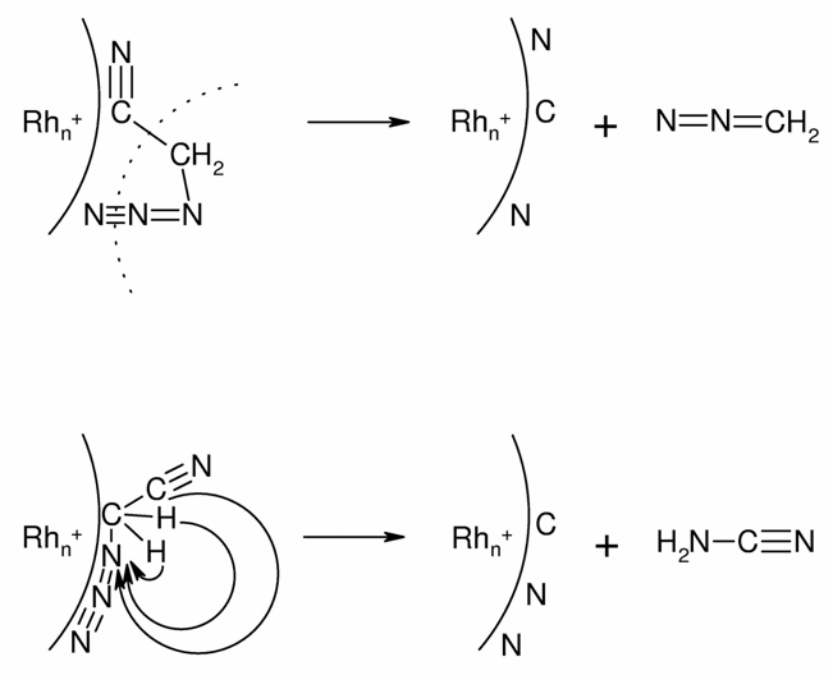

Figure 5: Possible routes to the formation of Rh_nCNN^+. The azide group is destroyed upon adsorption of azidoacetonitrile on the cluster, leading to formation of diazomethane (a) or cyanamide (b). Mechanistically speaking the formation of diazomethane (a) is much more likely because it does not require rearrangements of C-N bonds, in contrast to cyanamide (b). Thermochemically, (b) is favored by 81 kJ/mol over (a), the difference between the heat of formation of diazomethane and cyanamide.

will be deposited in the reaction product. This energy will consist of several contributions: the initial kinetic energy of the reactants, the adsorption energy of the unsaturated compound on the metal cluster surface, the enthalpy of the N_3CH_2CN reactant decomposition with N_2 and H_2 elimination, and finally of the enthalpy of the product ion formation. Overall, this large energy will be statistically distributed among the internal vibrational modes of the resulting product and will raise its effective temperature to a very high value.

Apparently the temperature may remain high enough so that even the evaporation of the remaining two nitrogen atoms as an N_2 molecule can take place, reaction (5). The overall amount of energy deposited will undoubtedly, in particular for the larger clusters, not depend

very strongly on the specific value of n. On the other hand, the number of internal vibrational modes and low-lying electronic states, over which this energy can be distributed will increase linearly with n, and consequently the effective cluster temperature must decrease with size. The net result of these effects will be the decrease in the effective temperature of the product cluster, which is then reflected in the suppression of the minor, presumably less exothermic side reactions for clusters $n \geq 13$.

In contrast to these presumably surface-like reactions (4-6), an almost completely different chemistry is observed for the smallest clusters, $n \leq 4$. This is undoubtedly due to the fact that when the number of rhodium atoms becomes too small, enough Rh-C and Rh-N bonds cannot form, and the stable interstitial carbide or nitride structure cannot develop. The exothermicity of the reaction of the azidoacetonitrile with the cluster decreases, so that the dehydrogenation reaction may not proceed to completion, and products with residual hydrogen appear.

Starting with the simple, monatomic rhodium cation, its observed reactions are described by equations (7), (8a), (9a).

$$Rh^+ + N_3CH_2CN \rightarrow RhN_3CH_2CN^+ \quad (7)$$

$$\rightarrow RhHCN^+ + N_2 + HCN \quad (8a)$$

$$\rightarrow RhH_2C_2N_2^+ + N_2 \quad (9a)$$

The simple adduct of Rh^+ with azidoacetonitrile according to reaction (7) is apparently sufficiently long lived so that it can be stabilized, either radiatively or collisionally. This stabilization is obviously facilitated by the presence of unsaturated bonds in the azide and nitrile groups.

Obviously stabilization of the complex is not the most probable outcome of the reaction, since the major product observed is an ion with the $RhHCN^+$ composition, according to reaction (8a). The time resolved profile of the product ion with $RhH_2C_2N_2^+$ composition suggests that it is at least partially a primary product formed according to reaction (9a). Two other ions are observed corresponding to $RhHCN(N_3CH_2CN)^+$ and $Rh(HCN)_3^+$, which are clearly the products of secondary reactions, as confirmed by their time resolved intensity profiles.

Reactions (8a) and (9a) can easily be rationalized with the help of the Curtius-rearrangement, reaction (1). As illustrated in Figure 6a, the standard Curtius-rearrangement leads to formation of NHCHCN, which may be stabilized on Rh^+, while N_2 evaporates. Unlike most other organic azides, however, azidoacetonitrile offers the possibility that the Curtius-rearrangement proceeds in the wrong direction, with the H atom attacking the nitrile carbon instead of the imine nitrogen. In this case, two HCN molecules are formed , together with N_2. One of the HCN stays attached to the Rh^+, the stabilization being helped by evaporation of two neutral molecules. In summary, the reactivity of Rh^+ with N_3CH_2CN can be rationalized by the unimolecular decomposition pathways of azidoacetonitrile illustrated in Figure 6.

In contrast with Rh^+, no complexes of Rh_n^+ with undecomposed azidoacetonitrile are observed for any cluster with $n \geq 2$. One can understand this observation in terms of an exothermic decomposition of the azidoacetonitrile on the rhodium metal, which is incomplete only in the case of the monatomic cation. The reactions of the small clusters in the intermediate range of $2 \leq n \leq 4$ can be described by the following set of equations, and the approximate relative yields are summarized in Table 1.

While for the larger clusters there is no analogue of the reaction (7), for the $n = 2$ dimer both the (8) and (9) analogue reactions occur. Besides, two new reactions (10) and (11)

$$Rh_n^+ + N_3CH_2CN \rightarrow Rh_nHCN^+ + N_2 + HCN, \quad n = 1 - 4 \quad (8)$$

$$\rightarrow Rh_n(HCN)_2^+ + N_2, \quad n = 1, 2 \quad (9)$$

$$\rightarrow Rh_nCN^+ + N_2 + CH_2N, \quad n = 2 \quad (10)$$

$$\rightarrow Rh_nN^+ + N_2 + CH_2CN \quad n = 2 - 4 \quad (11)$$

$$\rightarrow Rh_nC_2N_2^+ + N_2 + H_2 \quad n \geq 3 \quad (4)$$

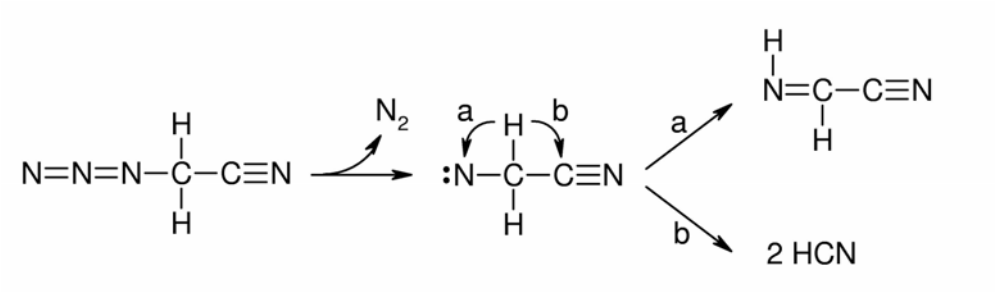

Figure 6: Curtius-rearrangement may proceed in two directions for the unimolecular decomposition of azidoacetonitrile. Standard Curtius-rearrangement leads to formation of NHCHCN (a), which may be stabilized on Rh^+, while N_2 evaporates. If an H atom attacks the nitrile carbon (b) instead of the imine nitrogen two HCN molecules are formed, together with N_2. During the process, one of the HCN attaches to the Rh^+, the stabilization being helped by the evaporation of two neutral molecules.

Table 1: Branching ratios in % of $Rh_n^+ + N_3CH_2CN \rightarrow$ products, n = 1 - 4.

n	$Rh_nN_3CH_2CN^+$ (7)	Rh_nHCN^+ (8)	$Rh_nH_2C_2N_2^+$ (9)	Rh_nCN^+ (10)	Rh_nN^+ (11)	$Rh_nC_2N_2^+$ (4)
1	15	75	10			
2		35	15	15	35	
3		35			60	5
4		30			50	15

are observed, with nominal masses of 26 and 14, respectively, remaining on the cluster. As already discussed, the corresponding gaseous products can only be inferred indirectly from the reaction stoichiometry and thermochemistry. Also the n = 3 and 4 clusters yield major products according to reactions (8) and (11), but the reactions (9) and (10) are not observed. They are replaced by the "large cluster" reaction (4) which is, as discussed above, the dominant reaction for all the clusters with $n \geq 5$.

In the case of reactions (10), the product $Rh_2C_2H_2^+$ with the same nominal mass can be ruled out based on the mass difference of 26.001 to the Rh_2^+ ion, which compares favorably with the 26.003 amu expected for CN, and is in heavy disagreement with the 26.016 expected for C_2H_2. Reaction (10) can be seen as reaction (8) proceeding somewhat further, with the formation of a bridged $[RhCNRh]^+$ structure, and the second HCN taking the remaining H atom away.

Again, the product of (11) is unambiguously assigned as Rh_nN^+ based on the measurement of the mass difference to the bare Rh_n^+ cluster. The reaction can be rationalized with a CH_2CN radical leaving the collision complex in the first step. The azide radical decomposes, yielding Rh_2N^+ and an N_2 molecule.

The analysis of consecutive reactions for larger cationic clusters is less unambiguous than for the anionic clusters, and is obviously complicated by the occurrence of the reactions (5) and (6). The presence of parallel processes makes the reaction scheme more complex, and dilutes the signal among more product ions. In spite of these difficulties, one can clearly say that the dominant reactions are again the cationic analogues of the reaction (3), with major products being the $Rh_nC_{2m}N_{2m}^+$ cation clusters.

4.3.3. Comparison of Cationic and Anionic Clusters

The variation of the rates of the primary reactions as a function of the rhodium cluster size n as well as of their charge is summarized graphically in Figure 7. For the anions the reaction rates increase almost monotonically with the cluster size n, and then level off above about n = 11-13. In contrast, there is a minimum of the observed reactivity of the cations for n = 6, which is explained by two overlapping processes: With increasing n, the rates of reactions (7-11), which are dominated by the gas-phase dissociation behavior of the azidoacetonitrile molecule, are decreasing. At the same time, the rates of the surface-driven reactions (4-6) are increasing. The slope of this rate increase is, however, faster for the cations than for the anions, so that just about at the point where the rates level off, the difference between the anions and cations essentially disappears. Above about n > 12 the reaction rates become almost size independent, and within the accuracy of the measurement, basically the same for anions and cations. The fundamental difference between cations and anions lies in the observation that the small cationic clusters are able to induce the unimolecular decomposition of azidoacetonitrile, presumably by offering thermochemically favorable positively charged rhodium compounds as potential products.

Several local deviations from the overall trends can be found in the data, but in the absence of any knowledge of the rhodium cluster structure, nothing more can be done than to note them in passing. Clearly visible is the somewhat lower overall reactivity of the n = 6 cation cluster, which reacts distinctly slower than either n = 5 or n = 7.

Another interesting observation is that the subsidiary reactions (5) and (6) do not occur for the anionic clusters, which react exclusively according to reaction (3). Following the arguments made above for larger cationic clusters, this might reflect a somewhat lower

exothermicity of the reaction for the small anions, and consequently lower effective temperature of the products formed.

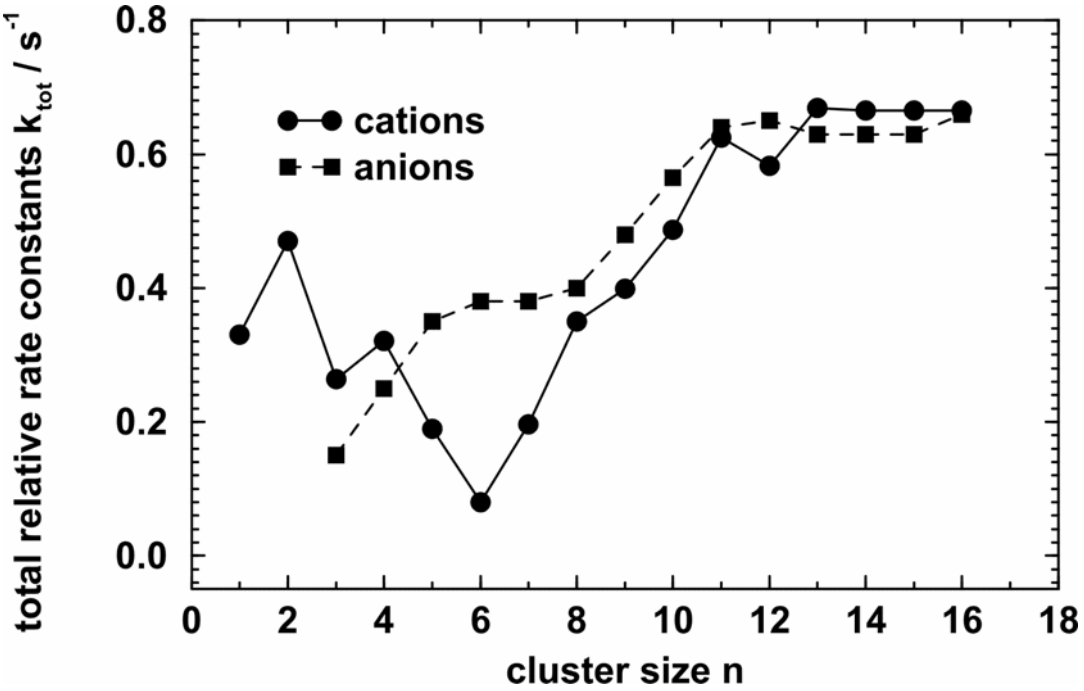

Figure 7: Total relative rate constants of the primary reactions of rhodium clusters with azidoacetonitrile as a function of their charge and size n. For the anions (■) the reaction rates increase almost monotonically with the cluster size n, and then level off around n = 11-13. In contrast there is a minimum of the observed reactivity of the cations (●) for n = 6, due to the fact that by increasing n the rates for unimolecular decomposition of azidoacetonitrile are decreasing and in the same time the rates of the surface-driven reaction are increasing. Above n > 12 the reaction rates become almost size independent. Starting with n = 8, the rates for anions and cations become the same.

One general conclusion which can be made, both for the reactions of anions and cations, is that for $n \geq 5$ no product clusters containing hydrogen are clearly identified, and that the "evaporation" of hydrogen from the clusters is in all cases complete. As noted previously, this can be understood based on the general reluctance of rhodium and nearby

metals to form bonds with hydrogen. Another observation perhaps worth repeating is that, again in agreement with previous results, no rhodium atom loss and no breakage of metal-metal bonds was observed, even in the reaction with the high-energy species azidoacetonitrile.

4.4. Conclusions

Reactions of anionic and large cationic rhodium clusters with azidoacetonitrile lead to the uptake of [2C,2N] into the cluster, either as interstitial carbides and nitrides or as CN groups, accompanied by full dehydrogenation and evaporation of neutral N_2 in consecutive steps. The reaction stops presumably when the cluster surface is saturated with the reaction products. The monomer Rh^+ reacts more or less as a spectator, with the azidoacetonitrile undergoing unimolecular reactions, whose products are stabilized as complexes with Rh^+. In the size region from two to five atoms, this unimolecular type of reaction becomes less important, and ceases to occur with n = 5, while formation of the surface-typical reaction products $Rh_nC_xN_y^+$ starts at n = 2 and becomes the dominant reactions at n = 3. The cationic clusters illustrate the gradual transition from metal ion gas phase chemistry to surface-like behavior. The reactivity of both cationic and anionic clusters shows that in the gas phase, the high-energy species azidoacetonitrile undergoes clean and defined reactions. The results suggest that azidoacetonitrile can be used to generate a stoichiometrically well-defined 1:1 carbide-nitride film or a film consisting of CN groups on a rhodium surface. Surface science experiments to test this prediction are highly desirable.

4.5. References

(1) T. Curtius, *Ber. Dtsch. Chem. Ges.*, **1890**, *23*, 3023.

(2) P. Griess, *Phil. Trans. Roy. Soc. (London)*, **1864**, *13*, 377.

(3) J. H. Boyer, F. C. Canter, *Chem. Rev.*, **1954**, *54*, 1.

(4) I. C. Tornieporth-Oetting, T. M. Klapötke, *Angew. Chem. Int. Ed. Engl.*, **1995**, *34*, 511.

(5) B. M. Jönsson, K. Håkansson, A. Liljas, *FEBS Lett*., **1993**, *322*, 186.

(6) R. Maurus, R. Bogumil, N. T. Nguyen, A. G. Mauk, G. Brayer, *Biochem. J.*, **1988**, *332*, 67.

(7) H. C. Ramsperger, *J. Am. Chem. Soc.*, **1929**, *51*, 2134.

(8) L. O. Brockway, L. Pauling, *Proc. Nat. Acad. Sci. USA*, **1933**, *19*, 860.

(9) L. Pauling, L. O. Brockway, *J. Am. Chem. Soc.*, **1937**, *59*, 13.

(10) V. R. P. Verneker, A. C. Forsyth, *J. Phys. Chem.*, **1968**, *72*, 111-115.

(11) V. R. P. Verneker, *J. Phys. Chem.*, **1968**, *72*, 1733-1736.

(12) T. L. Chant, K. B. Gross, R. G. Wooley, *Aerosol Sci. Tech.*, **1990**, *13*, 349-355.

(13) J. M. Berger, P. B. Butler, *Combust. Sci. Technol.*, **1995**, *104*, 93-114.

(14) T. Urano, K. Takahama, T. Yamaoka, *Imaging Sci. J.*, **1999**, *47*, 133-140.

(15) A. Marcos, J. L. de Benito, L. Ibarra, A. Rodriguez, L. Gonzalez, *Polym. Int.*, **1991**, *25*, 7-12.

(16) M. A. L. Manchado, J. M. Kenny, *Rubber Chem. Technol.*, **2001**, *74*, 198-210.

(17) R. A. Fischer, H. Sussek, A. Miehr, H. Pritzkow, E. Herdtweck, *J. Organomet. Chem.*, **1997**, *548*, 73-82.

(18) F. Falk, J. Meinschien, K. Schuster, H. Stafast, *Carbon*, **1998**, *35*, 765-769.

(19) J. J. Wang, E. G. Gillan, *Thin Solid Films*, **2002**, *422*, 62-68.

(20) R. A. Abramovitch, E. P. Kyba, *J. Am. Chem. Soc.*, **1977**, *96*, 480.

(21) H. Bock, R. Dammel, S. Aygen, *J. Am. Chem. Soc.*, **1983**, *105*, 7681.

(22) G. Bertrand, J.-P. Majoral, A. Baceiredo, *Acc. Chem. Res.*, **1986**, *19*, 17.

(23) H. Bock, R. Dammel, *Angew. Chem. Int. Ed. Engl.*, **1987**, *26*, 504.

(24) H. Bock, R. Dammel, *J. Am. Chem. Soc.*, **1988**, *110*, 5261.

(25) J. Baker, M. Barnes, M. G. R. Cockett, J. M. Dyke, A. M. Ellis, M. Fehér, E. P. F. Lee, A. Morris, H. Zamanpour, *J. Electron. Spectrosc.*, **1990**, *51*, 487.

(26) V. E. Bondybey, A. M. Smith, J. Agreiter, *Chem. Rev.*, **1996**, *96*, 2113.

(27) P. Klaeboe, C. J. Nielsen, H. Priebe, S. H. Schei, C. E. Soegren, *J. Mol. Struct.*, **1986**, *141*, 161.

(28) M. L. S. L. Costa, M. A. A. Ferreira, *J. Mol. Struct.*, **1988**, *175*, 417.

(29) M. L. Costa, B. J. C. Cabral, M. A. A. Ferreira, *J. Mol. Struct.*, **1990**, *220*, 315.

(30) J. M. Dyke, A. P. Groves, A. Morris, J. S. Ogden, A. A. Dias, A. M. S. Oliveira, M. L. Costa, M. T. Barros, M. H. Cabral, A. M. C. Moutinho, *J. Am. Chem. Soc.*, **1997**, *119*, 6883.

(31) J. M. Dyke, A. P. Groves, A. Morris, J. S. Ogden, M. I. Catarino, A. A. Dias, A. M. S. Oliveira, M. L. Costa, M. T. Barros, M. H. Cabral, A. M. C. Moutinho, *J. Phys. Chem. A*, **1999**, *103*, 8239.

(32) N. Hooper, L. J. Beeching, J. M. Dyke, A. Morris, J. S. Ogden, A. A. Dias, M. L. Costa, M. T. Barros, M. H. Cabral, A. M. C. Moutinho, A. M. C. *J. Phys. Chem. A*, **2002**, *106*(42), 9968-9975.

(33) M. T. Nguyen, D. Sengupta, T.-K. Ha, *J. Phys. Chem.*, **1996**, *100*, 6499.

(34) M. I. Catarino, B. J. Costa Cabral, M. L. Costa, *J. Mol. Struct. (Theochem)*, **1997**, *397*, 223.

(35) S. Sklenák, A. Gatial, S. Biskupi, *J. Mol. Struct. (Theochem)*, **1997**, *397*, 249.

(36) J. F. Arenas, J. I. Marcos, J. C. Otero, A. Sánchez-Gálvez, J. Soto, *J. Chem. Phys.*, **1999**, *111*, 551.

(37) J. F. Arenas, J. I. Marcos, I. López-Tocón, J. C. Otero, J. Soto, J. *J. Chem. Phys.*, **2000**, *113*, 2282.

(38) J. F. Arenas, J. I. Marcos, J. C. Otero, I. L. Tocón, J. Soto, *Int. J. Quantum Chem.*, **2001**, *84*, 241.

(39) M. N. D. S. Cordeiro, A. A. Dias, M. L. Costa, J. A. N. F. Gomes, *J. Phys. Chem. A*, **2001**, *105*, 3140.

(40) L. Ying, Y. Xia, H. Shang, X. Zhao, Y. Tang, *J. Chem. Phys.*, **1996**, *105*, 5798.

(41) W. Jing, S. Zheng, Z. Xinjiang, Y. Xiaojun, G. Maofa, W. Dianxun, *Angew. Chem. Int. Ed.*, **2001**, *40*, 3055.

(42) N. B. H. Jonathan, P. J. Knight, A. Morris, *Surf. Sci.*, **1992**, *275*, L640.

(43) J. C. S. Chu, Y. Bu, M. C. Lin, *Surf. Sci.*, **1993**, *284*, 281.

(44) C. Tindall, J. C. Hemminger, *Surf. Sci.*, **1995**, *330*, 67.

(45) A. A. Dias, R. Carrapa, M. T. Barros, T. Almeida Gasche, O. M. N. D. Teodoro, M. L. Costa, M. H. Vasconcelos Cabral, A. M. C. Moutinho, *Vacuum*, **2002**, *64*, 445.

(46) A. M. Oliveira, M. T. Barros, A. M. Martins, M. A. R. Cabral, A. A. Dias, M. L.Costa, M. H. Cabral, A. M. C. Moutinho, K. R. Jennings, *Rapid Commun. Mass Spectrom.*, **1999**, *13*, 559.

(47) M. F. Duarte, F. Martins, M. T. Fernandez, G. J. Langley, P. Rodrigues, M. T. Barros, M. L. Costa, *Rapid Commun. Mass Spectrom.*, **2003**, *17*, 957.

(48) M. P. Irion, *Int. J. Mass Spectrom.*, **1992**, *121*, 1.

(49) M. B. Knickelbein, *Annu. Rev. Phys. Chem.*, **1999**, *50*, 79.

(50) V. E. Bondybey, M. K. Beyer, *J. Phys. Chem. A*, **2001**, *105*, 951-960.

(51) K. M. Ervin, *Int. Rev. Phys. Chem.*, **2001**, *20*, 127.

(52) P. B. Armentrout, *Ann. Rev. Phys. Chem.*, **2001**, *52*, 423.

(53) C. Berg, M. Beyer, U. Achatz, S. Joos, G. Niedner-Schatteburg, V. E. Bondybey, *J. Chem. Phys.*, **1998**, *108*, 5398-5403.

(54) U. Achatz, C. Berg, S. Joos, B. S. Fox, M. K. Beyer, G. Niedner-Schatteburg, V. E. Bondybey, *Chem. Phys. Lett.*, **2000**, *320*, 53-58.

(55) I. Balteanu, U. Achatz, O. P. Balaj, B. S. Fox, M. K. Beyer, V. E. Bondybey, *Int. J. Mass Spectrom.*, **2003**, *229*, 61.

(56) C. Berg, T. Schindler, G. Niedner-Schatteburg, V. E. Bondybey, *J. Chem. Phys.*, **1995**, *102*, 4870.

(57) K. Freudenberg, H. Eichel, F. Leutert, *Ber. Dtsch. Chem. Ges.*, **1932**, *65*, 1183.

(58) H. Y. Afeefy, J. F. Liebman, S. E. Stein, "Neutral Thermochemical Data" in NIST Chemistry WebBook, NIST Standard Reference Database Number 69, Eds. P.J. Linstrom and W.G. Mallard, July 2001, National Institute of Standards and Technology, Gaithersburg MD, 20899 (http://webbook.nist.gov).

(59) W. Andreoni, C. M. Varma, *Phys. Rev. B*, **1981**, *23*, 437.

5. Reactions of Rhodium Cationic Clusters with Ethane

5.1. Introduction

Catalysts are one of the most important ingredients of chemical technology. They are essential in automotive applications, in refining fossil fuels, and production of chemicals. Most catalysts used in large volume applications are heterogeneous, with the reaction occurring on the catalyst's surface. Transition metals, with their multitude of oxidation states are among the most important industrial catalysts, and understanding the mechanisms of catalytic processes on atomic scale is a topic of considerable current interest. Their activity does not only depend on the chemical composition of the catalyst, but also very critically on the detailed structure of its surface. Small metal clusters, with their varied structures and varying degrees of coordinative saturation of the individual atoms are therefore very useful models for the catalytic process.

In the present study Fourier transform ion cyclotron resonance (FT-ICR) mass spectrometry was used to investigate the reactions of small cationic rhodium clusters Rh_n^+, n = 1 – 23 with C_2H_6.

Rhodium metal has a number of advantages for investigating hydrocarbon reactions. It lies in the area of the periodic table where the elements are rather reactive towards hydrogen, but do not have a very high affinity to carbon.[1] Obviously, any catalytic process requires adsorption of the reactants on the metal surface, occurrence of its reaction, and then desorption of the products. Metals which immediately and irreversibly react to metal carbide are of little interest from the point of view of chemical

catalysis. A great advantage of rhodium is that, unlike more typical catalysts like palladium or platinum, it is monoisotopic. While for such elements only one mass peak is observed for each cluster size, the signal for larger clusters of elements consisting of many isotopes will be progressively diluted into so many isotopic peaks, as to make the spectra extremely complex and difficult to analyze and interpret.

The reactions of rhodium clusters, anionic, neutral, and cationic with small molecules like CO, C_6H_6, O_2 have been studied previously.[2-9] More than a decade ago Kaldor and coworkers[10] have used the laser vaporization technique to generate neutral rhodium clusters, and investigated their reactions with D_2, N_2 and CH_4, and more recently, the reactions of cationic Rh_n^+ species with D_2 were also studied. Bondybey and coworkers have previously been able to generate both cationic and anionic rhodium clusters up to about n=30, and explored their reactions with benzene, methane, carbon monoxide, and azidoacetonitrile.[2,3,5,6,11]

5.2. Experimental Details

The experimental apparatus and techniques used were previously described,[4,5] and will be here presented only briefly. The studies are carried out on a commercial 4.7 T Bruker/Spectrospin CMS47X FT-ICR mass spectrometer. The rhodium clusters were produced by laser vaporization of the metal disk in the presence of high pressure (20 bar) helium carrier gas. The reactant gas, ethane, can be admitted to the instrument via adjustable leak valves. To study the bimolecular ion-molecule reactions the pressure inside the ICR cell was raised from the base value of around 4×10^{-10} mbar to about 9×10^{-9} mbar by controlled admission of the ethane reactant gas. Commercially available C_2H_6 (Messer-Griesheim) was used without further purification. Mass spectra were measured

after varying reaction times. The relative rate constants for the first reaction step were then obtained by fitting the observed time dependence of the parent and product cluster ion intensities, assuming pseudo-first order kinetics.

5.3. Computational Details

The geometry optimizations were carried out on a Pentium III based Lynux system using the B3LYP[12-14] hybrid Hartree-Fock density functional method implemented in the Gaussian98[15] program package. For both rhodium-ethane and rhodium-methane structures the 6-31+G(d,p) basis set was used on C, H and SDD on Rh. All the geometries were fully optimized and verified to be local minima on the potential energy surface by frequency calculations.

5.4. Results and Discussion

Since several preliminary experiments have shown that, consistent with previous experience with rhodium, the reactions never lead to cluster fragmentation, that is to a loss of rhodium atoms, a whole distribution of clusters could be studied simultaneously, without any need for mass selection. This has the considerable advantage that the entire distribution is investigated under exactly identical conditions, which obviously makes the measurement of the relative reaction rates and cross-sections for clusters of different sizes more consistent and reliable. The clusters produced in the source were trapped in the ICR cell, and typically accumulated over 20 pulses of the vaporization laser. The mass spectra were then acquired after varying reaction delays, beginning with 0 s, which means immediately after the completed accumulation. It should of course be noted, that since in

the course of the experiment the pressure in the cell remains constant, the clusters can, and do, react already during the accumulation time, so that even in the mass spectra corresponding to nominally zero reaction times some reaction products are observable.

The results are exemplified in Figure 1a by the data for n = 1, that is monatomic Rh^+, and in Figure 1b for n = 2, diatomic Rh_2^+. In the Figure 1a, plotted on a semi-logarithmic scale one can note over the first five seconds an exponential decay of the Rh^+, with a concurrent growth of the reaction product, which is easily identified as $Rh^+C_2H_4$. At longer time, the growth of a second product, $Rh^+C_4H_8$, can be detected. In the 1b panel, one observes a considerably faster decay of the more reactive Rh_2^+ dimer ion, and growth, it this case of two new mass peaks, both behaving as primary products. These can again be, based on exact measurement of their mass, unambiguously identified as $Rh_2^+C_2H_2$ and $Rh_2^+C_2H_4$, respectively.

The individual data points in Figure 1 represent the measured intensities of the Rh_n^+ reactant ions (full circles) and of the reaction products (other symbols). The thin lines shown in the figure represent then the theoretical fit to the experimental intensity data. With the help of similar fits like those exemplified in Figure 1, one can then derive fairly reliably the relative reaction rates and branching ratios for various sizes of clusters. All the clusters were investigated in this way in the range of about $1 \leq n \leq 23$. Usually different source conditions are needed to produce small or very large clusters, and it was therefore not possible to produce simultaneously adequate intensities of clusters over this entire range. The relative rates derived from the fit and presented in Figure 2 are the result of three different experiments involving three different, overlapping ranges of cluster sizes. For all the experiments, a constant pressure of 9×10^{-9} mbar was maintained in the

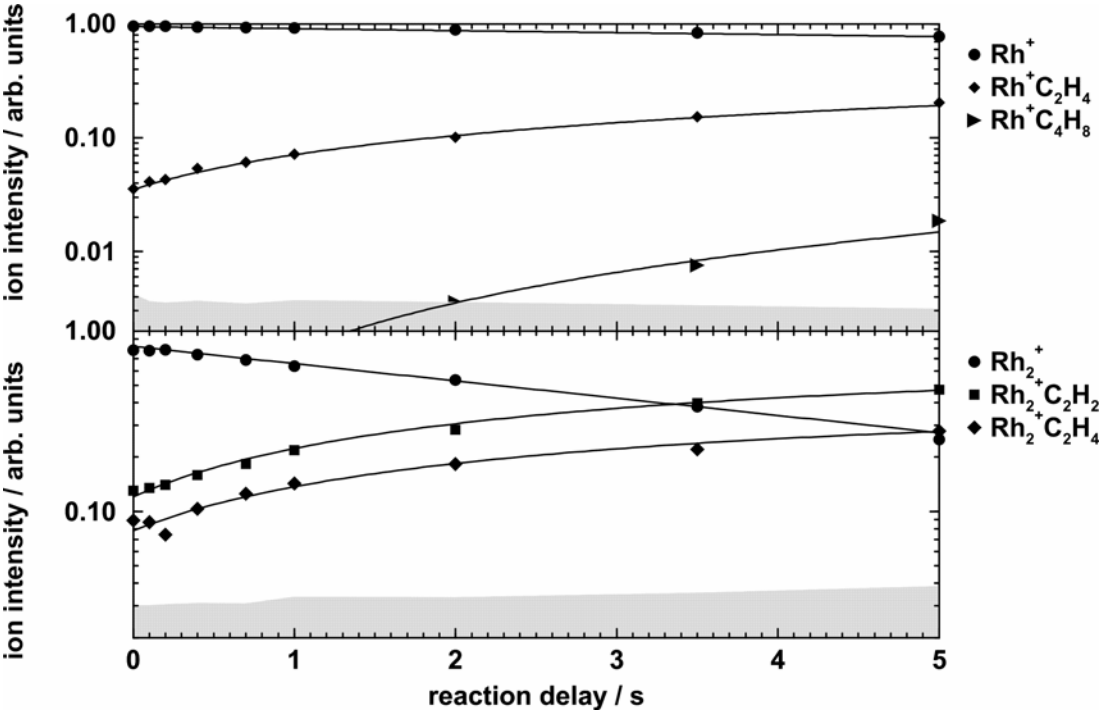

Figure 1: Time dependence of the reaction of Rh^+ (top) and Rh_2^+ (bottom) with about 9×10^{-9} mbar of ethane. Note the unique primary product, $RhC_2H_4^+$ (■) in the former, and two parallel products $Rh_2C_2H_4^+$ (■) and $Rh_2C_2H_2^+$ (◆) in the latter case. Gray shaded areas denote the noise level.

ICR cell. All the clusters react by the same two reactions exemplified already for n = 1 and n = 2 in the Figure 1, that is by partial dehydrogenation with the loss of one or two molecules of hydrogen:

$$Rh_n^+ + C_2H_6 \rightarrow Rh_n^+C_2H_4 + H_2 \quad (1)$$

$$\rightarrow Rh_n^+C_2H_2 + 2H_2 \quad (2)$$

Starting with about the n = 6 cluster, an additional product appears, corresponding to increase in mass of about 32 mass units. This is clearly due to the addition of molecular O_2 onto the cluster, due to the small amounts present in the background gas. While the

exact concentration of the molecular oxygen is not known, its reaction with the clusters still provides an interesting comparison with the reactions of the ethane, and therefore in also the reaction rates corresponding to the following reaction (3) is included in Figure 2 as triangles:

$$Rh_n^+ + O_2 \rightarrow Rh_n^+O_2 \qquad (3)$$

The presence of three parallel reactions (1), (2) and (3), and the presence of three primary products is exemplified for the fastest reacting cluster n = 10 in Figure 3a. As cursory examination of Figure 2 reveals, the reactions with oxygen have a fairly sharp onset around n = 6, and their rates are, at least over the range studied, relatively constant, with only small fluctuations, in most cases of the order the experimental error of the measurement. In contrast with that, the overall reaction rates with ethane, as well as the branching ratios between reactions (1) and (2) show wild fluctuations from size to size. Again as can be seen in Figure 2, even those clusters which do not react with ethane at all, or to be more exact, whose reactions are too slow to be detected in the present experiments, show an undiminished reactivity towards oxygen, as shown for the n = 17 cluster in panel 3b.

An examination of the rhodium cluster reactions with ethane becomes particularly interesting and revealing, when compared with the reactions with molecular O_2. While the Rh_n^+ clusters with $n < 6$ do not react with oxygen, or their reaction rates according to (3) are too slow to be detected under the condition of the present experiment, they exhibit clearly observable reactivities with the organic compound. Even more interestingly, unlike the reaction (3) which above the threshold around n = 6 shows only mild variations in

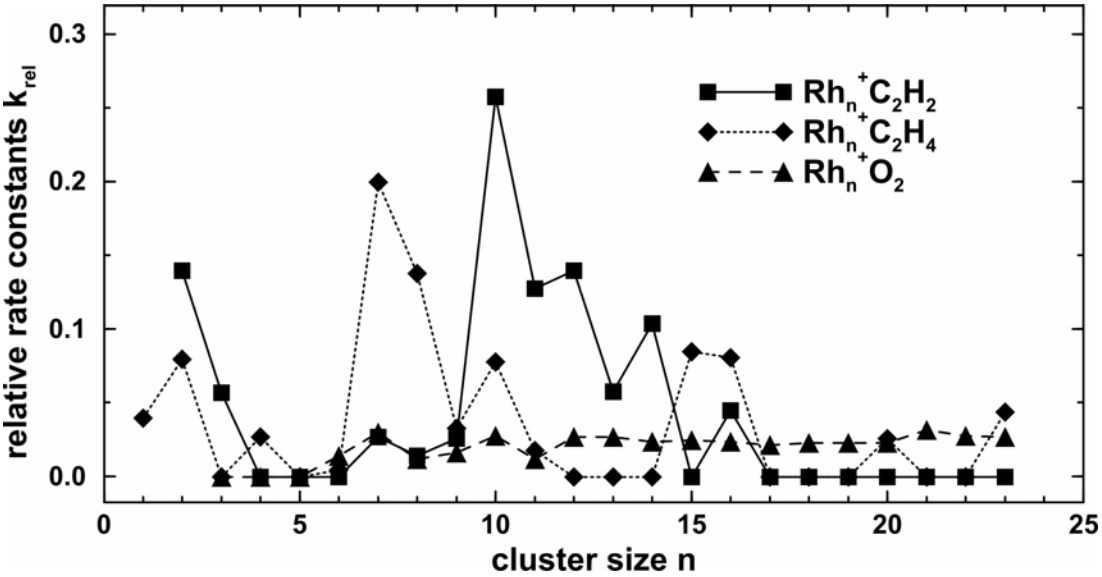

Figure 2: Relative rate constants for the first reaction step of the three observed primary reactions (1), (2) and (3). Squares - reaction (1), double dehydrogenation, diamonds - reaction (2), single dehydrogenation, and triangles - reaction (3), adsorption of O_2.

rates, both the rates of the reaction with ethane, as well as the branching ratio's between reactions (1) and (2) exhibit wild fluctuations as a function of the cluster size n, in some cases by orders of magnitude.

This can clearly be seen by examination of Figure 2 as well as of the numerical rate values in Table 1. Thus already the monatomic cation, n = 1, reacts with ethane according to (1), with the loss of two hydrogen atoms, almost certainly like an H_2 molecule. The diatomic cluster, Rh_2^+ exhibits both reactions (1) and (2), while for n = 3 exclusively loss of two hydrogen molecules, reaction (2) is detected. The n = 4 cluster reverts to reaction (1), but with a relatively low rate, while for the n = 5 no reaction at all is detected. The next, Rh_6^+ again reacts according to (1) with the loss of one H_2. All clusters between n = 7 and n = 11 exhibit both reaction (1) and (2) but with wildly varying rates and branching ratios. The n = 7 and 8 react fairly efficiently according to (1) with the

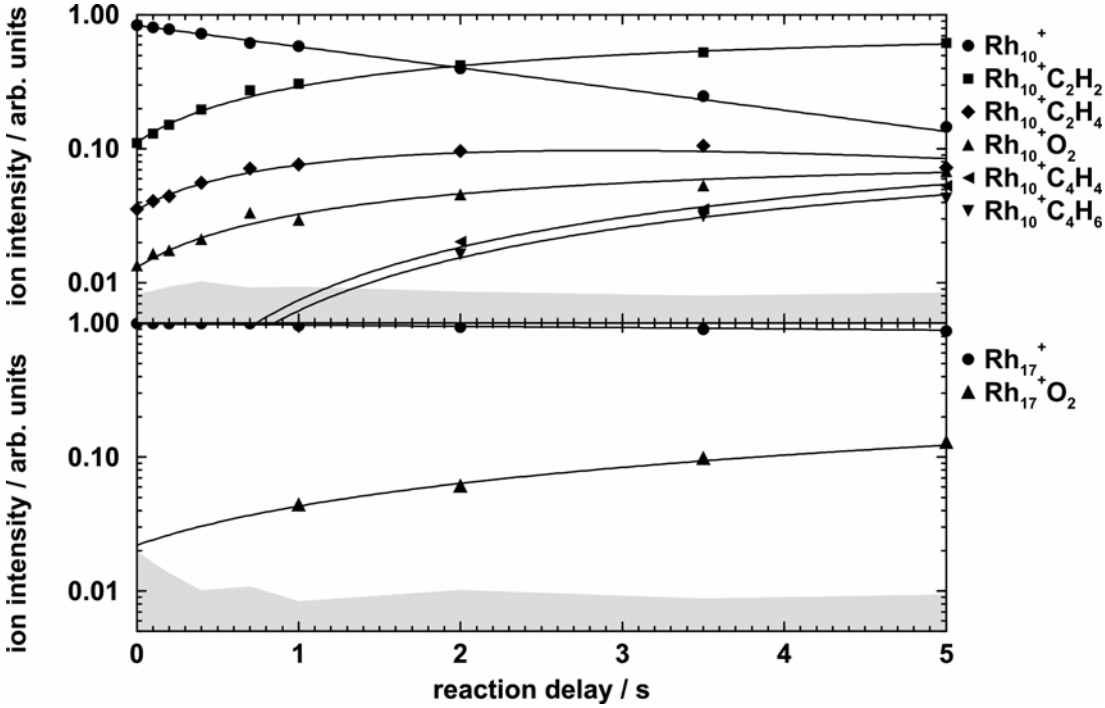

Figure 3: Top panel: reaction of the most reactive, Rh_{10}^+ cluster, and the growth of three parallel primary products, corresponding to reactions (1), (2), and (3), $Rh_{10}C_2H_4^+$ (diamonds), $Rh_{10}C_2H_2^+$ (squares), and $Rh_{10}O_2^+$ (triangles). Bottom panel: Rh_{17}^+ is unreactive towards ethane, but reacts efficiently with O_2 forming a binary complex $Rh_{17}O_2^+$. Note the slightly different shape of the time dependence of the product of reaction (2) (squares), which reacts efficiently to secondary products.

loss of one H_2, while double dehydrogenation dominates for the n = 10 - 14 clusters. The Rh_9^+ cluster is relatively unreactive, exhibiting small and comparable reaction rates according to (1), (2), and (3). For clusters n = 15, 16, 20 and 23 single dehydrogenation dominates, with only n = 16 showing some degree of double dehydrogenation according to (2). The other clusters with $n \geq 17$ are largely unreactive towards ethane.

The products of primary reaction are of course not necessarily stable, but may, and in many cases actually do react with a second molecule of ethane to form secondary product. While such sequential, secondary reactions were not investigated in detail, even

here one detects considerable variation from one cluster size to another. Thus already the product of the primary reaction of the monatomic rhodium cation, $Rh^+C_2H_4$ reacts again with the elimination of one H_2 molecule, forming an $Rh^+C_4H_8$ product, possibly rhodium with two ethylene ligands:

$$Rh^+C_2H_4 + C_2H_6 \rightarrow Rh^+C_4H_8 + H_2 \qquad (4)$$

On the other hand, the n = 7 cluster, for which the dominant first step reaction also was the elimination of a single hydrogen molecule, eliminates two H_2 in the secondary reaction:

$$Rh_7^+C_2H_4 + C_2H_6 \rightarrow Rh_7^+C_4H_6 + 2H_2 \qquad (5)$$

The most reactive n = 10 cluster forms relatively slowly two secondary products, $Rh_{10}^+C_4H_4$ and $Rh_{10}^+C_4H_6$, but in this case the exact secondary reactions are more difficult to untangle, since the cluster forms two primary products according to both reactions (1) and (2). It appears, though, that the minor primary product, $Rh_{10}^+C_2H_4$ must make a significant contribution, since its concentration goes quite rapidly through a maximum, and beyond about 3 seconds decreases again, as can in fact easily be seen in the Figure 3a, indicating that it is rather efficiently reacting away. Quite interesting is the case of the n = 15 cluster, which rather reluctantly dehydrogenates ethane to an $Rh_{15}^+C_2H_4$ primary product. This, however apparently reacts in a secondary reaction with the elimination of three hydrogen molecules so efficiently, that after 5 seconds the $Rh_{15}^+C_4H_4$ ion is already the most abundant product:

$$Rh_{15}^{+}C_2H_4 + C_2H_6 \rightarrow Rh_{15}^{+}C_4H_4 + 3H_2 \quad (6)$$

Mainly the clusters between 7 and 11 react efficiently with ethane in a secondary reaction with elimination of one or two hydrogen molecule, but $Rh_n^{+}C_4H_4$ complex was observed only for n = 10, 15 and 16.

As noted above, in view of the fact that a whole distribution of clusters is being reacted at the same time, the relative reaction rates can be fairly confidently determined. Table 1 also gives values for the absolute rate constants, collision frequencies determined from ADO theory and reaction efficiencies as the ratio of the two. Since two ill-defined scaling factors go into the absolute rate constant, namely the sensitivity of the ion gauge and the so-called geometry factor, which accounts for the position of the ion gauge relative to the ICR cell, the absolute values are probably reliable within 30%, while the relative rate constants deviate by less than 10%. Oxygen was present as an impurity on the order of 1-2 $\times 10^{-9}$ mbar. Absolute rate constants and efficiencies are given in Table 2 assuming a pressure $p(O_2) = 2.0 \times 10^{-9}$ mbar. On first sight, efficiencies above 100% seem to be clearly in error. However, the collision frequency is calculated from ADO theory, which assumes the reactant ion to be a point charge. Clearly, our quite sizeable rhodium clusters have considerably bigger collision cross sections than a point charge. Consequently, the real collision frequency will be higher than k_{ADO}. Still, the efficiencies are useful, and tell if the clusters react somewhat near collision frequency, or significantly below.

Tablel 1: Absolute bimolecular rate constants k_{abs}, collision frequency calculated by average dipole orientation theory k_{ADO},[16-18] and efficiencies k_{abs} / k_{ADO}.

Reactant	Product	k_{abs} (10^{-10} cm^3 s^{-1})	k_{ADO} (10^{-9} cm^3 s^{-1})	Efficiency (%)
Rh^+	$RhC_2H_4^+$	1.410	1.030	13.78
Rh_2^+	$Rh_2C_2H_2^+$	4.950	0.966	51.22
Rh_2^+	$Rh_2C_2H_4^+$	2.830	0.966	29.27
Rh_3^+	$Rh_3C_2H_2^+$	2.010	0.945	21.30
Rh_4^+	$Rh_4C_2H_4^+$	0.954	0.934	10.20
Rh_7^+	$Rh_7C_2H_2^+$	0.954	0.921	10.36
Rh_7^+	$Rh_7C_2H_4^+$	7.060	0.921	76.74
Rh_8^+	$Rh_8C_2H_2^+$	0.505	0.918	5.500
Rh_8^+	$Rh_8C_2H_4^+$	4.870	0.918	53.08
Rh_9^+	$Rh_9C_2H_2^+$	0.918	0.916	10.02
Rh_9^+	$Rh_9C_2H_4^+$	1.170	0.916	12.72
Rh_{10}^+	$Rh_{10}C_2H_2^+$	9.110	0.915	96.60
Rh_{10}^+	$Rh_{10}C_2H_4^+$	2.760	0.915	30.11
Rh_{11}^+	$Rh_{11}C_2H_2^+$	4.520	0.914	49.48
Rh_{11}^+	$Rh_{11}C_2H_4^+$	0.636	0.914	6.960
Rh_{12}^+	$Rh_{12}C_2H_2^+$	4.950	0.913	54.17
Rh_{13}^+	$Rh_{13}C_2H_2^+$	2.050	0.912	22.46
Rh_{14}^+	$Rh_{14}C_2H_2^+$	3.670	0.911	40.31
Rh_{15}^+	$Rh_{15}C_2H_4^+$	3.000	0.911	32.97
Rh_{16}^+	$Rh_{16}C_2H_2^+$	1.590	0.910	17.46
Rh_{16}^+	$Rh_{16}C_2H_4^+$	2.860	0.910	31.44
Rh_{20}^+	$Rh_{20}C_2H_4^+$	0.918	0.909	10.11
Rh_{23}^+	$Rh_{23}C_2H_4^+$	1.550	0.908	17.12

Table 2: Absolute bimolecular rate constants k_{abs}, collision frequency calculated by average dipole orientation theory k_{ADO},[16-18] and efficiencies k_{abs} / k_{ADO} for molecular oxygen addition.

Reactant	k_{abs} (10^{-10} cm^3 s^{-1})	k_{ADO} (10^{-10} cm^3 s^{-1})	Efficiency (%)
Rh_6^+	2.64	5.44	48.44
Rh_7^+	5.46	5.43	100.58
Rh_8^+	2.18	5.41	40.34
Rh_9^+	3.00	5.40	55.58
Rh_{10}^+	5.09	5.39	94.48
Rh_{11}^+	2.18	5.38	0.55
Rh_{12}^+	4.91	5.38	91.34
Rh_{13}^+	4.91	5.37	91.43
Rh_{14}^+	4.37	5.37	81.34
Rh_{15}^+	4.55	5.36	84.79
Rh_{16}^+	4.37	5.36	81.45
Rh_{17}^+	3.91	5.36	73.00
Rh_{18}^+	4.18	5.35	78.13
Rh_{19}^+	4.18	5.35	78.17
Rh_{20}^+	4.18	5.35	78.20
Rh_{21}^+	5.82	5.35	108.84
Rh_{22}^+	5.09	5.35	95.27
Rh_{23}^+	4.91	5.35	91.89

The relatively high efficiencies for a saturated hydrocarbon like ethane are somewhat at odds with the conclusions of previous investigations, for instance the trailblazing studies of El Sayed and coworkers.[19]

At this point it is perhaps useful to consider the mechanism of the molecular reactant-metal cluster reactions, occurring in binary gas phase collisions. The reactant, ethane in the present case, approaches with near thermal velocity the surface of the cluster, is accelerated by the attractive part of the intramolecular potential, “falls” into the potential well, and is then reflected on its inner, repulsive part, and if nothing else

happens, the two colliding partners will separate again unchanged. There is a finite probability that an adiabatic transition may occur from the potential of the reactant interaction potential onto a different electronic surface, leading to products - for instance a molecular hydrogen and ethylene adsorbed on the metal surface, but this requires a very efficient crossing, and extremely fast reaction which can occur on the several picosecond collision time scale.

An alternative is that during the collision an intramolecular vibrational energy redistribution, IVR, takes place, dispersing the kinetic energy originally in the one-dimensional ligand-cluster potential among other vibrational modes of the system - that is vibrational modes of the metal cluster, as well as those of the ligand. Once this happens, a much longer time scale “sticky” collision occurs. In reactants containing double or triple bonds, relatively strong interaction of the ligand π-orbitals with the metal atoms can take place, the cluster-ligand interaction potential is deep, and the density of internal states near the dissociation limit is high, making the probability of IVR occurring and a longer lived complex being formed high.

A system in which such energy redistribution has occurred still has enough energy to dissociate again, but the ligands only depart when the energy assembled in the two body interaction coordinate again exceeds the dissociation energy. The probability and rate at which this can occur depends on various properties of the system. In the first place, the lower the energy excess above that needed for dissociation, the lower will be its rate and the probability that it will occur. At least equally important is the number of degrees of freedom between which the energy was redistributed, and the density of states: in general, the deeper the interaction potential between the reactant and the cluster is, and the larger the system is, the slower and less efficient will be the dissociation.

In reactants containing double or triple bonds, relatively strong interaction of the ligand π-orbitals with the metal atoms can take place, the cluster-ligand interaction potential is deep, and the density of internal states near the dissociation limit is high, making the probability of IVR occurring and a long lived complex being formed high. Indeed, studies in the present laboratory, as well as in several others have clearly established, that complexes between metal clusters, or even monatomic ions and benzene, or similar unsaturated compounds can form readily even in the high vacuum, effectively collision-free environment of the ICR instrument. In such a long lived complex a nonadiabatic transition onto a product surface can then take place, even if the rate is relatively slow, or such complex can be completely stabilized without reacting either radiatively, or by a second collision. In saturated compounds without multiple bonds and π-orbitals, like in the present case of ethane, the interaction with the metal surface is much weaker, and the potential depth much smaller. Consequently, the probability of an IVR taking place and a longer lived collision complex being stabilized is rather small.

Consistent with the above picture, for none of the cluster sizes a stable binary complex with C_2H_6 has been detected. However, the reaction probabilities for some cluster sizes are quite high, and show wild fluctuations over the size region studied. On the other hand, for the oxygen molecule, with its multiple bond and π-orbitals, much stronger bonding to the surface can be expected, and binary complexes are observed for clusters with $n \geq 6$. For very small clusters, the number of vibrational modes in the collision complex is small, and the internal “temperature”, after the binding energy being distributed by the IVR between them is high, so that the complex is short lived, and redissociates before a stabilizing second collision, or emission of photon can take place. As the cluster size increases, so does the number of vibrational modes, and the density of states, so that above $n = 6$ the complexes with oxygen can survive and be stabilized.

The observed reactions of the clusters with ethane, and the seemingly random variations of reaction rates and branching ratios of reactions (1) and (2) as a function of number of atoms n just reflect the sensitivity of the CH bond activation and of the reaction rate to the details of the topography of the metal surface. Overall, one observes that above about n = 16 the reactivity is greatly reduced, and only a few, exceptional clusters, n = 20 and 23, still exhibit dehydrogenation reactions. This trend may represent overall the increasing coordinative saturation of the metal atoms with the increasing size of the cluster, with the reactive sizes representing clusters with awkward structure, with "ad-atoms" or "holes". Unfortunately, there is no experimental information about the structure of rhodium clusters, and also theoretical, quantum chemical computation of the geometry and other properties of species containing more transition metal atoms, with their open d-electron shells is still a very challenging problem. Clearly, a thorough computational study of the structure of at least small clusters might be of considerable interest. Figure 4 displays optimized structures of $RhCH_4^+$ and $RhC_2H_6^+$ generated from computed geometries.

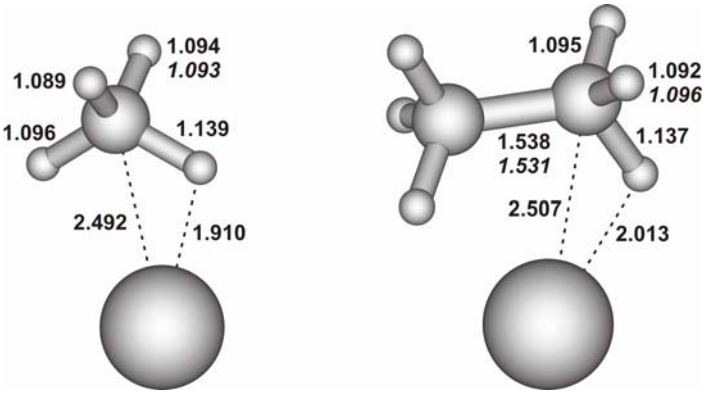

Figure 4: Optimized structures of $RhCH_4^+$ and $RhC_2H_6^+$. Bond lengths are displayed in angstroms. The zero point corrected binding energy for Rh-C_2H_6 is 85.14 kJ/mol, while for Rh-CH_4 is only 66.85 kJ/mol.

In view of the considerable reactivity of cationic rhodium cluster with ethane found here, it is of interest to compare the present results with earlier studies of the their reactions with methane.[2,10] In those studies it was shown, that with the exception of Rh_2^+ which reacts with methane with H_2 elimination and carbene formation, all the other "naked" cationic Rh_n^+ clusters were found to be completely unreactive. Interestingly, however, when one forced the reactants to form a long lived complex by ligand exchange reactions between cold $Rh_n^+Ar_m$ clusters and methane, also Rh_3^+ was found to react, yielding the dehydrogenated $Rh_3CH_2^+$ product. In the present case, instead the complex being stabilized by ligand exchange, the additional degrees of freedom, the presence of the low barrier internal rotation in ethane, and its higher binding energy as compared to methane might be responsible for extending the time scale of the collision, and making a reaction possible.

When the C_2H_6 molecule adsorbs on the cluster, the binding energy may heat the cluster sufficiently, so that the dehydrogenation can occur. As noted before, the sharply decreasing reaction rates for large rhodium cluster probably reflect the increasing degree of coordinative saturation of the rhodium atoms, but may also be due to the fact that as the cluster becomes larger, the temperature rise resulting from the adsorption of the reactant will become progressively smaller, reducing the probability that the barrier to reaction can be overcome. For large clusters the adsorption of C_2H_6 on a reactive site seems to become unfavorable, and the collision complex back-dissociates before the reaction can occur. The reason for the wild fluctuations would be the specific geometry of a certain cluster size.

5.5. Conclusions

In the present work cationic rhodium clusters in the range of about $1 \leq n \leq 25$ were generated and their reactions with ethane as a function of cluster size were investigated in an FT-ICR mass spectrometer under single collision conditions. Overall the reactivity of rhodium clusters towards ethane depends strongly on the cluster size. The primary products consist in a simple or double dehydrogenation or both for almost all the clusters, the most reactive rhodium cluster being n = 10. Rh_5^+ does not react at all with ethane and also do the larger sizes starting with 17, excepting n = 20 and n = 23. Besides the reactions with ethane, also addition of molecular oxygen, which is present in small amounts in the background gas, is observed, and comparison of the size dependence of this process with the ethane dehydrogenation provides interesting insights into the mechanisms of the occurring reactions.

5.6. References

(1) W. Andreoni, C. M. Varma, *Phys. Rew. B*, **1981**, *23 (2)*, 437-444.

(2) G. Albert, C. Berg, M.. Beyer, U. Achatz, S. Joos, G. N. Schatteburg, V. E. Bondybey *Chem. Phys. Lett.* **1997**, *268*, 235-241.

(3) C. Berg, M. Beyer, T. Schindler, G. N. Schatteburg, V. E. Bondybey, *J. Chem.. Phys.* **1996**, *104*, 20.

(4) Berg, C.; Schindler, T.; Niedner-Schatteburg, G.; Bondybey, V. E. *J. Chem. Phys.* **1995**, *102*, 4870.

(5) C. Berg, M. Beyer, U. Achatz, S. Joos, G. Niedner-Schatteburg, V. E. Bondybey, *J. Chem. Phys.* **1998**, *108*, 5398-5403.

(6) I. Balteanu, U. Achatz, O. P. Balaj, B. S. Fox, M. K. Beyer, V. E. Bondybey, *Int. J. Mass Spectrom.* **2003**, *229*, 61.

(7) D. Majumbar, S. Roszak, K. Balasubramanian, *J. Chem. Phys.* **1997,** 107, 408.

(8) D. Dai, K. Balasubramanian, *Chem. Phys. Lett.* **1996**, *263*, 703-709.

(9) W. Biemolt, A. P. J. Jansen, *J. Comp. Chem.* **1994**, *15*, 1053.

(10) M. R. Zakin, D. M. Cox, A. Kaldor, J. Chem.. Phys. **1988**, *89(2)*, 1201.

(11) I. Balteanu, O. P. Balaj, B. S. Fox, P. Godriguez, M. T. Barros, A. M. C. Mouthino, M. L. Costa, M. K. Beyer, V. E. Bonbybey, *Organometallics,* **2004**, *23*, 1978-1985

(12) A. D. Becke, *Phys. Rev. A,* **1988**, *38*, 3098.

(12) A. D. Becke, *J. Chem. Phys.,* **1993**, *98*, 1372.

(14) A. D. Becke, *J. Chem. Phys.,* **1993**, *98*, 5648.

(15) Gaussian 98 (Revision A.11), M. J. Frisch, G. W. Trucks, H. B. Schlegel, G. E. Scuseria, M. A. Robb, J. R. Cheeseman, V. G. Zakrzewski, J. A. Montgomery, Jr., R. E. Stratmann, J. C. Burant, S. Dapprich, J. M. Millam, A. D. Daniels, K. N. Kudin, M. C. Strain, O. Farkas, J. Tomasi, V. Barone, M. Cossi, R. Cammi, B. Mennucci, C. Pomelli, C. Adamo, S. Clifford, J. Ochterski, G. A. Petersson, P. Y. Ayala, Q. Cui, K. Morokuma, P. Salvador, J. J. Dannenberg, D. K. Malick, A. D. Rabuck, K. Raghavachari, J. B. Foresman, J. Cioslowski, J. V. Ortiz, A. G. Baboul, B. B. Stefanov, G. Liu, A. Liashenko, P. Piskorz, I. Komaromi, R. Gomperts, R. L. Martin, D. J. Fox, T. Keith, M. A. Al-Laham, C. Y. Peng, A. Nanayakkara, M. Challacombe, P. M. W. Gill, B. Johnson, W. Chen, M. W. Wong, J. L. Andres, C. Gonzalez, M. Head-Gordon, E. S. Replogle, and J. A. Pople, Gaussian, Inc., Pittsburgh PA, 2001.

(16) T. Su, M. T. Bowers, *J. Chem. Phys.*, **1973**, *58*, 3027-3037.

(17) L. Bass, T. Su, M. T. Bowers, *Int. J. Mass Spectrom. Ion Processes*, **1978**, *28*, 389-399.

(18) L. Bass, T. Su, W. J. Chesnavich, M. T. Bowers, *Chem. Phys. Lett.*, **1975**, *34*, 119-122.

(19) M. A. El-Sayed, *J. Phys. Chem.*, **1991**, *95 (10)*, 3898-3906.

6. Isotopically Enriched Platinum Cluster Studies. Reactions of Platinum Clusters $^{195}Pt_n^{\pm}$, n = 1 - 23, with N_2O and CO

6.1. Introduction

Transition metals and their compounds, with their multitude of oxidation states, are efficient and frequently used catalysts. The reactions of ionic metal clusters, in particular those involving transition metals, with small gas phase molecules represent convenient, relatively simple models for heterogeneous catalysis, and for these reasons they were in the last two decades extensively investigated by mass spectrometry.[1-5] Platinum, palladium and rhodium are useful dehydrogenation catalysts,[6,7] but are also used extensively in removing toxic oxides such as carbon monoxide or nitrogen oxides from automotive exhaust.[8,9]

Several groups have investigated dehydrogenation of simple hydrocarbons, such as methane, ethane, ethylene or acetylene on platinum cluster ions, and their reactions with various simple molecules, like CO, N_2O, or CH_4 .[7,9-22] The Garching group has previously studied methane activation by gas phase $Pt_n^{\pm}$ cluster ions in the n = 1-9 size range.[7] Schwarz and coworkers succeeded, by mass-selecting the most intense peak, and then thermalizing the ions in argon collisions, in studying the reactions of $^{195}Pt_n^+$ with N_2O and other small molecules up to n = 5.[9] Larger clusters up to n = 30 have also been investigated in flow reactors,[11,21] albeit without resolving the individual isotopomers, which made interpretation of the data somewhat difficult. Heiz et al. succeeded in depositing size selected platinum clusters with up to 20 atoms on surfaces and investigated their chemical reactivity.[23,24] Chemisorption

of CO on smaller platinum clusters was studied in a flow tube reactor[12] and using photoelectron spectroscopy.[25] Irion and coworkers demonstrated catalytic formation of benzene from ethylene catalyzed by Fe_4^+ in the gas phase,[26] where collision-induced desorption of C_6H_6 from the cluster was necessary to close the catalytic cycle. Ervin and coworkers demonstrated that the elementary steps of the catalytic cycle of CO oxidation with N_2O are possible on anionic platinum clusters.[12-14,17] Schwarz and coworkers showed that the platinum cation Pt^+ already exhibits catalytic activity, including full cycles of CO and methane oxidation.[27-33] Andersson and Rosén provided strong evidence for catalytic oxidation of H_2 with O_2, forming H_2O in a flow reactor, albeit without resolving the detailed kinetics of the reaction.[21]

While gas phase reactivity studies on metals like niobium or rhodium can easily be done for clusters of sizes ranging up to thirty atoms,[6,34,35] large clusters of platinum and palladium have been studied in less detail. The reason for this is that unlike rhodium or niobium, which are monoisotopic elements, both palladium and platinum have six stable isotopes each. For larger clusters, this very quickly leads to dilution of the signal among many isotopomers, and overlapping of the products with the reactants. Both effects together so far have limited the cluster sizes accessible in reactivity studies. All works in which the reactivity was probed in the gas phase by mass spectrometry with at least unit mass resolution, have therefore been restricted to smaller clusters, with ten atoms or less.[7,9,14,19,20,22]

A laser vaporization source requires only minor amounts of materials, permitting work with isotopically enriched samples.[36] A first step in each heterogeneous catalytic process is adsorption of the reactants on the surface of the metal. In the present chapter highly isotopically enriched platinum was used to investigate the reactions of $^{195}Pt_n^{+/-}$ clusters, n = 1-24, with small molecules like N_2O and CO as well the saturation reactions with CO and

catalytic oxidation of CO on gas phase platinum clusters.

6.2. Experimental Details

In the present study isotopically enriched platinum (97.28% ^{195}Pt, Oak Ridge National Laboratories) was used to investigate the reactions of $^{195}Pt_n^{+/-}$ clusters, n = 1 - 24, with N_2O and CO under binary collision conditions in a Fourier tranform ion cyclotron resonance (FT-ICR) mass spectrometer. The platinum sponge was pressed into a disk and subjected to zonal melting. The resulting pearl was rolled into a foil which was used as a target for the home-built laser vaporization source.[35-39] In the source, the firing of the laser is synchronized with a helium pulse from a home-built piezo-electric valve. From the laser generated plasma, cold clusters form in the supersonic expansion of the high pressure gas into high vacuum. Ionic clusters are guided by a series of electrostatic lenses through several stages of differential pumping, and trapped and stored inside the ICR cell in the ultrahigh vacuum of the FT-ICR mass spectrometer. For each mass spectrum, clusters generated in 20 laser shots over a period of 2 s are accumulated in the cell. To study ion-molecule reactions, the pressure inside the ICR cell was raised from its base value of about 1×10^{-10} mbar to a constant value of 9.0×10^{-9} mbar by controlled admission of the reactant gas N_2O (99.5%, Messer Griesheim) at room temperature, to 4.5×10^{-9} mbar or to a higher value of 5.1×10^{-8} mbar for the saturation experiments, by controlled admission of carbon monoxide, CO (Messer-Griesheim 99.997%) at room temperature. For the catalytic oxidation of CO on platinum clusters the reactant gases CO (99.98%) and N_2O (99.8%) were admitted via two needle valves to the UHV region of the FT-ICR instruments at constant partial pressures. In the 1:6 mixture, $p(CO) = 1.6 \times 10^{-8}$ mbar and $p(N_2O) = 9.9 \times 10^{-8}$ mbar. In the 5:3 mixture, $p(CO) = 1.6 \times 10^{-8}$ mbar and $p(N_2O) = 9.8 \times$

10^{-9} mbar. Mass spectra were acquired after a series of varying reaction delays. A crude selection of a cluster size range was accomplished by adjusting the timing of the cell trapping, effectively selecting a fraction of ions within a certain time of flight window from the source to the ICR cell. Relative rate constants were obtained by fitting the experimental data to pseudo-first order reaction kinetics, and converted to absolute rate constants and reaction efficiencies using the average dipole orientation (ADO) theory.[40-42]

6.3. Results and Discussion

Previous studies of ionic metal cluster chemistry have demonstrated that only in a very few exceptional cases does a chemical reaction result in a loss of a metal atom from the cluster, and that metal clusters otherwise react as unbreakable units. This is quite helpful in making the data interpretation more unambiguous, and it also makes it possible to study the entire, usually fairly broad size distribution of clusters produced in the source, in a single experiment, without mass selection. In this way, the clusters of different sizes are investigated under exactly identical experimental conditions, which makes comparisons and measurement of relative reaction rates more meaningful.

The advantage of using isotopically enriched platinum is exemplified by the n = 7 cluster in Figure 1. In the top trace, obtained with a non-enriched sample, the intensity is distributed over at least seventeen isotopic peaks. In the bottom panel, obtained with the isotopically enriched target, a strong $^{195}Pt_7^+$ peak is present. The weak side peaks corresponding to $^{194}Pt^{195}Pt_6^+$ and $^{195}Pt_6{}^{196}Pt^+$ clusters exhibit intensities that are consistent with the specified enrichment grade of the sample.

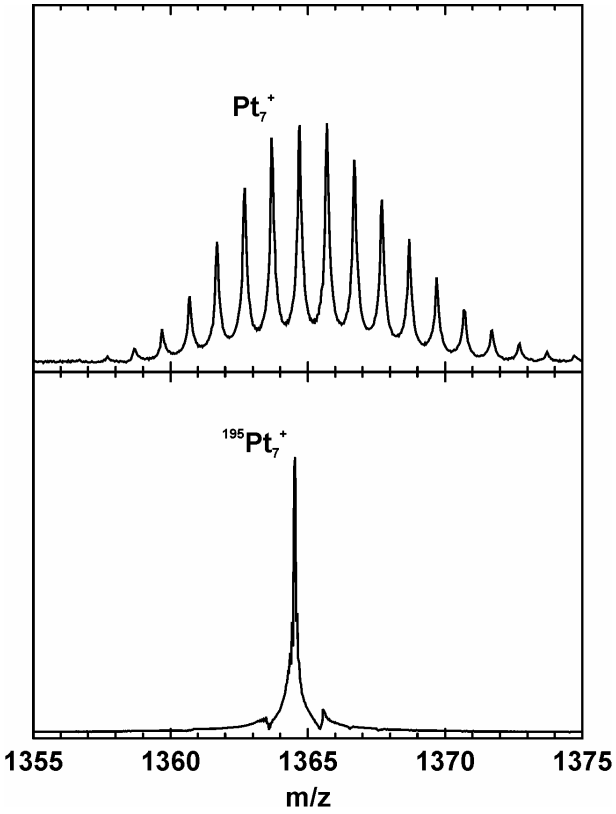

Figure 1: Mass spectrum of Pt_7^+ obtained with a target with natural isotope distribution (top) and ^{195}Pt enriched to 97.28% (bottom).

6.3.1. Reactions of Platinum Clusters $^{195}Pt_n^{\pm}$, n = 1 - 23, with N_2O

A typical mass spectrum of cationic clusters $^{195}Pt_n^+$ with n = 10 - 21 after a reaction delay of 5 s is shown in Figure 2. The reactions occurring are quite simple, and similar to those observed previously for smaller clusters:[9,14] Oxide clusters, $^{195}Pt_nO^+$ are formed and N_2 is lost. Apparent is a size-specific variation in reactivity. While n = 11, 12, 15 and 20 are very reactive, n = 10, 13, 14, 19 and 21 show very little to no reactivity. One can also see that in the case of n = 18, and to some extent n = 16, reaction with a second N_2O occurs, resulting in the loss of another N_2 molecule, and formation of a dioxide cluster, $^{195}Pt_nO_2^+$.

More detailed insight and quantitative reaction rates are obtained by actually fitting the

time-intensity profile to pseudo-first order kinetics, as exemplified in Figure 3. $^{195}Pt_8^+$ is shown in the top panel. In this case, one can follow an exponential decay of the reactant cluster, and the oxide product, $^{195}Pt_8O^+$ reacts further with a second molecule of N_2O, resulting in a dioxide cluster $^{195}Pt_8O_2^+$. The figure also reveals, that already at a nominal time t = 0 some product is present. This is due to reactions occurring during the cluster accumulation period. As a second example, in the bottom panel the exponential decay of the $^{195}Pt_{20}^+$ cluster is shown and concurrent growth of the only product, $^{195}Pt_{20}O^+$. The reaction proceeds faster for n = 20 than for n = 8, but only one reaction step is observed.

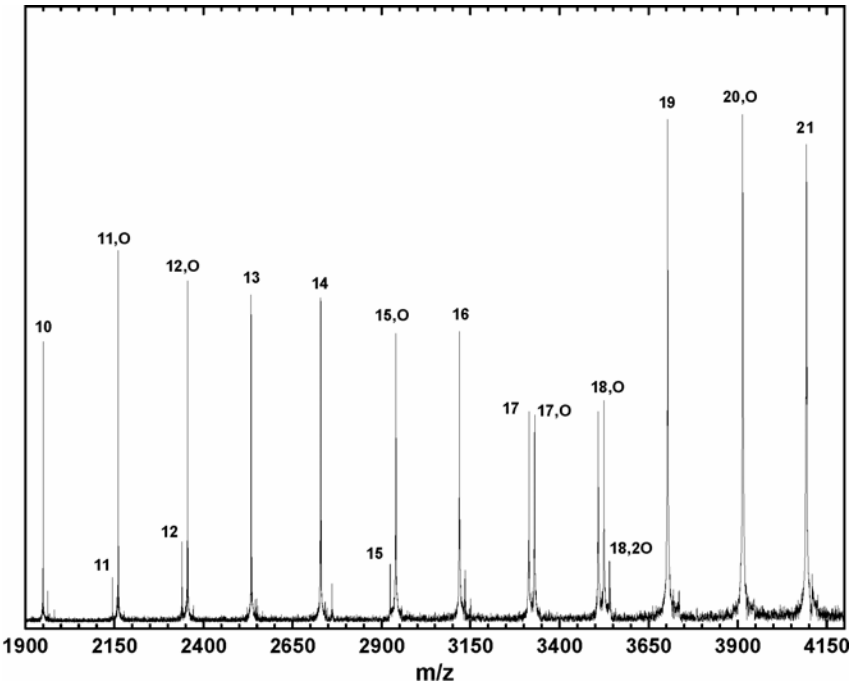

Figure 2: Mass spectrum of the reaction of large cationic platinum clusters Pt_n^+, n = 10 - 21, with N_2O after 5 s, using the isotopically enriched target. Peaks are labelled with their cluster size and reaction product O or 2O. The clusters show a quite irregular reactivity pattern, not only with respect to their rate constant, but also to the number of reaction steps they undergo. The peaks accompanying n = 10 and n = 14 are $Pt_{10}C^+$ and $Pt_{14}C_2^+$, presumably formed in reactions with minor hydrocarbon impurities in the ion source.

Overall, the chemistry pattern found for all of the clusters, both anions and cations, within the range studied is quite simple. No evidence for loss of a platinum atom from the cluster was observed, which would in the present analysis lead to a curvature of the reactant ion decay in the semi-logarithmic plots of Figure 3. When reaction upon collision with N_2O does occur, the N_2 molecule is lost, and the single oxygen atom oxidizes the cluster. While in some cases, $^{195}Pt_nO^{\pm}$ appears unreactive, in others it reacts further to form the respective

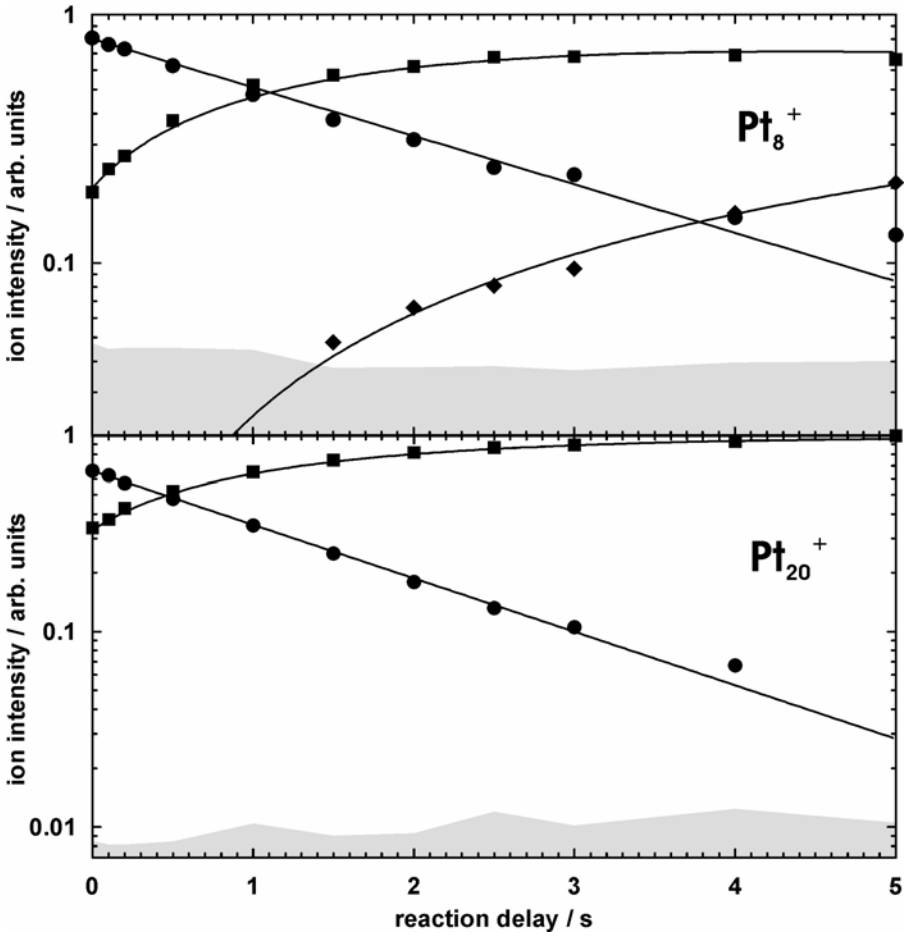

Figure 3: Kinetic fit of the reaction of Pt_8^+ (top) and Pt_{20}^+ (bottom) with N_2O (● Pt_n^+ , ■ Pt_nO^+, ◆ $Pt_nO_2^+$). While Pt_{20}^+ reacts only once, forming $Pt_{20}O^+$, Pt_8^+ undergoes a second reaction step. The grey area denotes the noise level.

dioxide, $^{195}Pt_nO_2^{\pm}$. In a few cases, also a third step resulting in $^{195}Pt_nO_3^{+}$ is detected, so that the reactions can be described by the simple equation pattern:

$$^{195}Pt_n^{\pm} + N_2O \rightarrow {}^{195}Pt_nO^{\pm} + N_2 \quad (1)$$

$$^{195}Pt_nO^{\pm} + N_2O \rightarrow {}^{195}Pt_nO_2^{\pm} + N_2 \quad (2)$$

$$^{195}Pt_nO_2^{\pm} + N_2O \rightarrow {}^{195}Pt_nO_3^{\pm} + N_2 \quad (3)$$

Figure 4 shows a graphical comparison of the observed rates, on a logarithmic scale, of the first reaction step (1) for cations and anions as a function of cluster size. Numerical data for the first reaction step are summarized in Table 1, and for the second, and in the few cases it is observed, third reaction step in Table 2. One finds that the rates of the reaction, as well as the number of oxidation steps observed in the time frame of the experiment vary appreciably, and in a seemingly random manner from cluster to cluster, and the reactivity pattern is also strongly dependent on the cluster charge.

Among the cations, the n = 6 and 20 clusters exhibit the fastest reaction according to equation (1), with rates above the ADO collision efficiency. This indicates that the collision probability for large clusters is higher than predicted by the ADO theory. In neither case does the primary product $^{195}Pt_nO^{+}$ react further, and after about five seconds, these clusters are almost completely converted to the primary product. The clusters n = 7, 8, 11, 12, 15 exhibit an appreciable reactivity, with the primary product reacting further (2). On the other hand, no reaction could be established for clusters n = 10, 14, 23, and upper limits for their reactivity are derived. Also rather unreactive are very small clusters $^{195}Pt_n^{+}$, $n \leq 5$, with n = 1, 2, and 5 reacting only marginally, and no detectable reaction for n = 2 - 4. For n = 15 and n = 18, also

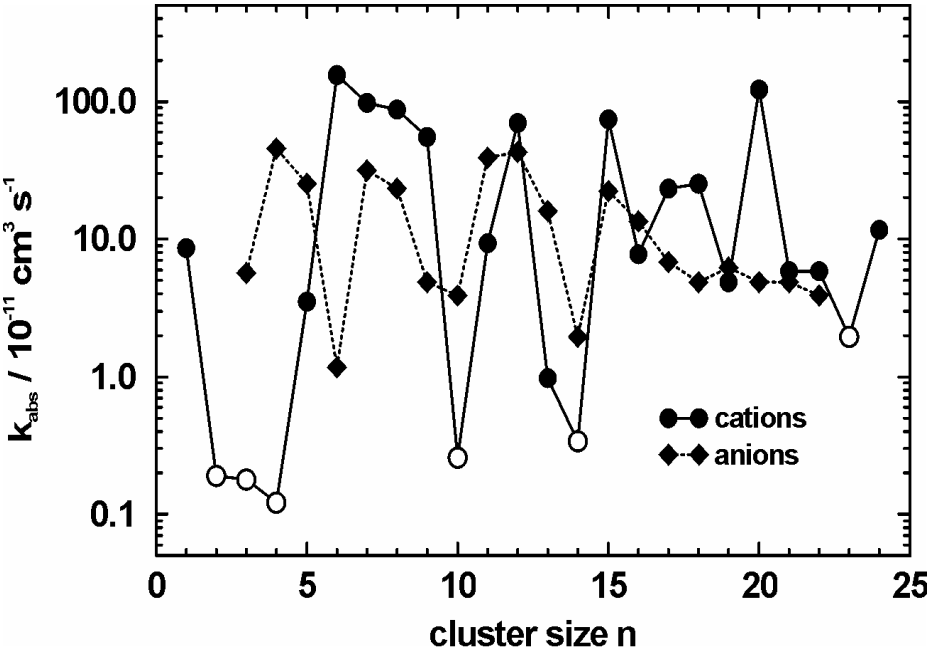

Figure 4: Absolute rate constants of the first reaction step of $Pt_n^{\pm}$ clusters on a semi-logarithmic scale. Open symbols denote upper limits of the rate constant for cluster sizes where no reaction was observed.

a third reaction step, according to (3), is observed, which is in both cases faster than the second step.

The negative cluster ions overall react somewhat slower than the cations, and the size dependence is considerably different. Interestingly, the n = 6 cluster, which was the fastest reacting cluster among the cations, represents in fact a deep reactivity minimum among the anions, with the $^{195}Pt_6^-$ cluster reacting twenty times slower than the neighboring n = 4, 5, 7, 8 clusters. The n = 4 cluster, which is completely unreactive among the cations, is in fact the fastest reacting anion, and also exhibits a fast second reaction step to form $^{195}Pt_4O_2^-$. On the other hand, the n = 10 and 14 clusters, which appear completely inert as cations, are also as anions quite unreactive.

Table 1: Absolute rate constants and efficiencies calculated from ADO theory[40-42] for reactions step (1) of ionic platinum clusters.

	Cations		Anions	
Cluster	$10^{11}k_{abs}/cm^3s^{-1}$	Efficiency (%)	$10^{11}k_{abs}/cm^3s^{-1}$	Efficiency (%)
$Pt_1^{+/-}$	8.58	12.6	-	-
$Pt_2^{+/-}$	<0.191	<0.295	-	-
$Pt_3^{+/-}$	<0.179	<0.281	5.66	8.88
$Pt_4^{+/-}$	<0.122	<0.193	45.8	72.7
$Pt_5^{+/-}$	3.51	5.60	25.4	40.4
$Pt_6^{+/-}$	156	250	1.17	1.80
$Pt_7^{+/-}$	97.5	156	31.8	51.0
$Pt_8^{+/-}$	87.8	141	23.4	37.6
$Pt_9^{+/-}$	55.6	89.5	4.88	7.84
$Pt_{10}^{+/-}$	<0.258	<0.416	3.90	6.28
$Pt_{11}^{+/-}$	93.6	151	39.0	62.9
$Pt_{12}^{+/-}$	70.2	113	42.9	69.3
$Pt_{13}^{+/-}$	0.975	1.58	16.0	25.8
$Pt_{14}^{+/-}$	<0.339	<0.548	1.95	3.15
$Pt_{15}^{+/-}$	74.1	120	22.4	36.3
$Pt_{16}^{+/-}$	7.80	12.6	13.5	21.8
$Pt_{17}^{+/-}$	23.4	37.9	6.83	11.1
$Pt_{18}^{+/-}$	25.4	41.1	4.88	7.90
$Pt_{19}^{+/-}$	4.86	7.89	6.24	10.1
$Pt_{20}^{+/-}$	123	199	4.88	7.90
$Pt_{21}^{+/-}$	5.85	9.48	4.88	7.90
$Pt_{22}^{+/-}$	5.85	9.48	3.90	6.32
$Pt_{23}^{+/-}$	<1.95	<3.16	-	-
$Pt_{24}^{+/-}$	11.7	19.0	-	-

Table 2: Absolute rate constants and efficiencies calculated from ADO theory[40-42] for reaction steps (2) and (3) of ionic platinum clusters.

	Cations		Anions	
Cluster	$10^{11}k_{abs}/cm^3s^{-1}$	Efficiency (%)	$10^{11}k_{abs}/cm^3s^{-1}$	Efficiency (%)
$Pt_1O^{+/-}$	11.9	17.6	-	-
$Pt_3O^{+/-}$	-	-	31.2	49.1
$Pt_4O^{+/-}$	-	-	33.2	52.6
$Pt_5O^{+/-}$	11.3	18.0	1.37	2.18
$Pt_6O^{+/-}$	-	-	35.1	56.2
$Pt_7O^{+/-}$	48.8	78.2	5.66	9.07
$Pt_8O^{+/-}$	13.7	21.9	4.68	7.52
$Pt_{10}O^{+/-}$	-	-	19.5	31.4
$Pt_{11}O^{+/-}$	2.15	3.46	-	-
$Pt_{12}O^{+/-}$	3.32	5.35	1.37	2.20
$Pt_{13}O^{+/-}$	-	-	1.95	3.15
$Pt_{15}O^{+/-}$	3.90	6.31	1.95	3.15
$Pt_{16}O^{+/-}$	9.75	15.8	5.85	9.47
$Pt_{17}O^{+/-}$	-	-	5.85	9.47
$Pt_{18}O^{+/-}$	11.7	19.0	1.95	3.16
$Pt_{19}O^{+/-}$	5.85	9.48	2.93	4.74
$Pt_{20}O^{+/-}$	-	-	1.95	3.16
$Pt_{21}O^{+/-}$	3.90	6.32	-	-
$Pt_{22}O^{+/-}$	15.6	25.3	-	-
$Pt_{15}O_2^{+/-}$	31.2	50.5	-	-
$Pt_{18}O_2^{+/-}$	12.1	19.6	-	-

To summarize the observations, one can understand the reactions as a decomposition of the nitrous oxide on the metal cluster surface, yielding an oxygen atom and molecular N_2. While the oxygen atom oxidizes the platinum, the weakly bound nitrogen is released. No stabilization of the undecomposed N_2O on the surface was observed, and no trace of products containing nitrogen was seen. The nearly three orders of magnitude wide variation in the reaction rates between various clusters may reflect their structural differences, and the presence of differently efficient “sites” on the cluster surface. The fact that anions and cations behave differently may suggest considerable differences between their structures.

For small anions, n = 3 - 7, where our data overlap with earlier results of Hintz and Ervin,[13,14] as well as for cations, n = 1 – 5, measured by Schwarz and coworkers,[9] there is good quantitative agreement in the measured rates. Over the entire range of sizes explored, addition or subtraction of a single atom can change the reactivity by orders of magnitude.

6.3.2. Saturation Reactions of Platinum Clusters $^{195}Pt_n^{+/-}$, n = 1 - 24, with CO

As noted above, one of practical uses of platinum catalysts involves conversion of carbon monoxide to CO_2, and here is presented the first, necessary reaction step, that is adsorption of CO on the catalyst surface, by letting the $Pt_n^{+/-}$ clusters in the size range of n = 1 - 23, to interact with gaseous carbon monoxide. In a typical experiment, the clusters are first accumulated over about 20 laser pulses, and the spectrum is then measured first immediately after the completed accumulation at the nominal time t = 0, and measurements are then repeatedly made allowing various times, up to about 60 seconds for the reaction to occur. Over the entire size range studied, both for anionic and cationic clusters, the only reaction observed is addition of the CO to the cluster, as exemplified by the data shown in the Figure 5, which shows a part of the cationic cluster size distribution between 8 to 12 platinum atoms, first at the nominal t = 0 time in panel a), and then after 2 and 3 s delays in Figure 5b and 5c, respectively.

The advantage of using isotopically highly enriched platinum metal is apparent from the spectra. If a sample with natural isotopic abundance is used, the signal for, for instance, the n = 12 cluster, as well as for each of its product, would be distributed over nearly 20 isotopic peaks, with the situation becoming progressively worse for the still larger clusters. The product peak groups for subsequent numbers of CO ligands would overlap and

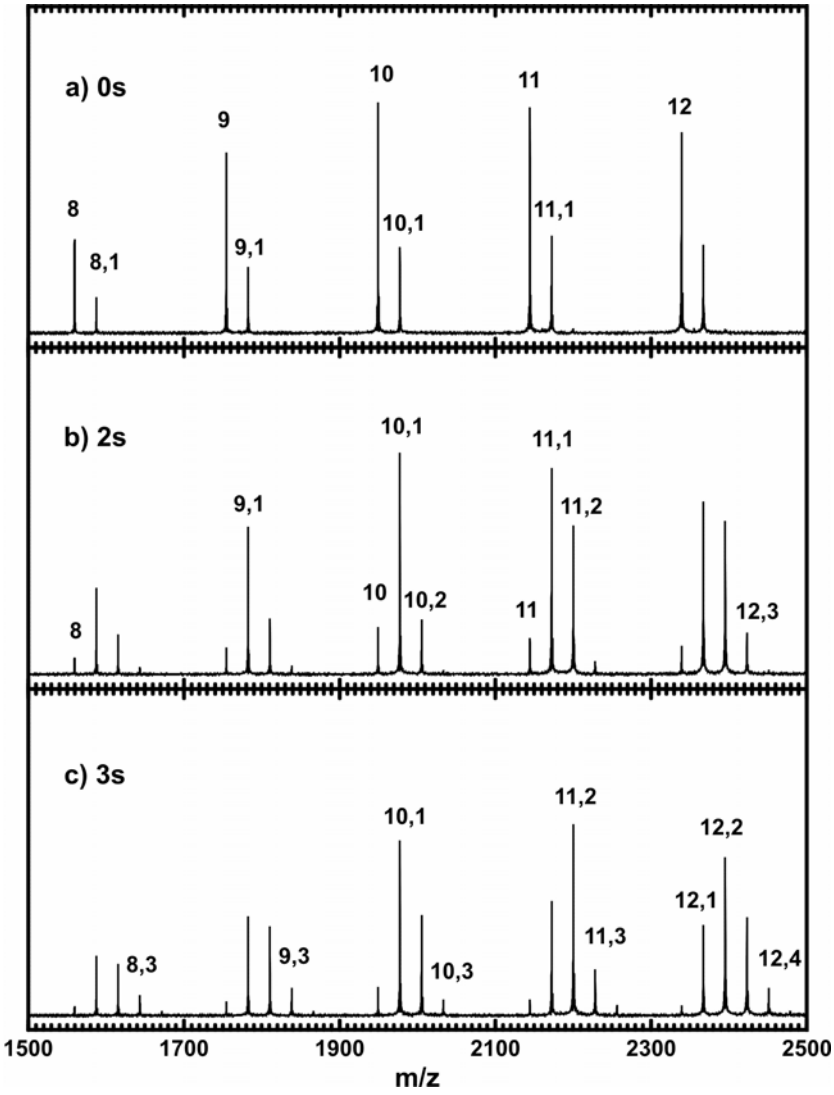

Figure 5: Mass spectra showing cationic clusters Pt_n^+, $8 \leq n \leq 12$ and their reaction products $Pt_n(CO)_m^+$ at the nominal time t = 0 (a) and after reaction delays of 2 s (b) and 3 s (c). The numbers denote the species n, m. The only reaction products correspond to the sequential addition of carbon monoxide to the clusters, $Pt_n(CO)_m^+$.

quantitative data evaluation would be impossible. With the enriched sample used here, one prominent peak appears for each reactant cluster, as well as for each of its reaction products, leading to quite clear, unambiguous spectra.

Since the CO reactant is continuously present in the trap even during the cluster accumulation, one can clearly see already in Figure 5a reaction products, that is clusters containing adsorbed CO, since the nominal t = 0 actually corresponds to approximately 0.5 second reaction delay. One can also clearly see by examining Figure 5b and Figure 5c that the reaction does not stop after adsorbing a single molecule of CO, but that consecutive adsorbtions of additional carbon monoxide take place:

$$Pt_n (CO)_m^{+/-} + CO \rightarrow Pt_n(CO)_{m+1}^{+/-} \qquad n = 1 - 24,\ m \leq n + 2 \qquad (1)$$

One can see that after 2 s in Figure 5c almost all the bare clusters have already reacted, and products with up to four CO molecules are easily observable.

By allowing the clusters to react for various time delays, one can follow the course of the reactions, and typical data of reactant concentration versus time are exemplified for the Pt_8^+ cationic cluster by the Figure 6. By least square fitting the decay of the original bare cluster signal at the early reaction times, one can extract the reaction rate for adsorption of the first carbon monoxide molecule on the cluster. It can be seen in the Figure 6, that the Pt_8^+ reactant decay is not a perfect exponential, and the fit quality can be improved by assuming the decay is a sum of two, or even more exponentials. This could, of course imply the presence of two different isomeric structures, or several electronic states. More probably, however, it simply reflects a distribution of clusters with different internal energies and vibrational temperatures.

Such measurements and fits as shown in the Figure 6 were carried out for all the clusters up to n = 23, relative rate constants, both for the anions and the cations were extracted, converted into absolute rate constants and summarized in Figure 7. Small cationic

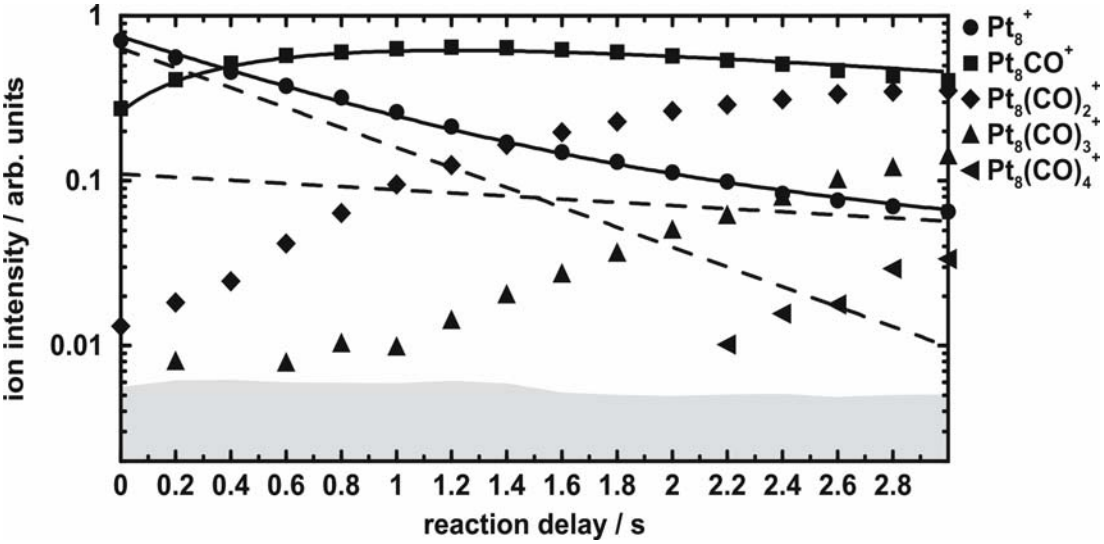

Figure 6: Time profile for the reaction of Pt_8^+ with CO. The only reaction observed is sequential addition of CO to the cluster. The relative rate constant for the first reaction step is: $k_{rel} = 1.39\ s^{-1}$. Grey shaded area denotes the noise level.

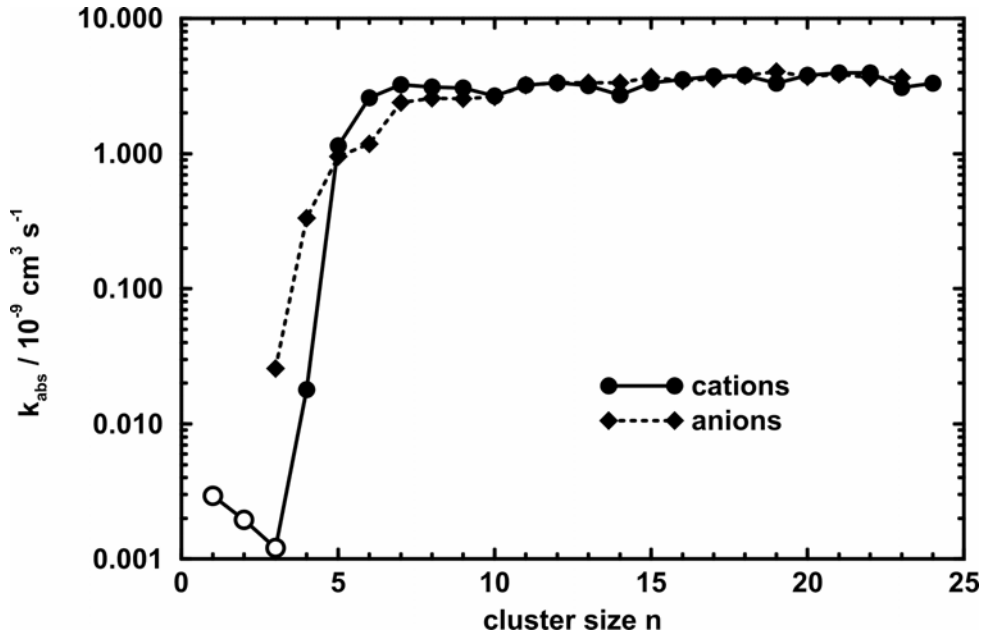

Figure 7: Absolute rate constants of the first reaction step of $Pt_n^{+/-}$, n = 1 - 24. Open symbols denote upper limits of the rate constant for the cluster sizes where no reaction was observed.

clusters, n = 1 - 3 are almost unreactive, and only a rather slow reaction is observed for n = 4. For the next larger cluster, n = 5, the rate increases by nearly an order of magnitude, and starting with n = 6 all clusters adsorb CO very efficiently, with the rate of the reaction probably approaching the collisional rate. The lack of reactivity of the small clusters almost certainly does not represent a lack of bonding between the small clusters and CO, but rather the difficulty of stabilizing the hot Pt_n^+-(CO) complex in the high vacuum, nearly collision free environment. With increasing size of the cluster and number of atoms, the internal density of states increases drastically, so that the internal energy of the collision complex can be redistributed, and it can survive long enough to be stabilized either by infrared radiation, or by a subsequent collision.

Somewhat differently from the cationic clusters behave the anions. The anion monomer and dimer are not produced in the source in appreciable quantities, but the anion trimer, unlike the cation trimer, already exhibits an observable reactivity. Also for the anions, the reaction rates increase with cluster size, however the increase is more gradual than in the cations, and only for n > 10 does the reaction rate reach a nearly constant value, with all the large anions and cations reacting with almost identical rates basically independent of the cluster charge. The slightly different behavior of the anions may be due to the negative charge on the surface of the small cluster hindering the reaction, since CO is binding with the negative end of the dipole $C^{\delta+}O^{\delta-}$, with the effect ceasing in the larger clusters, where the negative charge is distributed over a larger cluster surface.

As can be clearly seen in Figures 5 and 6, the reaction of the clusters with CO does not end with the adsorption of a single CO, but it continues according to equation (1) further, with already after 3 seconds products with up m = 5, that is with five adsorbed carbon monoxide molecules being observable. Useful information about the chemical properties of the clusters,

with possibly some insights into their structure can provide saturation experiments, that is establishing the maximum number of adsorbate molecules which can be attached to the cluster surface.[12] In order to establish this number, the pressure in the ICR cell was increased by roughly an order of magnitude to about 5×10^{-8} mbar, in order to reach the saturation point in an experimentally manageable length of time. Typical data from such a saturation experiment for n = 8, that is again for the Pt_8^+ cation, where the products were followed for over 50 seconds, are presented in the Figure 8, and plotted graphically in Figure 9. At the higher pressure already after 2 s products with up to m = 8 are observed, with most intense being clusters with m = 2 - 4. After additional 3 seconds, m = 8 clusters are dominant, and also weak signals due to m = 9 and m = 10 are detectable. Finally, after 30 seconds, almost all clusters have been converted to m = 10, that is each of the original Pt_8^+ cations has adsorbed ten CO molecules, and only a few percent of the m = 9 cluster remain. After still longer times, traces of m = 11 and m = 12 clusters are detectable.

More insight into the occurring processes can be gained by examining the Figure 9, which is a graphic representation of the mass spectroscopic data, plotting ion intensities as a function of time. One sees that the original Pt_8^+ cluster adds CO molecules one by one, and is gradually converted to the m = 8, and eventually m = 10 cluster, $Pt_8^+(CO)_{10}$. Just by superficially examining the curves in the Figure 9 one can see that the adsorption according to the reaction (1) is initially fast, but decreases with increasing value of m. This trend can, of course, be easily qualitatively understood. Initially the entire surface of the cluster is free, and so the CO molecule colliding with the cluster will inevitably come to contact with bare metal. As the value of m increases, however, the surface becomes covered by CO, and the probability of direct Pt-gas phase molecule contact decreases proportionately. The new CO ligand is less

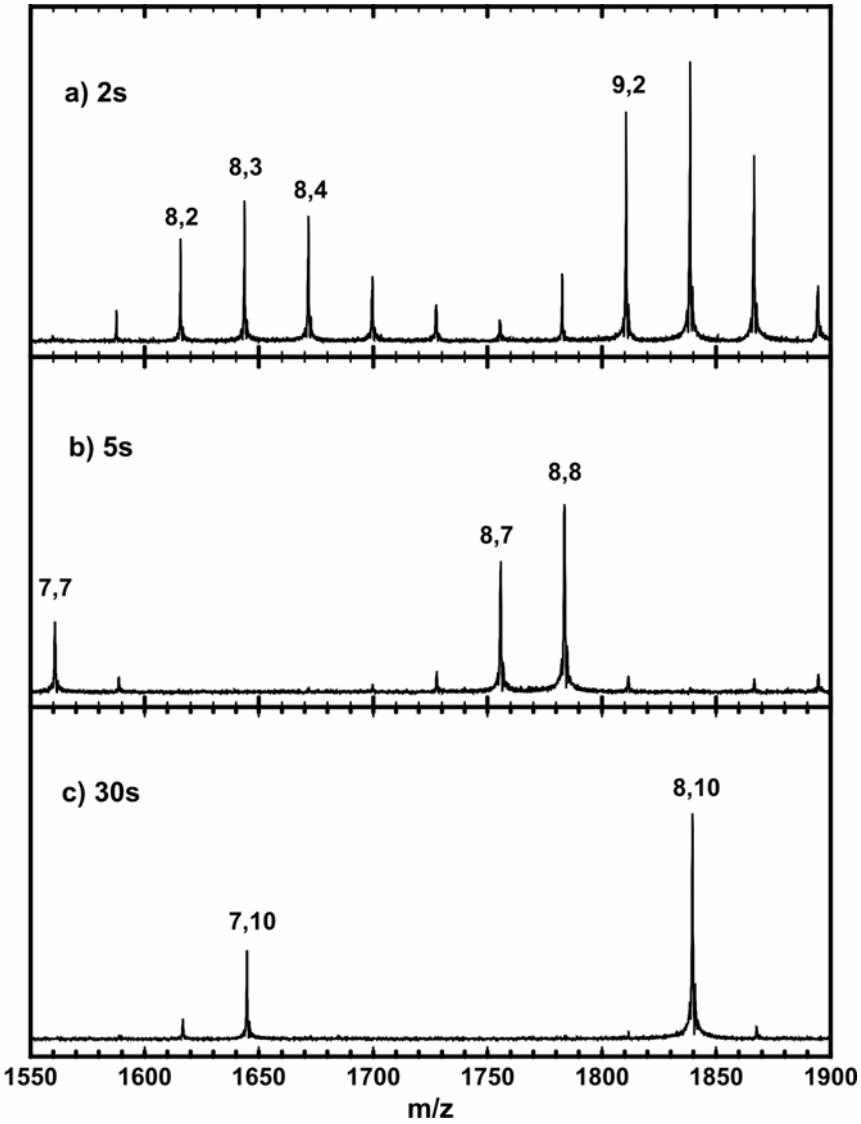

Figure 8: Mass spectra showing Pt_8^+ and its products after reaction delays of 2s (a), 5s (b) and 30s (c). After 30s almost all the clusters have been converted to m = 10.

likely to adhere to already present CO molecules, and furthermore, a ligand exchange type reaction becomes possible, where the incoming CO ligands with excess energy will dislodge an already present CO, resulting in no net increase in the m value.

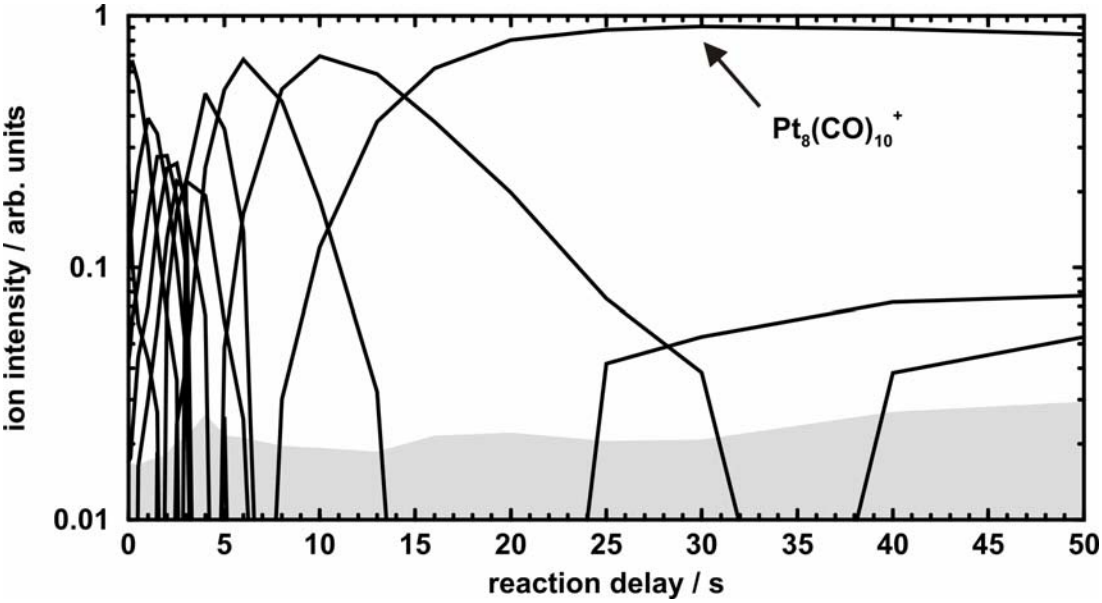

Figure 9: Time profile for the reaction of Pt_8^+ with CO. The adsorption of CO molecules is initially fast, but decreases with increasing the value of m. After very long time weak signals appear beyond the saturation product, m = 10, however they do not grow further.

The most conspicuous change in the rate of further adsorption occurs after m = 8 is reached, that is after there is just one CO ligand per platinum atom. Examination of the structure of metal carbonyls reveals, that the CO ligands can be bound to metal surface in a variety of ways, as a “terminal” CO bound to a single atom, or as an “edge” atom, bound to two surface atoms, or finally as a “face” atom, simultaneously to three neighboring atoms on the metal surface. It is interesting to note that at least for the Pt_8^+ cluster, the most noticable change in rate takes place after one CO ligand per atom has been adsorbed, and perhaps this reflects the change in ligand bonding, and change in the corresponding binding energies for the ligands 9 and 10. Finally, as can be seen in Figure 9, after very long times weak signals appear beyond the m = 10 saturation peak, due to m = 11 and 12 species. These, however, do not seem to grow further. They might be attributed to the presence of a minor quantity of an isomeric structure, but much more likely they are due to the establishment of a stationary

state, where a very weakly bound 11^{th} or 12^{th} ligand can be transiently attached, but again lost in subsequent collisions.

Data similar to those presented in Figure 8 and Figure 9 have been acquired for anionic and cationic clusters up to n = 24, and these results are summarized in Figure 10 and Table 3. A superficial glance reveals that the "saturation" number m_{max} increases roughly linearly with n, the number of atoms in the cluster, but the increase is not quite smooth, and not even always monotonic: the n = 5 cation saturates at m = 7, while n = 4 at m = 8, and similarly n = 22 saturates at m = 23, less than the m_{max} = 24 saturation for n = 21.

Even at the higher pressure used in the "saturation" experiment, the n = 1 - 3 cations are essentially nonreactive. Very small signals due to the m = 1 and 2 species can be detected, but they do not grow significantly with time, again suggesting a stationary state where the rate of attachment is matched by a similar rate of fragmentation. It is interesting to note, that there is not necessarily a clear correlation between the rate of attachment of the first ligand, and the saturation value. As noted above, the n = 3 anion, Pt_3^- adsorbes the first ligand very slowly, but then relatively rapidly attaches five further CO, saturating as an m = 6, $Pt_3(CO)_6^-$ complex. The explanation clearly again lies in the density of states argument. In Pt_3^- itself, the density of states is small, and it is difficult to stabilize the collision complex before it can re-dissociate. On the other hand, once one or several CO ligands are present, the density of vibrational states increases drastically, so that additional ligands can be attached, and the cluster can be radiatively or collisionally stabilized with a relative ease. Among the cations, the first clearly reactive species Pt_4^+ adds sequentially CO molecules until saturation is reached at m = 8, that is a saturated product $Pt_4(CO)_8^+$ is obtained. The largest investigated species was Pt_{24}^+, which saturated at 26 CO molecules adsorbed.

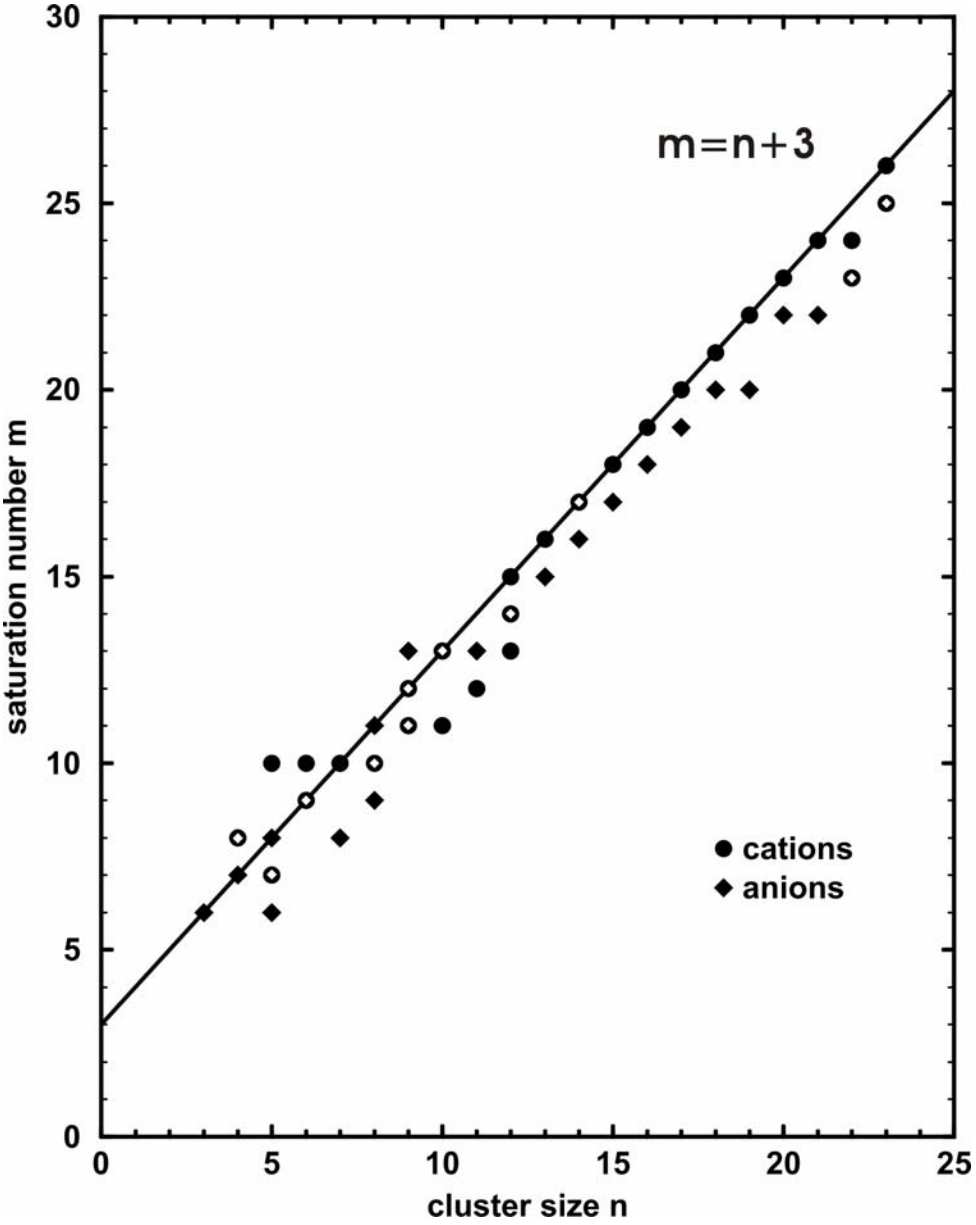

Figure 10: Saturation numbers m plotted as a function of cluster size n for both cations (circles) and anions (diamonds). m increases roughly linearly with n, plot line: m = n + 3 represents the upper limit for most clusters

Table 3: Saturation number m for the reaction of ionic platinum clusters $Pt_n^{+/-}$ with CO.

Cluster size n	Saturation number m	
	Cations	Anions
1	-	
2	-	
3	-	6
4	8	7, 8[f)]
5	7, 10	6, 7, 8[b)]
6	9, 10[a)]	9
7	10	8
8	10	9, 10, 11[d)]
9	11, 12[b)]	11, 12, 13[e)]
10	11, 13[a)]	13
11	12	13
12	13, 14, 15[b,c)]	14
13	16	15
14	17	16, 17[b)]
15	18	17
16	19	18
17	20	19
18	21	20
19	22	20
20	23	22
21	24	22
22	23, 24[b)]	23
23	25, 26[b)]	

[a)] m = 10 appears after 200s.
[b)] no change in relative abundance between 150s and 300s reaction delay.
[c)] only m = 13 reaches 100%.
[d)] only m = 11 reaches 100%.
[e)] m = 12, 13 grow slowly.
[f)] slow increase for m = 8, after longer time it may reach the maximum.

It might be noted, that seven CO ligands have a nominal mass of 196 AMU, only one unit more than the mass of the ^{195}Pt atom, and thus one might worry about overlap of the addition products of one cluster, with the bare clusters (or m = 7 product clusters) of the next higher n cluster. However, since all the clusters attach ligands at a similar rate, this proved not

to be a problem, and in general clusters and products corresponding to different values of n remained well separated during the experiment, given the high resolution of the FT-ICR instrument.

It might be interesting to discuss the saturation numbers for individual cluster sizes, and try to correlate these with their structure. Unfortunately, there is at present virtually no experimental information available about their structures, and theoretical computation of the structure of larger transition metal clusters is notoriously difficult. In general, it is assumed that for $n > 3$ linear structures are not stable and can be dismissed. Xiao et al have suggested that for platinum clusters up to nine atoms planar structures should be comparably stable as their three dimensional isomers, except for Pt_6 they find the planar structure to be considerably more stable.[43] This similarity between planar and three-dimensional structures would suggest that several isomeric structures could be present. A reason is that in these experimental data for some species the saturation converges to two or even three different values of m_{max}. Larger Pt clusters are almost certainly three dimensional. Also little studied is the influence of charge upon the cluster structure, although one might expect that for larger species the influence of the addition or removal of a single electron might be minor. In this context it is interesting to mention, that although the saturation numbers m_{max} for anions and cations are in most cases similar, for some cluster sizes they may differ somewhat. Thus, for instance for $n = 10$ the $m_{max} = 11$ for the cation, but 13 for the anion. Conversely, for $n = 7$, $m_{max} = 8$ for the anion, but 10 for the cation.

Previous studies for the saturation of the anionic platinum clusters with CO, assuming the18-electron rule, predicted a planar butterfly arrangement for the platinum tetramer which saturates forming $Pt_4(CO)_8^-$ compound and a three-dimensional structures for Pt_5^- and Pt_6^-.[12] Fortunelli et al. have found also for the anionic tetramer the planar structure to be the most

stabile using the density functional theory, while the cationic tetramer prefers the tetrahedron structure.[44] For large ionic platinum clusters data about the electronic structure and the geometric structure are not yet available.

6.3.3. Catalytic Oxidation of CO on Gas Phase Platinum Clusters

When platinum cluster cations in a size range from 5 to 10 are stored in the ICR cell together with a 1:6 mixture of CO and N_2O, for some sizes sequential addition of CO is observed, while for others, equilibrium of the bare platinum cluster with its oxides is established. Although Pt_5^+ forms Pt_5O^+ and $Pt_5O_2^+$, it efficiently reacts away by attaching CO molecules. Pt_6^+ is in equilibrium with Pt_6O^+, and, to a small extent, also $Pt_6O_2^+$ and $Pt_6O_3^+$ are visible. Pt_7^+ establishes equilibrium with Pt_7O^+ and $Pt_7O_2^+$ in a ratio of about 1:2:4. Pt_8^+ behaves somewhat similar to Pt_7^+, with Pt_8^+ and Pt_8O^+ as dominant species. Pt_9^+ and Pt_9O^+ keep a constant branching ratio, but their intensities decrease, because Pt_9^+ sequentially attaches CO ligands. Pt_{10}^+ efficiently attaches CO without any indication of catalytic activity.

Mass selection experiments confirm that indeed a dynamic equilibrium is established. When Pt_7O^+ was mass selected after 2 s, as can be seen in Figure 11, the equilibrium between Pt_7^+, P_7O^+, and $Pt_7O_2^+$ is again established within 3 s after mass selection, which proves that catalytic oxidation of CO is taking place, involving the four reactions:

$$Pt_7^+ + N_2O \rightarrow Pt_7O^+ + N_2 \quad (1)$$

$$Pt_7O^+ + N_2O \rightarrow Pt_7O_2^+ + N_2 \quad (2)$$

$$Pt_7O_2^+ + CO \rightarrow Pt_7O^+ + CO_2 \quad (3)$$

$$Pt_7O^+ + CO \rightarrow Pt_7^+ + CO_2 \quad (4)$$

After very long reaction delays of 150 s, $Pt_7CO_{8\text{-}10}^+$ species are observed to a very small extent. Obviously, by addition of multiple CO molecules, some bare Pt_7^+ escape the catalytic cycle. To learn more about this process of catalyst poisoning, and to establish the number of CO molecules necessary to quench the oxidation reaction, the experimental conditions have been changed in favour of poisoning. Using a 5:3 mixture of CO and N_2O in the ICR cell, we mass selected Pt_7CO^+ after 1 s. Following the reaction further, Pt_7CO^+ is with almost equal probability converted back to Pt_7^+, which is available for the catalytic cycle described above, or it attaches a second CO molecule to form $Pt_7(CO)_2^+$:

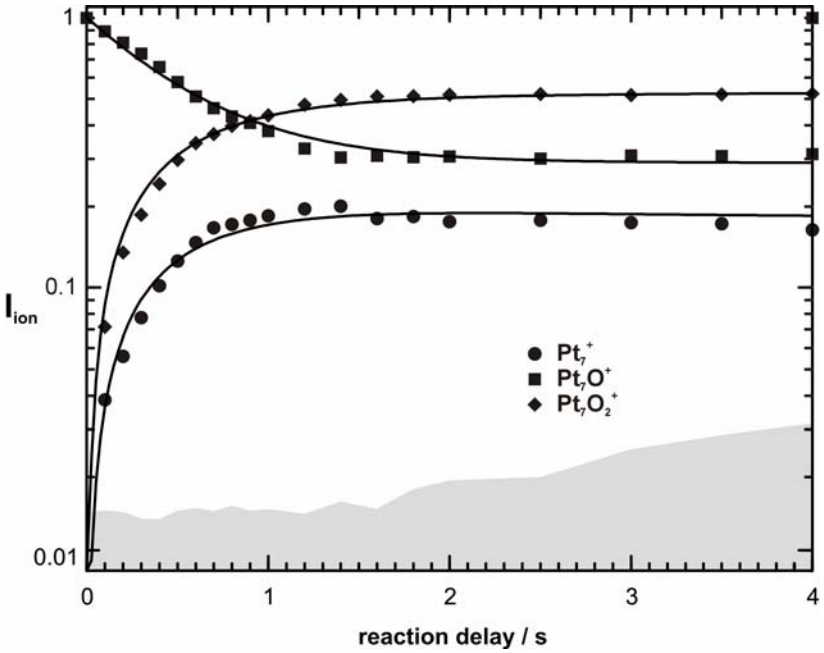

Figure 11: Kinetic fit of the reaction of mass selected Pt_7O^+ with a mixture 1:6 of CO and N_2O. Very fast ■ Pt_7O^+ either reacts back to ● Pt_7^+, or forms ◆ $Pt_7O_2^+$ and the equilibrium is reestablished between the three species. The gray area denotes the noise level. Due to the mass selection, the clusters are kinetically excited, thus the total ion signal is reduced, and Pt_7CO^+ lies below the noise level.

$$Pt_7^+ + CO \rightarrow Pt_7CO^+ \quad (5)$$

$$Pt_7CO^+ + N_2O \rightarrow Pt_7^+ + CO_2 + N_2 \quad (6)$$

$$Pt_7CO^+ + CO \rightarrow Pt_7(CO)_2^+ \quad (7)$$

Two CO ligands seem to be sufficient to quench the oxidation reaction, and the cluster sequentially and fast adds CO molecules until the surface is fully saturated:

$$Pt_7(CO)_n^+ + CO \rightarrow Pt_7(CO)_{n+1}^+ , n = 2 - 9 \quad (8)$$

Figure 12 shows the kinetics of the Pt_7^+ catalytic cycle using a 1:6 mixture of CO and N_2O without mass selection, since this yields the best signal to noise ratio. In order to reduce the number of fit parameters, previous absolute reaction rates of reactions (1) and (2) from 6.3.1. were used. In addition, the rate constant of reaction (6) was taken from the mass selection of Pt_7CO^+. As seen in Figure 12, the dynamic equilibrium between Pt_7^+, Pt_7O^+, $Pt_7O_2^+$ and Pt_7CO^+ is established within 5 s. Towards longer reaction times, the intensities slowly decrease, and the poisoned clusters become more and more intense. Extrapolating the exponential decrease of the ions involved in the catalytic cycle, the active life time of a cluster in the cycle is estimated to be 750 s. From the reaction rate constants and the intensities of the reactant ions in reactions (3), (4) and (6), one can estimate that each Pt_7^+ cluster converts 0.687 CO molecules into CO_2 per second. Over the lifetime of the cluster in the cycle, this amounts to a total of 515 CO_2 molecules formed.

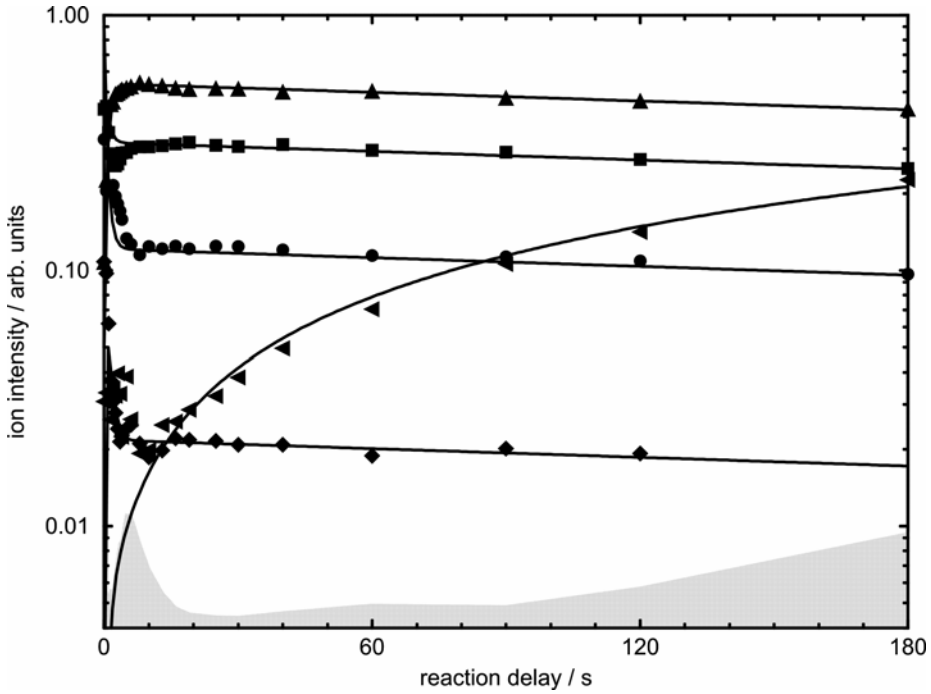

Figure 12: Kinetic fit of the Pt_7^+ reactions with a mixture 1:6 of CO and N_2O. ● Pt_7^+ reacts very fast to ■ Pt_7O^+ and ▲ $Pt_7O_2^+$. The described equilibrium is established between the three species within 5 s. Pt_7^+ also reacts efficiently with CO forming ◆ Pt_7CO^+ which in turn can either react back to ● Pt_7^+ or can very slowly attach a second CO molecule forming $Pt_7(CO)_2^+$. Additional CO molecules are then very fast attached until the cluster is fully saturated. The final product of CO attachment is $Pt_7(CO)_{10}^+$. The visible ◀ $Pt_7(CO)_n^+$, n = 2, 8, 9, 10, are summed together for clarity. The gray area denotes the noise level.

The full catalytic cycle together with the poisoning mechanism is summarized in Figure 13. Catalytic conversion of CO to CO_2 is achieved in three different ways, either by CO colliding with the oxide species Pt_7O^+ or $Pt_7O_2^+$, reactions (3), (4), or by N_2O oxidizing preadsorbed CO on Pt_7CO^+, reaction (6).

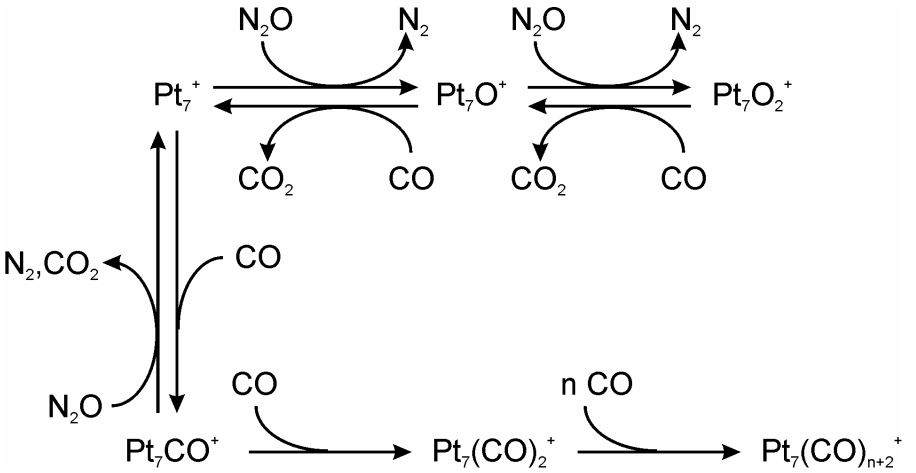

Figure 13: Schematic representation of the catalytic cycle of the Pt_7^+ ion in a 1:6 mixture of CO and N_2O.

If N_2O is present in sufficient excess, the concentration of Pt_7^+ in the equilibrium is small, and the catalytic cycle runs mostly via reactions (2), (3) between Pt_7O^+ and $Pt_7O_2^+$.Very few Pt_7CO^+ ions are formed, and these are in turn almost entirely converted back to Pt_7^+, before attachment of a second CO can occur. This gas phase catalytic cycle thus exhibits a typical characteristic of large scale catalytic processes: The partial pressures of the reactants can be adjusted to suppress catalyst poisoning.

Preliminary data for other cluster sizes indicate that the catalytic activity with respect to CO oxidation by N_2O is determined by the reactivity of the bare cluster with N_2O.[45] This seems eminently reasonable: A high reactivity with N_2O shifts the equilibrium in favour of the oxide species and thus hinders the poisoning reaction by sequential CO addition to the bare cluster. For larger clusters, however, the picture becomes more complicated. Due to their larger surface, adsorption of CO on Pt_nO^+ becomes feasible, presumably at a site which is remote from the oxygen atom. E.g. for Pt_{20}^+, it seems that $Pt_{20}OCO^+$ becomes an observable intermediate in the catalytic cycle. For the anionic tetramer Pt_4^- four CO ligands seem to be

sufficient to stop the oxidation reaction, as displayed in Figure 14 and 15, and the cluster sequentially adds CO molecules until the surface is fully saturated. Such anionic species as well as larger cationic clusters are currently under investigation.

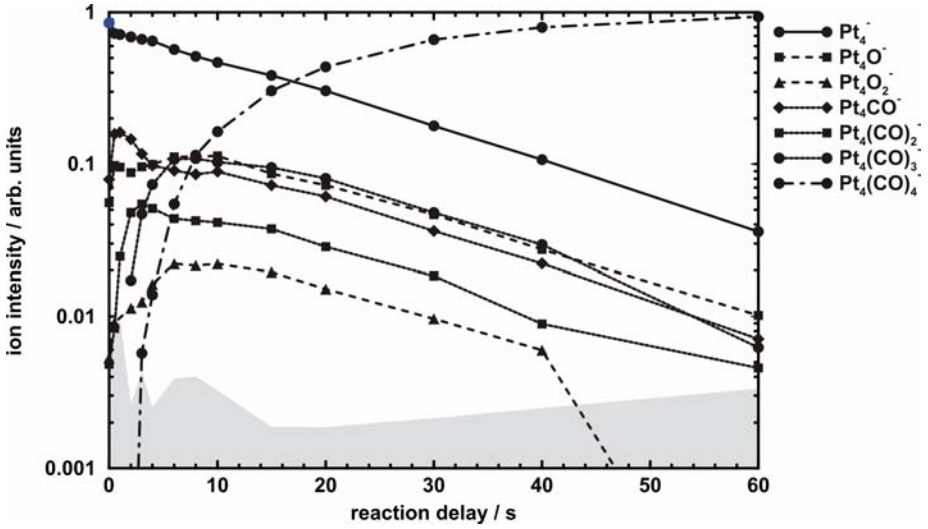

Figure 14: Reaction course of the anionic platinum Pt_4^- with a mixture 1:2 CO and N_2O. Pt_4O^- and $Pt_4O_2^-$ forms back until four CO molecules are attached, when the poisoning of the cycle starts.

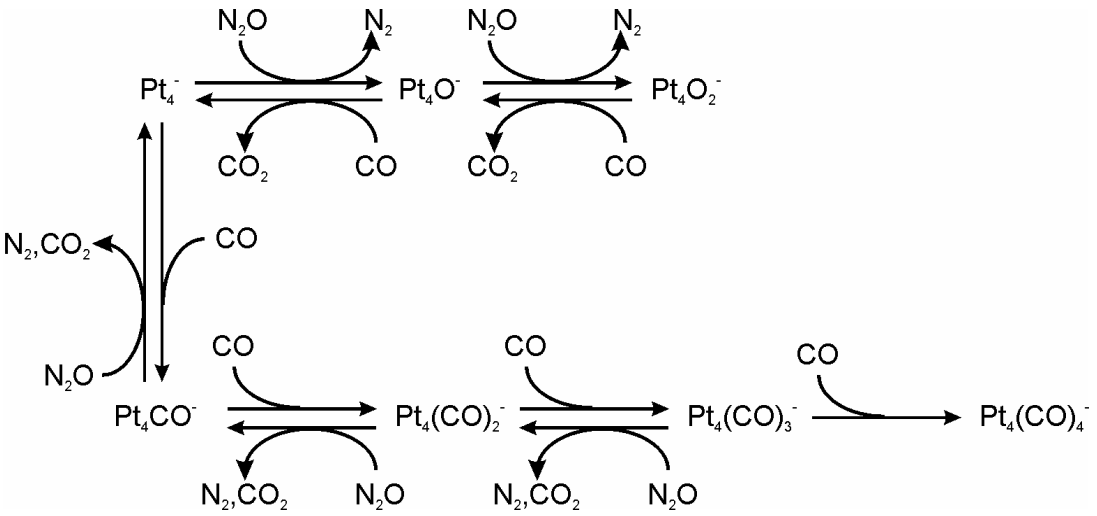

Figure 15: Schematic representation of the catalytic cycle of the Pt_4^- ion in a 1:2 mixture of CO and N_2O.

6.4. Conclusions

Isotopically enriched platinum allows the quantitative investigation of size-dependent reactivities of platinum clusters. The present work demonstrates the feasibility and the potential of this approach to further substantiate the notion introduced by Schwarz and coworkers that small platinum clusters can serve as model system for surface catalytic reactions.[9] They also indicate, however, that, as was previously shown for supported platinum clusters by Heiz et al.,[24] also in the gas phase "each atom counts."

6.5. References

(1) M. P. Irion, *Int. J. Mass Spectrom. Ion Processes*, **1992**, *121*, 1-47.

(2) M. B. Knickelbein, *Annu. Rev. Phys. Chem.*, **1999**, *50*, 79-115.

(3) P. B. Armentrout, *Annu. Rev. Phys. Chem.*, **2001**, *52*, 423-461.

(4) V. E. Bondybey, M. K. Beyer, *J. Phys. Chem. A*, **2001**, *105*, 951-960.

(5) K. M. Ervin, *Int. Rev. Phys. Chem.*, **2001**, *20*, 127-164.

(6) C. Berg, M. Beyer, T. Schindler, G. Niedner-Schatteburg, V. E. Bondybey, *J. Chem. Phys.*, **1996**, *104*, 7940-7946.

(7) U. Achatz, C. Berg, S. Joos, B. S. Fox, M. K. Beyer, G. Niedner-Schatteburg, V. E. Bondybey, *Chem. Phys. Lett.*, **2000**, *320*, 53-58.

(8) S. H. Yang, D. A. Drabold, J. B. Adams, P. Ordejon, K. Glassford, *Journal of Physics-Condensed Matter*, **1997**, *9*, L39-L45.

(9) K. Koszinowski, D. Schroder, H. Schwarz, *J. Phys. Chem. A*, **2003**, *107*, 4999-5006.

(10) D. J. Trevor, R. L. Whetten, D. M. Cox, A. Kaldor, *J. Am. Chem. Soc.*, **1985**, *107*,

518-519.

(11) D. J. Trevor, D. M. Cox, A. Kaldor, *J. Am. Chem. Soc.*, **1990**, *112*, 3742-3749.

(12) X. L. Ren, P. A. Hintz, K. M. Ervin, *J. Chem. Phys.*, **1993**, *99*, 3575-3587.

(13) P. A. Hintz, K. M. Ervin, *J. Chem. Phys.*, **1994**, *100*, 5715-5725.

(14) P. A. Hintz, K. M. Ervin, *J. Chem. Phys.*, **1995**, *103*, 7897-7906.

(15) A. Grushow, K. M. Ervin, *J. Am. Chem. Soc.*, **1995**, *117*, 11612-11613.

(16) A. Grushow, K. M. Ervin, *J. Chem. Phys.*, **1997**, *106*, 9580-9593.

(17) Y. Shi, K. M. Ervin, *J. Chem. Phys.*, **1998**, *108*, 1757-1760.

(18) Y. Shi, V. A. Spasov, K. M. Ervin, *Int. J. Mass Spectrom.*, **2001**, *204*, 197-208.

(19) G. S. Jackson, F. M. White, C. L. Hammill, R. J. Clark, A. G. Marshall, *J. Am. Chem. Soc.*, **1997**, *119*, 7567-7572.

(20) T. Hanmura, M. Ichihashi, T. Kondow, *J. Phys. Chem. A*, **2002**, *106*, 11465-11469.

(21) M. Andersson, A. Rosén, *J. Chem. Phys.*, **2002**, *117*, 7051-7054.

(22) K. Koszinowski, D. Schroder, H. Schwarz, *Organometallics*, **2003**, *22*, 3809-3819.

(23) U. Heiz, A. Sanchez, S. Abbet, W. D. Schneider, *European Physical Journal D*, **1999**, *9*, 35-39.

(24) U. Heiz, A. Sanchez, S. Abbet, W. D. Schneider, *J. Am. Chem. Soc.*, **1999**, *121*, 3214-3217.

(25) G. Gantefoer, G. Schulze Icking-Konert, H. Handschuh, W. Eberhardt, *Int. J. Mass Spectrom.*, **1996**, *159*, 81-109.

(26) P. Schnabel, K. G. Weil, M. P. Irion, *Angew. Chem. Int. Edit.* **1992**, *31*, 636-638.

(27) M. Brönstrup, D. Schröder, I. Kretzschmar, H. Schwarz, J. N. Harvey, *J. Am. Chem. Soc.*, **2001**, *123*, 142-147.

(28) R. Wesendrup, D. Schröder, H. Schwarz, *Angew. Chem. Int. Edit.*, **1994**, *33*, 1174-

1176.

(29) M. Pavlov, M. R. A. Blomberg, P. E. M. Siegbahn, R. Wesendrup, C. Heinemann, H. Schwarz, *J. Phys. Chem. A*, **1997**, *101*, 1567-1579.

(30) M. Aschi, M. Brönstrup, M. Diefenbach, J. N. Harvey, D. Schröder, H. Schwarz, *Angew. Chem. Int. Edit.*, **1998**, *37*, 829-832.

(31) M. Brönstrup, D. Schröder, H. Schwarz, *Organometallics*, **1999**, *18*, 1939-1948.

(32) H. Schwarz, *Angew. Chem. Int. Edit.*, **2003**, *42*, 4442-4454.

(33) M. Diefenbach, M. Brönstrup, M. Aschi, D. Schröder, H. Schwarz, *J. Am. Chem. Soc.*, **1999**, *121*, 10614-10625.

(34) C. Berg, M. Beyer, U. Achatz, S. Joos, G. Niedner-Schatteburg, V. E. Bondybey, *J. Chem. Phys.*, **1998**, *108*, 5398-5403.

(35) C. Berg, T. Schindler, G. Niedner-Schatteburg, V. E. Bondybey, *J. Chem. Phys.*, **1995**, *102*, 4870-4884.

(36) V E. Bondybey, Science, **1985**, *227*, 125-131

(37) V. E. Bondybey, J. H. English, *J. Chem. Phys.*, **1981**, *74*, 6978-6979.

(38) T. G. Dietz, M. A. Duncan, D. E. Powers, R. E. Smalley, *J. Chem. Phys.*, **1981**, *74*, 6511-6512.

(39) S. Maruyama, L. R. Anderson, R. E. Smalley, *Rev. Sci. Instrum.*, **1990**, *61*, 3686-3693.

(40) T. Su, M. T. Bowers, *J. Chem. Phys.*, **1973**, *58*, 3027-3037.

(41) L. Bass, T. Su, M. T. Bowers, *Int. J. Mass Spectrom. Ion Processes*, **1978**, *28*, 389-399.

(42) L. Bass, T. Su, W. J. Chesnavich, M. T. Bowers, *Chem. Phys. Lett.*, **1975**, *34*, 119-122.

(43) L. Xiao, L. Wang, *J. Phys. Chem.*, **2004**, *108*, 8605-8614

(44) A. Fortunelli, *J. Mol. Struct.*, **1999**, *493*, 233-240

(45) I. Balteanu, O. P. Balaj, M. K. Beyer, V. E. Bondybey, *Phys. Chem. Chem. Phys.* **2004**, *6*, 2910-2913.

7. Methane and Deuterated Methane Activation by Platinum Cluster Ions

7.1. Introduction

Reactions of transition metal clusters with small molecules were intensively studied in the last decades because of their importance in catalysis. Their very rich chemistry is determined by the fact that usually only the s and d-electrons participate to the bindings. Platinum, as well palladium and rhodium besides their using as dehydrogenation catalysts are also used extensively in oxidation of toxic oxide pollutants, like carbon monoxide, nitrous oxide and also some hydrocarbons from automotive exhaust.[1,2]

It is well known that transition metals can activate unreactive C-H bonds of different molecules. Several groups have investigated in detail the interaction between the methane and the catalysts in order to understand the methane activation mechanism.[3-8] Kaldor et al. investigated in a flow reactor dehydrogenation of methane on neutral platinum clusters with up to 24 atoms and found that the dehydrogenation degree decreases with the cluster size.[3] The Garching group has previously studied methane activation by gas phase $Pt_n^{+/-}$ cluster ions with a normal isotopic distribution for small species up to nine atoms $Pt_n^{+/-}$.[7] The dehydrogenation of the methane on the platinum clusters proceeds by activation of one of the methane C-H bonds and formation of a hydrido-methyl platinum complex. The natural platinum distribution, with six stabile isotopes complicated the mass spectra and diluted considerably the signal, therefore the

study was limited to clusters with up to nine atoms. In the present chapter highly isotopically enriched platinum ^{195}Pt was used to investigate the reactions of $^{195}Pt_n^{+/-}$ clusters, n = 1-24, with methane CH_4 and deuterated methane CD_4.

7.2. Experimental Details

Isotopically enriched platinum (97.28% ^{195}Pt, Oak Ridge National Laboratories)[9] was used to investigate the reactions of platinum clusters $^{195}Pt_n^{+/-}$, n = 1 - 24 with methane CH_4 and deuterated methane CD_4 under binary collision conditions in a Fourier transform ion cyclotron resonance (FT-ICR) mass spectrometer. The experimental setup was described in details previously.[10] Briefly the platinum ions are produced by pulsed laser vaporisation of a rotating platinum disk. The hot metal plasma produced by the laser, which contains enough ions without need for post-ionization, is cooled down and clustered by supersonic expansion of the high pressure gas into high vacuum. Ionic clusters are accelerated along the magnetic field axis by a series of electrostatic lenses, trapped and stored inside the ICR cell in the ultrahigh vacuum of the FT-ICR mass spectrometer. To study the bimolecular cluster ion-molecule reactions the pressure in the ICR cell was raised from the base value of 1×10^{-10} mbar to the constant pressure of typically 9.1×10^{-9} mbar by controlled admission of the reactant gas CH_4 and CD_4 at room temperature. Commercially available methane CH_4 (Messer-Griesheim 99.9%) and deuterated methane CD_4 (Cambridge Isotope Laboratories 99%) were used without further purification. For each mass spectrum, clusters generated in 20 laser shots over a period of 2 s were accumulated in the cell. Mass spectra were taken after different reaction delays and relative rate constants were extracted.

7.3. Results

7.3.1. Reactions of Cationic Clusters

Platinum clusters $Pt_n^{+/-}$, n = 1 - 24, react with CH_4 and CD_4 as an unbreakable unit, thus the reactions for all cluster sizes have been studied under exactly the same conditions, without mass selection. The reactivity of both positively and negatively charged platinum clusters towards CH_4 and CD_4 was investigated as a function of cluster size. A typical mass spectrum taken after 2 s reaction delay for the reaction of cationic platinum clusters Pt_n^+ with CH_4 is presented in Figure 1, showing a part of the mass spectrum which contains clusters with 4 to 11 atoms. At the first sight one can observe that their reactivity depends strongly on the cluster size not only with respect to their rate constant, but also to the number of reaction steps they undergo. The first species displayed in Figure 1, Pt_4^+ shows a very low reactivity towards CH_4, after 2 s reaction delay only few product is visible in the spectrum. Mainly the clusters in the range of $5 \leq n \leq 9$ display an appreciable reactivity. For all these species the reaction consists in simple dehydrogenation of the methane on the cluster surface. The reaction takes place in sequential steps, a second reaction product being already observed for most of the species, as described by the equation pattern:

$$Pt_n^+ + CH_4 \rightarrow Pt_nCH_2^+ + H_2 \quad (1)$$

$$Pt_nCH_2^+ + CH_4 \rightarrow Pt_nC_2H_4^+ + H_2 \quad (2)$$

Clusters with 6 and 9 atoms react slower to a secondary step than the previous clusters. Quite different is the behaviour of n = 10 cluster which reacts considerably

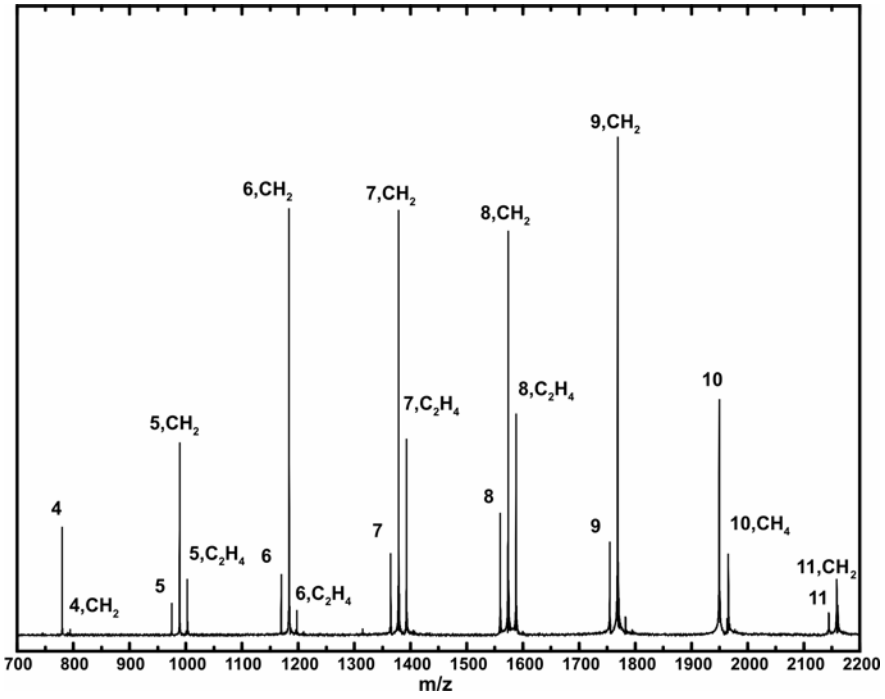

Figure 1: Mass spectrum of the reaction of cationic platinum clusters Pt_n^+, n = 4 - 11, with CH_4 after 2 s reaction delay, using the isotopically enriched target. Peaks are labelled with their cluster size and primary reaction products, addition of CH_2, CH_4 or for some species secondary C_2H_4. The clusters show a quite irregular reactivity pattern, not only with respect to their rate constant, but also to the number of reaction steps they undergo.

slower than the previous clusters and is the first species which adsorbs a complete CH_4 complex, according to the equation:

$$Pt_{10}^+ + CH_4 \rightarrow Pt_{10}CH_4^+ \qquad (3)$$

In a typical experiment, spectra similar to that exemplified in Figure 1 were measured after 14 different reaction delays ranging from the nominal time t = 0 up to 3 s. Relative intensities of the parent and reaction product ions are extracted from these spectra

and exemplified in Figure 2 for Pt_9^+, assuming pseudo-first order reaction kinetics. The parent ion decay is linear in the semi-logarithmic scale indicating the absence of the platinum cluster fragmentation. The first reaction step, addition of CH_2 with elimination of molecular H_2 proceeds efficiently while the secondary CH_2 is significantly more slowly attached.

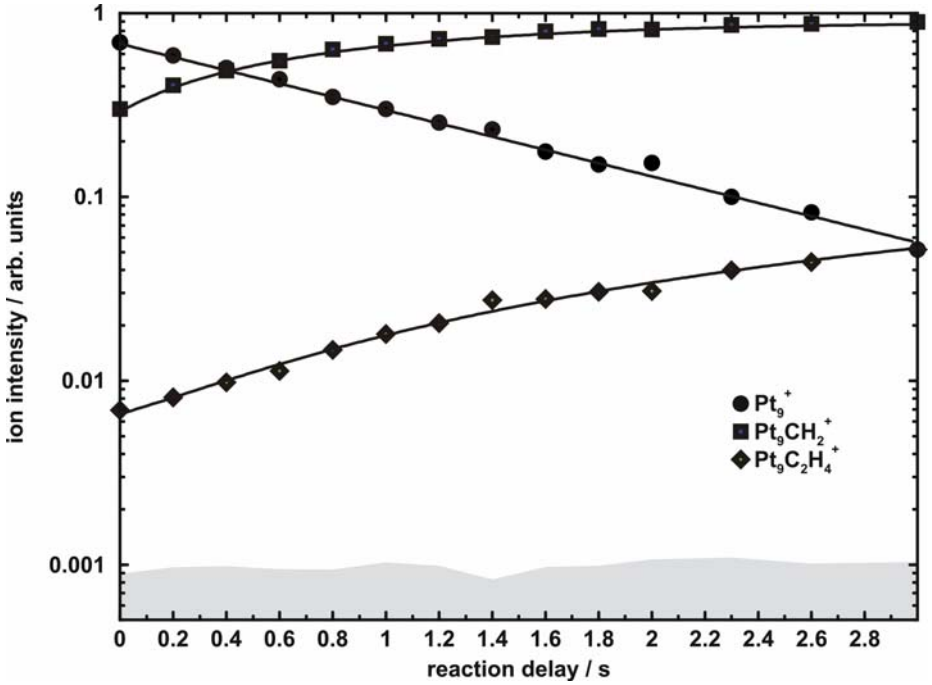

Figure 2: Kinetic fit for the reaction of Pt_9^+ with CH_4. The first reaction step, addition of CH_2, proceeds efficiently while the secondary CH_2 is significantly more slowly attached. Grey shaded area denotes the noise level.

Kinetic evaluation of the data analogous to n = 9 species was undertaken for all the cations ranging from 1 to 24 atoms and they will be shown later. Different results were obtained using deuterated methane CD_4 as reactant gas instead of methane. Figure 3 displays a typical mass spectrum taken after 2 s reaction delay for a cluster distribution from n = 9 to n = 12 reacting with CD_4. A major difference can be observed for the n = 9

and 11 species which beside the expected CD_2 addition with loss of molecular D_2 display a

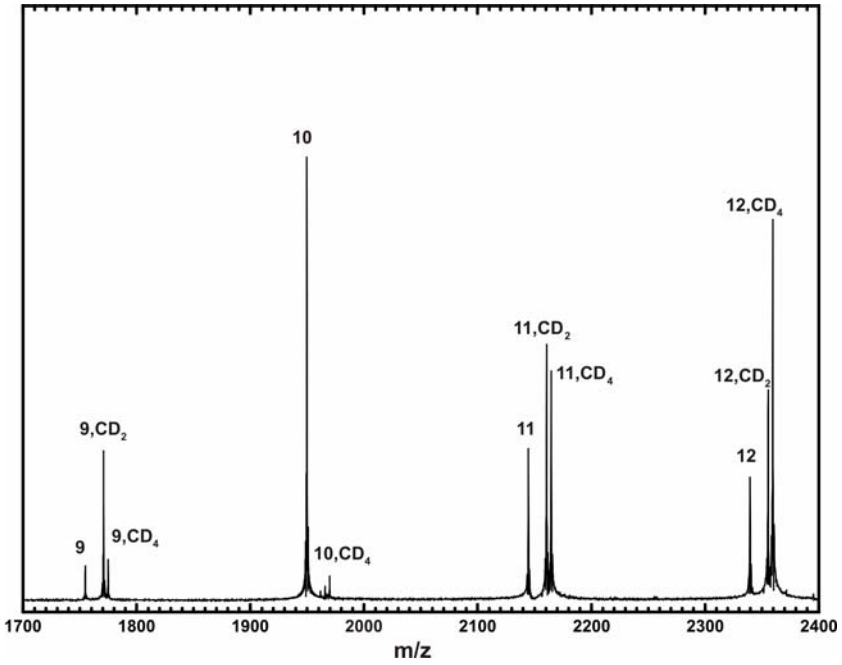

Figure 3: Mass spectrum of the reaction of cationic platinum clusters Pt_n^+, n = 9 - 12, with CD_4 after 2 s reaction delay. The clusters show beside the CD_2 addition, a second primary product, $Pt_nCD_4^+$.

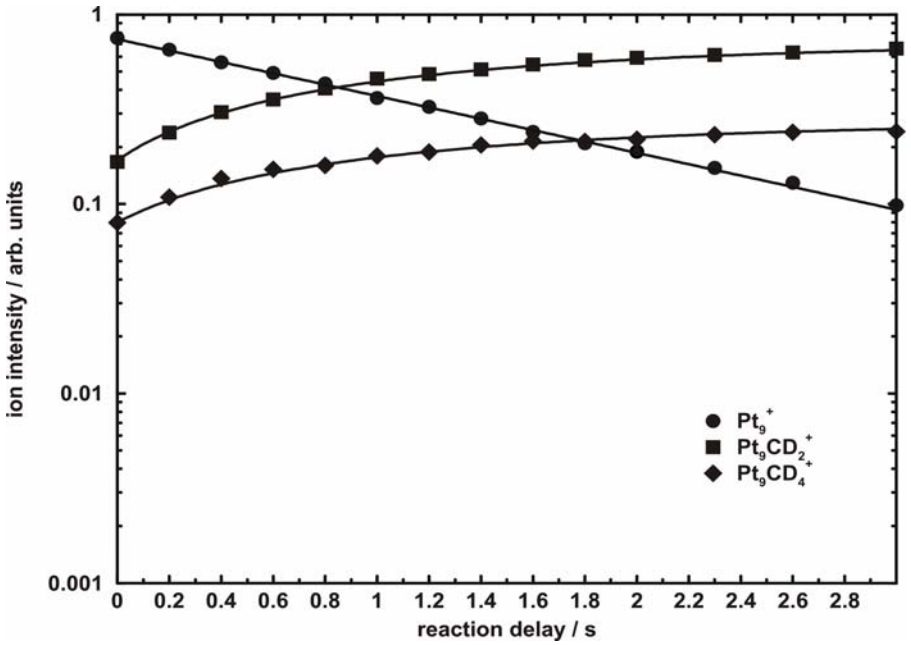

Figure 4: Kinetic fit for the reaction of Pt_9^+ with CD_4. Pt_9^+ reacts to the primary reaction products

$Pt_9CH_2^+$ and $Pt_9CH_4^+$ efficiently respective less than half efficient.

second primary reaction product which is for both cluster sizes attachment of CD_4 to the cluster surface. The time intensity profile is again exemplified for Pt_9^+ in Figure 4. The two primary products are attachment of CD_2 with elimination of molecular D_2 and complete attachment of CD_4 complex to the cluster, the last one being less efficient.

$$Pt_9^+ + CD_4 \rightarrow Pt_9CD_2^+ + D_2 \quad (4)$$

$$Pt_9^+ + CD_4 \rightarrow Pt_9CD_4^+ \quad (5)$$

Similar kinetic evaluation of the reactions were undertaken for all the cationic clusters, $1 \leq n \leq 24$, relative rate constants for the first reaction step for both reactions with CH_4 and CD_4 were extracted from the kinetic fits and further converted into absolute rate

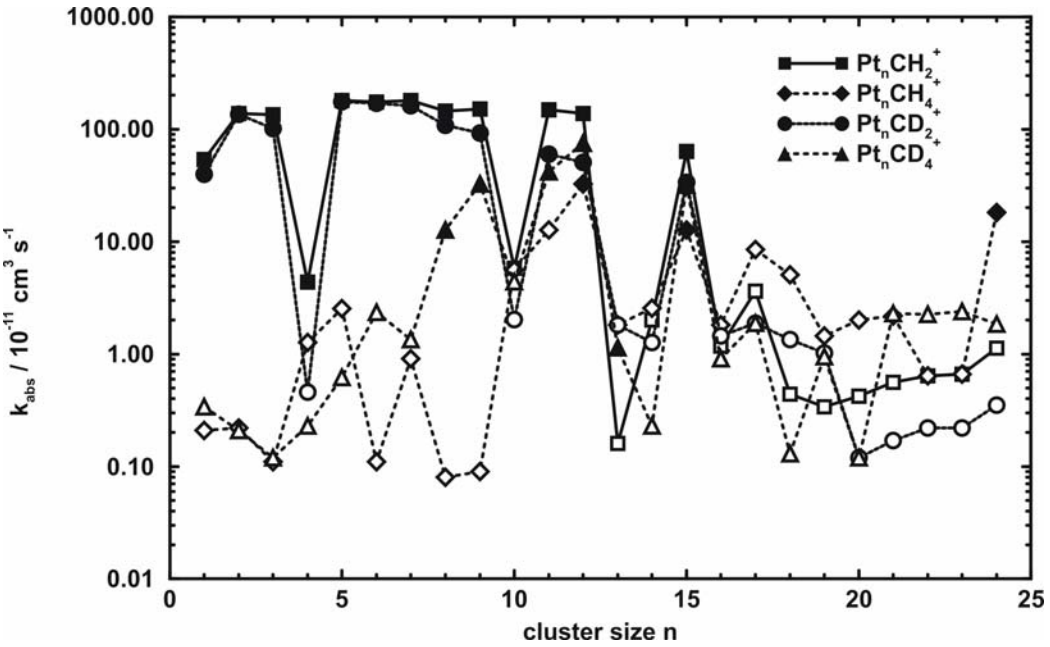

Figure 5: Absolute rate constants of the first reaction step of Pt_n^+ clusters with CH_4 and CD_4 on a semi-logarithmic scale. Open symbols denote upper limits of the rate constants for the unreactive or reactive cluster sizes, where the product intensity was not sufficient to determine a rate constant.

Table 1: Absolute rate constants for the first reactions step of cationic platinum clusters.

	$10^{11}k_{abs}/cm^3s^{-1}$			
	Reaction products			
Cluster	$Pt_nCH_2^+$	$Pt_nCH_4^+$	$Pt_nCD_2^+$	$Pt_nCD_4^+$
Pt_1^+	53.52	<0.21	39.92	<0.34
Pt_2^+	137.89	<0.22	135.17	<0.21
Pt_3^+	134.26	<0.11	101.60	<0.12
Pt_4^+	4.35	<1.27	<0.46	<0.23
Pt_5^+	179.62	<2.56	175.99	<0.62
Pt_6^+	174.18	<0.11	170.55	<2.36
Pt_7^+	179.62	<0.91	161.48	<1.34
Pt_8^+	145.15	<0.08	107.95	12.70
Pt_9^+	150.59	<0.09	92.53	32.66
Pt_{10}^+	<5.81	<5.62	<2.03	<4.39
Pt_{11}^+	148.78	<12.70	59.87	41.73
Pt_{12}^+	137.89	32.66	50.80	74.93
Pt_{13}^+	<0.16	<1.81	<1.81	1.14
Pt_{14}^+	<2.01	<2.56	<1,27	<0.23
Pt_{15}^+	63.50	<12.70	33.57	31.75
Pt_{16}^+	<1.18	<1.81	<1.45	<0.91
Pt_{17}^+	<3.64	<8.53	<1.87	<1.88
Pt_{18}^+	<0.44	<5.08	<1.34	<0.13
Pt_{19}^+	<0.34	<1.45	<1.02	<0.95
Pt_{20}^+	<0.42	<2.00	<0.12	<0.12
Pt_{21}^+	<0.56	<2.18	<0.17	<2.30
Pt_{22}^+	<0.64	<0.64	<0.22	<2.26
Pt_{23}^+	<0.66	<0.66	<0.22	<2.40
Pt_{24}^+	<1.13	18.14	<0.35	<1.85

constants, displayed in Figure 5 and summarized in Table 1. The differences between the two kinds of reactions are not very significant, however the reactivity of platinum clusters towards CH_4 for the dehydrogenation reaction is slightly stronger. For cationic species like 8, 9, 11 atoms two primary reaction products corresponding to $Pt_nCD_2^+$ and $Pt_nCD_4^+$ were

observed while the same cluster sizes reacting with CH_4 showed only one reaction product, simple dehydrogenation of the methane. Pt_4^+ represents an exception, showing a very poor reactivity towards both reactant gases, in contrast with the rest of the small cluster sizes. A drastic change in reactivity can be observed for Pt_{24}^+ which reacts well with CH_4 but no reaction was observed with CD_4. The open symbols in Figure 5 denote upper limits determined by considering the initial parent ion intensities and the noise level after a certain reaction delay.

7.3.2. Reactions of Anionic Clusters

The anionic platinum clusters Pt_n^-, n = 3 - 24, were investigated under similar conditions. Monomer and dimer platinum anions are not produced in sufficient quantities in the present ion source. For all anionic platinum clusters above mentioned was undertaken a kinetic evaluation analogous to that of Pt_9^+ and the absolute rate constants for the first reaction step were extracted and summarized in Figure 6 and Table 2. The anions behave differently from the cations, overall they exhibit a much slower reactivity towards both reactant gases, CH_4 and CD_4, the only reaction observed being simple dehydrogenation, according to:

$$Pt_n^- + CH_4 \rightarrow Pt_nCH_2^- + H_2 \quad (6)$$

$$Pt_n^- + CD_4 \rightarrow Pt_nCD_2^- + D_2 \quad (7)$$

Overall there are not significant differences between the reactions of the anions with methane and deuterated methane. They follow almost the same path in reactivity, however, except species like n = 3 and n = 11 the reactivity of the anions towards CD_4 is

slightly smaller than CH_4. The most reactive anion studied is Pt_4^- cluster in contrast with the cation Pt_4^+ which exhibits a deep minimum in reactivity pattern of Figure 5. The anion n = 6 is almost unreactive, while the corresponding cationic species shows a quite strong reactivity towards both reactants. Starting with n = 12 the anions are almost unreactive and upper limits for their reactivity were calculated.

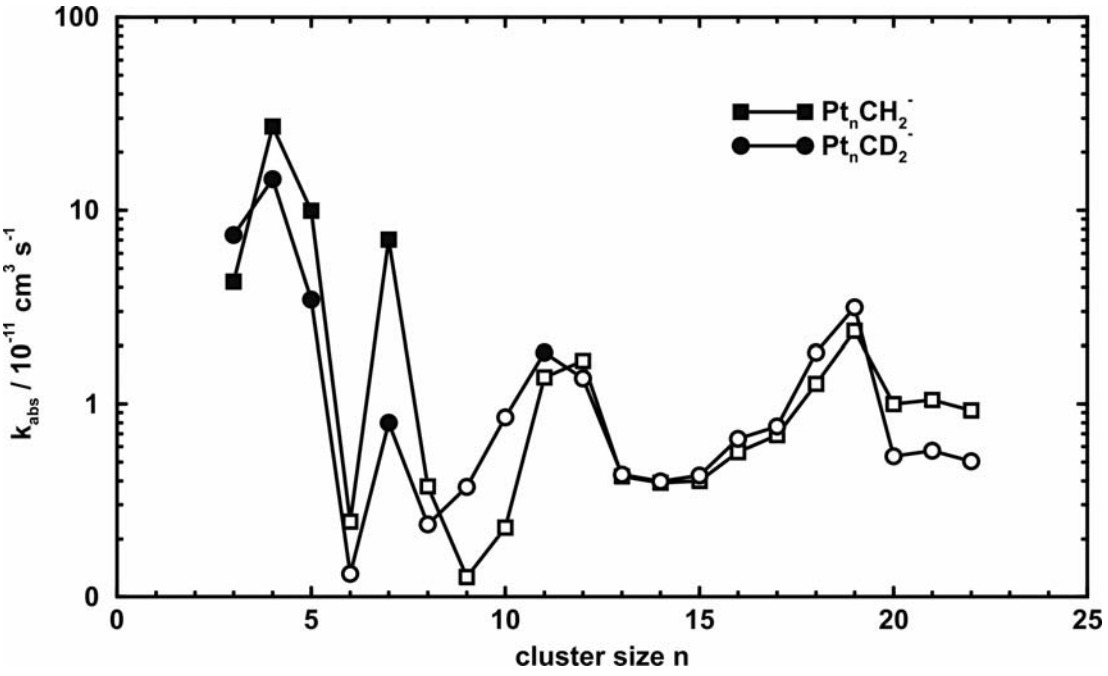

Figure 6: Absolute rate constants of the first reaction step of Pt_n^+ clusters with CH_4 and CD_4 on a semi-logarithmic scale. Open symbols denote upper limits of the rate constants for the unreactive or very few reactive cluster sizes. Monomer and dimer platinum anions are not produced in sufficient quantities in the present ion source.

Table 2: Absolute rate constants for the first reactions step of anionic platinum clusters.

	$10^{11}k_{abs}/cm^3s^{-1}$	
	Reaction products	
Cluster	$Pt_nCH_2^-$	$Pt_nCD_2^-$
Pt_3^-	4.26	7.43
Pt_4^-	27.21	14.51
Pt_5^-	9.97	3.44
Pt_6^-	<0.24	<0.13
Pt_7^-	7.07	0.79
Pt_8^-	<0.37	<0.23
Pt_9^-	<0.12	<0.37
Pt_{10}^-	<0.22	<0.85
Pt_{11}^-	<1.37	<1.83
Pt_{12}^-	<1.66	<1.35
Pt_{13}^-	<0.42	<0.43
Pt_{14}^-	<0.39	<0.39
Pt_{15}^-	<0.39	<0.42
Pt_{16}^-	<0.56	<0.65
Pt_{17}^-	<0.68	<0.76
Pt_{18}^-	<1.27	<1.83
Pt_{19}^-	<2.37	<3.13
Pt_{20}^-	<0.99	<0.53
Pt_{21}^-	<1.05	<0.57
Pt_{22}^-	<0.92	<0.50

7.4. Discussion

Density functional calculations have shown that the dehydrogenation of the methane on Pt^+ proceeds via a hydrido-methyl platinum complex, which represents a global minimum on the potential energy surface.[5-7] Generally, when a CH_4 molecule collides with a platinum cluster an electrostatically bound complex is formed, $Pt_n^{+/-}CH_4$. This step is followed by the insertion of the platinum atom into one of the C-H bonds of methane, resulting into a hydrido-methyl platinum structure, $HPt_n^{+/-}CH_3$. In a next step of

the reaction path, a second hydrogen atom migrates from the methyl radical to the platinum cluster, forming a collisionally stabilized long lived complex corresponding to another global minimum on the potential energy surface. Further rearrangements due to the vibrational moving can lead to formation of a dihydrogen complex of the platinum carbene, $H_2Ptn^{+/-}CH_2$ and finally to dehydrogenation of the methane by releasing the hydrogen molecule H_2.

$$Pt_n^{+/-} + CH_4 \rightarrow Pt_n^{+/-}\cdots CH_4 \rightarrow HPt_n^{+/-}CH_3 \rightarrow$$
$$\rightarrow [2H]Pt_n^{+/-}CH_2 \rightarrow H_2\cdots Pt_n^{+/-}CH_2 \rightarrow Pt_n^{+/-}CH_2 + H_2 \qquad (8)$$

This reaction mechanism favours the cationic platinum clusters. The monomer Pt^+ for example has a very low-lying excited state $5d^86s^1$ with three half occupied orbitals, which are needed to covalently bind the methyl complex and the hydrogen atoms. Conversely, the anionic monomer, Pt^-, instead of these three unpaired electrons needed for the covalent bounds, possesses only one, a d-electron from the electronic configuration $5d^96s^2$. This would be the reason why the anionic platinum clusters exhibit a significantly lower reactivity towards CH_4 than the cationic clusters. Very interesting is the behaviour of platinum tetramer, which is almost unreactive as cation while as anion shows a maximum in the reactivity pattern. Achatz et al. assumed that the reactivity of this species is subject of the geometric structure rather than the electronic configuration.[7] The cationic tetramer structure is a tetrahedron in which every platinum atom is coordinated to the other three. A completely different structure shows the anionic tetramer, whose geometry is rhombohedric, with low coordinated atoms and potentially higher reactivity.[7]

On the other hand for small clusters formation of the hydrogen molecule and its releasing from the cluster surface is more favourable than for the large clusters because the

bigger the cluster is the larger the surface is and the more difficult for the two hydrogen atoms to find each other and to form the molecule. This is the case of n = 10, 12 and 15 cationic species which show beside the dehydrogenation reaction another primary product, corresponding to attachment of a CH_4 complex. Another example is Pt_{24}^+ cluster for which the only observable reaction product was addition of CH_4 without dehydrogenation, $Pt_{24}CH_4^+$.

The reaction path for the deuterated methane, CD_4 undergoes in a similar way, as illustrated in equation (8). Having a larger mass than hydrogen, for the deuterated atoms is more difficult to migrate on the cluster surface and find the other D atom. Therefore formation of a deuterated molecule is less probable and the dehydrogenation reaction is less favourable than for CH_4. One can assume that for the reaction of positively charged clusters with CD_4 the reactivity is shifted favouring the CD_4 attachment. This behaviour is exemplified by cationic clusters with 8, 9, 11, 12 and 13 atoms which exhibit beside the dehydrogenation reaction a comparable intense reaction product which corresponds to addition of CD_4 to the cluster. A reason why Pt_{24}^+ exhibits a quite good reactivity towards CH_4 while towards CD_4 no reaction was observed might be the tunnelling effect, which is presumably less feasible for the deuterated atoms due to their larger mass.

7.5. Conclusions

Cationic and anionic platinum clusters with up to 24 atoms were generated and the cluster size and charge state dependence of their reactivity towards methane and deuterated methane was investigated. The reactions observed are dehydrogenation of the methane and attachment of a CH_4 respectively CD_4 complex to the clusters. The dehydrogenation of the methane on the platinum clusters proceeds by activation of one of

the methane C-H bonds and formation of a hydrido-methyl platinum complex. The reactivity depends strongly on the cluster size and charge state showing that adding or subtracting one electron can affect dramatically their electronic and geometric structure. The anions show a lower reactivity towards both reactant gases than the cations presumably due to their electronic structure. For the cations by increasing the cluster size the reactivity is shifted in the favour of CH_4 addition to the cluster. Reaction with deuterated methane compared with methane occurs without significant differences for the anions, while for the cations the reactivity is shifted favouring the CD_4 attachment. Starting with n = 15 both cations and anions are almost uneactive.

7.6. References

(1) S. H. Yang, D. A. Drabold, J. B. Adams, P. Ordejon, K. Glassford, *Journal of Physics-Condensed Matter*, **1997**, *9*, L39-L45.

(2) K. Koszinowski, D. Schroder, H. Schwarz, *J. Phys. Chem. A*, **2003**, *107*, 4999-5006.

(3) D. J. Trevor, R. L. Whetten, D. M. Cox, A. Kaldor, *J. Am. Chem. Soc.*, **1985**, *107*, 518-519.

(4) C. Heinemann, R. Wesendrup, H. Schwarz, *Chem. Phys. Lett.*, **1995**, *239*, 75

(5) M. Pavlov, M. R. A. Blomberg, P. E. M. Siegbahn, R. Wesendrup, C. Heinemann, H. Schwarz, *J. Phys. Chem. A*, **1997**, *101*, 1567-1579.

(6) U. Achatz, M. K. Beyer, S. Joos, B. S. Fox, G. Niedner-Schatteburg, V. E. Bondybey, *J. Phys. Chem. A*, **1999**, *103*, 8200-8206.

(7) U. Achatz, C. Berg, S. Joos, B. S. Fox, M. K. Beyer, G. Niedner-Schatteburg, V. E. Bondybey, *Chem. Phys. Lett.*, **2000**, *320*, 53-58.

(8) G. Albert, C. Berg, M. K. Beyer, U. Achatz, S. Joos, G. Niedner-Schatteburg, V. E. Bondybey, *Chem. Phys. Lett.*, **1997**, *268*, 235-241.

(9) I. Balteanu, O. P. Balaj, M. K. Beyer, V. E. Bondybey, *Phys. Chem. Chem. Phys.*, **2004**, *6*, 2910-2913.

(10) C. Berg, T. Schindler, G. Niedner-Schatteburg, V. E. Bondybey, *J. Chem. Phys.*, **1995**, *102*, 4870-4884.

8. Summary

Understanding of the interactions between transition metal clusters, both cations and anions and different adsorbed substances offers information about their geometric and electronic structure. This work investigated the reactivity of the cations and anions of the transition elements towards many small molecules as a function of the cluster size and their charge.

Fourier transform ion cyclotron resonance mass spectrometry proved to be a very useful technique to investigate the reactions of transition metal clusters with different molecules. The versatile laser vaporisation source used can produce a large variety of transition metal clusters both cations and anions. Gold, rhodium and platinum clusters were generated by the source and their reactions with small molecules were investigated. For the first time isotopically enriched platinum clusters were generated and their reactivity towards different complexes investigated. The results show that isotopically enriched samples allow for the investigation of large cluster sizes together with an unambiguous assignment of the reaction products and quantitative determination of the rate constants.

The results of each chapter can be summarized in the following way:

First results on the reactivity of gold anionic clusters Au_n^- with up to 16 atoms towards CO are reported. A novel approach was developed in order to extract absolute bimolecular rate constants from a pulsed-valve experiment in an FT-ICR, due to the fact

that the rate constants observed were in most cases too low to be measured by the standard method with a constant backing pressure. A sequence of reaction gas pulses was employed in order to acquire sufficient product intensity of these exceedingly inefficient reactions. The clusters in the size range of n = 2 - 17 exhibit an amazing diversity in their reactivity patterns, suggesting that perhaps their distinct molecular geometries and structures are of comparable importance as electronic shell closing predicted by the jellium model. The most reactive species is Au_{11}^- whose reactivity was studied also in an experiment with a constant backing pressure. The overall reactivities towards CO somewhat seem to favor odd n clusters, thus n = 5, 7, 9, and 11 all are highly reactive. The complete lack of reactivity of Au_{13}^- might be explained by its presumably icosahedral close-packed geometry. The results suggest that geometric effects will be at least equally important for their reactivity, as the electronic shell structure.

Gas phase reactions of anionic and cationic rhodium clusters with azidoacetonitrile were studied under near-thermal conditions. All anionic and large cationic clusters react by adding [2C, 2N] in consecutive steps, either by forming interstitial carbides and nitrides or by adding two CN groups to the cluster surface, accompanied by full dehydrogenation and evaporation of neutral N_2. Small cationic clusters behave differently, with the unimolecular decomposition of the azide determining the reactivity. The monomer Rh^+ reacts more or less as a spectator, with the azidoacetonitrile undergoing unimolecular reactions, whose products are stabilized as complexes with Rh^+. In the size region from two to five atoms, this unimolecular type of reaction becomes less important, and ceases to occur with n = 5, while formation of the surface-typical reaction products $Rh_nC_xN_y^+$ starts at n = 2 and becomes the dominant reaction at n = 3. The cationic clusters illustrate the gradual transition from metal ion gas phase chemistry to surface-like behavior with

increasing cluster size. Saturation is identified via the size dependent efficiency of consecutive reaction steps.

These results are the first study of the organic azide on transition metal clusters. The reactivity of both cationic and anionic clusters shows that in the gas phase, the high-energy species azidoacetonitrile undergoes clean and defined reactions. The observed selectivity of the reaction is in contrast to the high exotermicity of any reaction with azide species. The results suggest that azidoacetonitrile can be used to generate a stoichiometrically well-defined 1:1 carbide-nitride film or a film consisting of CN groups on a rhodium surface.

Cationic rhodium clusters in the range of about $1 \leq n \leq 25$ were generated and their reactions with ethane as a function of cluster size were investigated under single collision conditions. Overall the reactivity of rhodium clusters towards ethane depends strongly on the cluster size. The primary products consist in a simple or double dehydrogenation or both for almost all the clusters, the most reactive rhodium cluster being n = 10. Rh_5^+ does not react at all with ethane and also do the larger sizes starting with 17, except n = 20 and n = 23. Besides the reactions with ethane, also addition of molecular oxygen, which is present in small amounts in the background gas, is observed, and comparison of the size dependence of this process with the ethane dehydrogenation provides interesting insights into the mechanisms of the occurring reactions.

Platinum is known as a very good catalyst; however it has been studied in less detail because unlike rhodium which is a monoisotopic element, platinum has six stable isotopes. In this work first studies using an isotopically enriched platinum (97.28% ^{195}Pt, Oak Ridge National Laboratories) target are reported. In this way the dilution of the signal

and the overlapping of the reaction products with the reactants are avoided, large clusters with up to 25 atoms being generated, each cluster showing up in the mass spectrum as one clean and dominant peak. Isotopically enriched platinum was used to investigate the reactions of $^{195}Pt_n^{+/-}$ clusters, n = 1 - 24, with N_2O and CO under binary collision conditions.

The reaction of $^{195}Pt_n^{+/-}$ clusters with N_2O can be understood as a decomposition of the nitrous oxide on the metal cluster surface, yielding an oxygen atom and molecular N_2. While the oxygen atom oxidizes the platinum, the weakly bound nitrogen is released. No stabilisation of the undecomposed N_2O on the surface was observed. The nearly three orders of magnitude wide variation in the reaction rates between various clusters may reflect their structural differences, and the presence of differently efficient “sites” on the cluster surface. The fact that anions and cations behave differently may suggest considerable differences between their structures.

Saturation experiments of $^{195}Pt_n^{+/-}$ clusters with CO revealed that the “saturation” number m_{max}, representing the maximum number of adsorbate molecules which can be attached to the cluster surface, increases roughly linearly with n, the number of atoms in the cluster, for both cations and anions but the increase is not quite smooth, and not even always monotonic. For some species the saturation converges to two or even three different values of m_{max}. This suggests that some isomeric structures can be present. At large clusters the influence of the charge is minor, addition or subtracting of a single electron does not affect significantly the saturation number.

A catalytic cycle was observed for Pt_7^+ when the reactant gas used was a mixture 1:6 of CO and N_2O. Pt_7^+ establishes equilibrium with Pt_7O^+ and $Pt_7O_2^+$ in a ratio of about 1:2:4. Two CO molecules are enough to quench the oxidation reaction, and the cluster sequentially and fast adds CO molecules until the surface is fully saturated.

The dehydrogenation of the methane on the platinum clusters proceeds by activation of one of the methane C-H bonds and formation of a hydrido-methyl platinum complex. Reactivity of platinum clusters, both cations and anions towards CH_4 and CD_4 was investigated. For the cations by increasing the cluster size the reactivity is shifted in the favour of CH_4 addition to the cluster, presumably due to the fact that for larger surfaces the probability for the combining the two hydrogen atoms and releasing the molecule is smaller. Reaction with deuterated methane compared with methane occurs without significant differences for the anions, while for the cations the reactivity is shifted favouring the CD_4 attachment.

A List of Publications

1. **Single Molecule Precipitation of Transition Metal(I) Chlorides in Water Clusters**
   B. S. Fox, O. P. Balaj, I. Balteanu, M. K. Beyer, V. E. Bondybey
   J. Am. Chem. Soc. **2002**, *124*, 172-173.

2. **Black Body Radiation Induced Hydrogen Formation in Hydrated Vanadium Cations $V^+(H_2O)_n$**
   B. S. Fox, I. Balteanu, O. P. Balaj, H. C. Liu, M. K. Beyer, V. E. Bondybey
   Phys. Chem. Chem. Phys. **2002,** *4*, 2224-2228.

3. **Reactions of Hydrated Aluminum Ions with Methanol and Formic Acid**
   O. P. Balaj, E. P. F. Lee, I. Balteanu, B. S. Fox, M. K. Beyer, J. M. Dyke, V. E. Bondybey
   Int. J. Mass Spectrom. **2002,** *220*, 331-341.

4. **Aqueous Chemistry of Transition Metals in Oxidation State (I) in Nanodroplets**
   B. S. Fox, O. P. Balaj, I. Balteanu, M. K. Beyer, V. E. Bondybey
   Chem. Eur. J. **2002,** *8*, 5534-5540.

5. **Very Low Rate Constants of Bimolecular CO Adsorption on Anionic Gold Clusters: Implications for Catalytic Activity**
   I. Balteanu, O. P. Balaj, B. S. Fox, M. K. Beyer, Z. Bastl, V. E. Bondybey
   Phys. Chem. Chem. Phys. **2003,** *5*, 1213-1218.

6. **Addition of a Hydrogen Atom to Acetonitrile by Hydrated Electrons in Nanodroplets**

   O. P. Balaj, I. Balteanu, B. S. Fox-Beyer, M. K. Beyer, V. E. Bondybey

   Angew. Chem. Int. Ed. **2003**, *42*, 5516-5518.

7. **The Effect of Charge upon CO-Adsorption by Ionic Group 5 and Group 9 Transition Metal Clusters**

   I. Balteanu, U. Achatz, O. P. Balaj, B. S. Fox, M. K. Beyer, V. E. Bondybey

   Int. J. Mass Spectrom. **2003,** *229*, 61-65.

8. **Size- and Charge-State-Dependent Reactivity of Azidoacetonitrile with Anionic and Cationic Rhodium Clusters $Rh_n^{\pm}$**

   I. Balteanu, O. P. Balaj, B. S. Fox-Beyer, P. Rodrigues, M. T. Barros, A. M. C. Moutinho, M. L. Costa, M. K. Beyer, V. E. Bondybey

   Organometallics **2004**, *23*, 1978-1985.

9. **Base-Catalyzed Hydrogen/Deuterium Exchange between Water and Acetonitrile in Anionic Water Clusters**

   O. P. Balaj, C.-K. Siu, I. Balteanu, B. S. Fox-Beyer, M. K. Beyer, V. E. Bondybey

   J. Phys. Chem. **2004**, *108*, 7506-7512.

10. **Reactions of Platinum Clusters $^{195}Pt_n^{\pm}$, n=1-24, with N_2O Studied with Isotopically Enriched Platinum**

    I. Balteanu, O. P. Balaj, M. K. Beyer, V. E. Bondybey

    Phys. Chem. Chem. Phys. **2004**, *6*, 2910-2913.

11. **Generation of $C_6H_4^{+\cdot}$ by Laser Vaporization of Magnesium with *o*-$C_6H_4F_2$ in Argon Carrier Gas**

    H. Liu, S. Yang, I. Balteanu, O. P. Balaj, B. S. Fox-Beyer, M. K. Beyer, V. E. Bondybey

    Rapid Commun. Mass Spectrom. **2004**, *18*, 1479-1481

12. Free Electrons, the Simplest Radicals of them all: Chemistry of Aqueous Electrons as Studied by Mass Spectrometry

O. P. Balaj, C.-K. Siu, I. Balteanu, M. K. Beyer, V. E. Bondybey

Int. J. Mass Spectrom. **2004**, *238*, 65-74.

13. Reactions of Hydrated Electrons $(H_2O)_n^-$ with Carbon Dioxide and Molecular Oxygen: Hydration of the CO_2^- and O_2^- Ions

O. P. Balaj, C.-K. Siu, I. Balteanu, M. K. Beyer, V. E. Bondybey

Chem. Eur. J. **2004**, *10*, 4822-4830.

14. Catalytic Oxidation of CO with N_2O on Gas-Phase Platinum Clusters

O. P. Balaj, I. Balteanu, T. T. I. Roßteuscher, M. K. Beyer, V. E. Bondybey

Angew. Chem. **2004**, *116*, 6681-6684.

15. Reactions of Rhodium Cationic Clusters with Ethane

I. Balteanu, O. P. Balaj, M. K. Beyer, V. E. Bondybey

In preparation.

16. Saturation Reactions of Platinum Clusters $^{195}Pt_n^{\pm}$, n=1-23, with CO Studied with Isotopically Enriched Platinum

I. Balteanu, Z. Sun, O. P. Balaj, M. K. Beyer, V. E. Bondybey

In preparation.

17. Reactions of Hydrated Electrons with Hydrogen Chloride: Formation of Atomic Hydrogen

C.-K. Siu, O. P. Balaj, I. Balteanu, M. K. Beyer, V. E. Bondybey

In preparation.

B List of Presentations at Scientific Workshops and Conferences

1. **The Effect of Charge upon CO Adsorption by Ionic Group 5 and Group 9 Transition Metal Clusters**
   I. Balteanu, O. P. Balaj, B. S. Fox, M. K. Beyer, V. E. Bondybey
   3rd Meeting of the RTN Network on "Reactive Intermediates Relevant in Atmospheric Chemistry and Combustion", 11-14 October 2001, Garching b. München, Germany
   Talk

2. **The Effect of Charge upon CO Adsorption by Ionic Metal Clusters**
   I. Balteanu, O. P. Balaj, B. S. Fox, M. K. Beyer, V. E. Bondybey
   6th European workshop on Fourier Transform Ion Cyclotron Resonance Mass Spectrometry, 16-19 October 2001, Rolduc Monastery, Kerkrade, The Netherlands
   Talk

3. **Effect of Charge upon CO Adsorption by Coinage Metal Clusters**
   I. Balteanu, O. P. Balaj, B. S. Fox, M. K. Beyer, V. E. Bondybey
   35. DGMS-Diskussionstagung, 3-6 March 2002, Heidelberg, Germany
   Poster

4. **Effect of Charge upon CO Adsorption by Ionic Coinage Metal Clusters**
   I. Balteanu, O. P. Balaj, B. S. Fox, M. K. Beyer, V. E. Bondybey
   66. Frühjahrstagung der Deutschen Physikalischen Gesellschaft, 4-8 March 2002, Osnabrück, Germany
   Talk

5. Black Body Radiation Induced Hydrogen Formation in Hydrated Vanadium Cations $V^+(H_2O)_n$

B. S. Fox, I. Balteanu, O. P. Balaj, M. K. Beyer, V. E. Bondybey

4th Meeting of the RTN Network on "Reactive Intermediates Relevant in Atmospheric Chemistry and Combustion", 18-23 April 2002, Heraklion, Crete

Talk and Poster

6. Reactions of Ionic Rhodium Clusters with Organic Azides

I. Balteanu, O. P. Balaj, B. S. Fox, M. K. Beyer, V. E. Bondybey

5th Meeting of the RTN Network on "Reactive Intermediates Relevant in Atmospheric Chemistry and Combustion", 8-11 September 2002, Southampton, UK

Talk and Poster

7. Very Low Rate Constants of Bimolecular CO Adsorption on Anionic Gold Clusters: Implications for Catalytic Activity

I. Balteanu, O. P. Balaj, B. S. Fox, M. K. Beyer, V. E. Bondybey

4th International Conference on Cryocrystals and Quantum Crystals, 27-31 October 2002, Freising, Germany

Poster

8. Very Low Rate Constants of Bimolecular CO Adsorption on Anionic Gold Clusters

I. Balteanu, O. P. Balaj, B. S. Fox, M. K. Beyer, V. E. Bondybey

6th Meeting of the RTN Network on "Reactive Intermediates Relevant in Atmospheric Chemistry and Combustion", 26-30 March 2003, Bremen, Germany

Poster

9. Reactions of Large Ionic Platinum Clusters $Pt_n^{+/-}$, n = 1 – 26, with Small Molecules

I. Balteanu, O. P. Balaj, M. K. Beyer, V. E. Bondybey

7th Meeting of the RTN Network on "Reactive Intermediates Relevant in Atmospheric Chemistry and Combustion", 3-7 September 2003, Saint Lambert des Bois, France

Talk and Poster

10. Cluster Size and Charge Dependence Reactions of the Highly Exothermic Azidoacetonitrile on Anionic and Cationic Rhodium Clusters

I. Balteanu, O. P. Balaj, B. S. Fox, M. K. Beyer, V. E. Bondybey

68. Frühjahrstagung der Deutschen Physikalischen Gesellschaft, 22-26 March 2002, München, Germany

Talk

11. Use of Isotopically Enriched Material in Gas Phase Cluster Studies

I. Balteanu, O. P. Balaj, B. S. Fox, M. K. Beyer, V. E. Bondybey

7th European workshop on Fourier Transform Ion Cyclotron Resonance Mass Spectrometry, 28 March -1 April 2004, Konstanz, Germany

Talk

Acknowledgement

This thesis would not have been possible without help and support from a team of wonderful people. First I would like to thank with deepest gratitude my supervisor Prof. Dr. Vladimir E. Bondybey for the brilliant ideas, world wide recognized experience and critical advice which shaped my work.

I want to cordially thank Dr. Martin Beyer, the head of the Garching group, for the overwhelming knowledge, open friendly leadership, energy and scientific enthusiasm. His guiding in the scientific research has been invaluable for my professional formation.

I will greatly miss the collaboration and helpful discussions with the other active members of the ICR group, Dr. Brigitte S. Fox-Beyer, Ovidiu Balaj, Dr. Chi-Kit Siu and recently Dr. Sun Zheng, all great friends and extraordinary team players. Matthias' work was very useful to the whole group.

Special thanks to Sabine Kullick, our secretary, who is the heart and soul of the group for her priceless help and to Peter Kämmerer for his dedication in fighting (and winning) all kinds of IT battles.

I would like to thank the other members of the Bondybey group, Dr. Marcin Frankowski, Alexey Ponomariov, Dr. Alice Smith-Gicklhorn, Dr. Elena Savchenko and, as well as former members of the group, Dr. Dieter Kraus and Dr. Bernhard Urban for their helpful attitude.

It was a great pleasure and experience to be one of the young researchers (YR) of the European Union's "Reactive Intermediates Relevant in the Atmospheric Chemistry and Combustion" network. I would like to thank all the people involved and especially to

Prof. Dr. John Dyke from University of Southampton and Prof. Dr. C. A. de Lange from Vrije Univeriteit. The network's financial support is gratefully acknowledged.

Special thanks to Dr. Horia Porteanu from Physics Department Garching who helped me a lot to get the visa for Germany.

Financial support by the Deutsche Forschungsgemeinschaft and the Fonds der Chemischen Industrie is gratefully acknowledged.

The deepest "thank you" is reserved for my grandfather Buni and for Eugen.